Supplementary Information (SI) for Dalton Transactions.

Electronic Supporting Information

Ruthenium Complexes Bearing Terpyridyl Ligands of Distinct Donor-Acceptor Configuration for Solar Energy Conversion

Tanu Singh[‡a], *Angelina Mary*[‡a], *Tanushree Gupta*[#a], *Pooja Sharma*[#a], *Vinod Kumar*[b], *Amilan D. Jose*[b], *and Abbas Raja Naziruddin*[a*]

[a]*Malaviya National Institute of Technology Jaipur, Rajasthan, India,*

[b]National Institute of Technology Kurukshetra, India.

Contents **Page**

Photophysical studies

Electrochemistry

Dye – TiO_2 interfacial studies

Experimental details

Dimethyl-6-bromo-[2,2'-bipyridine]-4,4'-dicarboxylate(**a**)[1], 2-methyl-6-tributyltin (**b**)[2], 4-carboxylate terpyridine (**L_1**)[3], 4, 4', 4''-tricarboxy terpyridine (**L_3**),[3] and 4'-^{tert}butyl-2,2'6,6'-terpyridine (**L_4**)[4] were prepared by following the reported protocols. The photovoltaic and electron impedance spectroscopy studies of [**S1**] – [**S3**] and **N3** dye is displayed in Tables S11 and S12 (a) and (b) respectively.

Preparation of 4-carboxylate terpyridine (L_1):

(**L_1**): 4-carboxylate terpyridine was isolated by following the reported protocol with slight modifications.

Preparation of 4, 4', 4''-tricarboxy terpyridine (L_3):

(**L_3**): Initially, ethyl-2-isonicotinate was isolated as yellow solids by refluxing the mixture of paraldehyde (8.20 g, 62.00 mmol) and ethyl isonicotinate (1.90 g, 12.70 mmol), $FeSO_4{\cdot}7H_2O$ (60.00 mg, 0.20 mmol), trifluoroacetic acid (1.50 g, 13.00 mmol) and 70% ^{t}BuOOH (3.20 g, 0.25 mmol) in acetonitrile (26.00 mL) for 4 h at 80 °C. Subsequently, acetonitrile was removed *in vacuo*, and the residue was taken up in a 20.00 mL of sodium carbonate (*aq.*). The aqueous layer was extracted with benzene. The combined organic fractions were dried over Na_2SO_4, filtered, and then the solvent was removed *in vacuo*. The reaction mixture containing ethyl-2-isonicotinate (2.00 g, 10.70 mmol) was reacted with freshly distilled furfural (0.49 g, 5.18 mmol) potassium hydroxide (1.33 g, 2.44 mmol), and 10.00 mL of 25 % NH_3 (aq.) in 12.00 mL of absolute ethanol under inert atmosphere at ambient temperature for 24 h. After the completion of the reaction, the reaction mixture was filtered using buchner funnel and the precipitate of 4′-furyl-2,2′:6′,2''- terpyridine-4,4''-dicarboxylate was washed with acetonitrile till the drops were colourless resulting in light brown solids. Further, 4′-furyl-2,2′:6′,2''- terpyridine-4,4''-dicarboxylate (2.46 g, 5.30 mmol) was reacted with $KMnO_4$ (4.00 g, 25.31 mmol) in water (100 mL). The solution was adjusted to pH 10 by adding potassium hydroxide (0.04 g). The resulting mixture was stirred at room temperature for 24 h. The resulting mixture was filtered and then the filtrate was acidified with 37 % HCl till pH 5 resulting in white precipitate. The precipitate was filtered and thoroughly washed with H_2O. Product was obtained as white solids. Further esterification was done in methanol by following the procedure reported in the literature.[3]

Preparation of 4'-^{tert}butyl-2,2'6,6'-terpyridine (L_4):

(**L_4**): 4'-^{tert}butyl-2,2'6,6'-terpyridine was isolated by following the reported protocol.[4]

Dimethyl-6-bromo-[2,2'-bipyridine]-4,4'-dicarboxylate (a):

The titled compound was prepared using a slight modification of the reported protocol.[1, 5] In a flame-dried Schlenk tube, dimethyl-6-chloro-[2,2'-bipyridine]-4,4'-dicarboxylate (1.00 g, 3.30 mmol, 1.00 eq.) was dissolved in propionitrile (60.00 mL) under an atmosphere of nitrogen gas. Subsequently, bromotrimethylsilane (4.00 g, 3.40 mL, 26.10 mmol, 8.00 eq.) was added to the mixture. Attention should be given to the vigorous evolution of bromine fumes. The reaction mixture was refluxed at 100 °C for 4 days. After this time, the content of the Schlenk flask was cooled down, and the mixture was neutralized to pH 7 using a 2.00 M aqueous sodium carbonate solution. The product was extracted in dichloromethane, and the organic layer was dried over magnesium sulfate. Column chromatography using silica gel (100 – 200 mesh) and the solvent mixture of dichloromethane: methanol (97:3, *v*: *v*) separated the products with an R_f value of 0.90. Removal of the solvents gave the product as white solids, in 80% yield. Analytical data matches the reported literature.[1]

Synthesis of 2-methyl-6-tributyltin (b): In a flame-dried Schenck flask of 100.00 mL volume, 2-bromo-6-picoline (1.00 g, 5.80 mmol) was dissolved in tetrahydrofuran (20.00 mL). Subsequently, 1.20 M ^{n}Butyl lithium (5.00 mL, 6.40 mmol) was added dropwise into the reaction mixture stirring under inert atmosphere at –78 °C for a period of 20.00 minutes. After 1.50 h, tributyl tin chloride (1.90 mL, 6.90 mmol) was added at –78 °C. The color of reaction mixture turned into pale-yellow. Yellow coloured mixture was stirred for 6.00 hours at room temperature. Then the reaction was stopped by quenching the excess ^{n}butyl lithium using water. Product was extracted in ethyl acetate and organic layer was dried over $MgSO_4$. Product was purified using column chromatography (60 mesh silica) using a solvent mixture of hexane: ethyl acetate (9:1)., Yield: 90%, pale yellow coloured liquid. Analytical data matches the reported literature. R_f value: 0.90

Syntheses of (**L_2**): Dimethyl-6-bromo-[2,2'-bipyridine]-4,4'-dicarboxylate (a) (0.30 g, 0.90 mmol) and 2-methyl-6-tributyltin (b) (0.32 g, 0.90 mmol) were dissolved in toluene in a 100.0 mL Schenck flask under an inert atmosphere of N_2 gas. Subsequently, $[Pd(PPh_3)_4]$ (3.20 mg, 0.01 mmol) was added to this mixture. Then, the reaction mixture was refluxed under 110 °C for 48 h. After this time, the content of the Schenck flask was transferred into a 100.00 mL round-bottomed flask and dried using a rotary evaporator. Further purification was done using silica gel column chromatography (60 mesh) using an eluent mixture of dichloromethane: methanol (97:3 *v*: *v*). R_f value: 0.90, Yield: 70%, white solid. ^{1}H NMR (400.00 MHz, $CDCl_3$): δ 9.1 (s, 1H), 9.0 (s, 1H), 8.9 (s, 1H), 8.8 (s, 1H), 8.4 (s, 1H), 7.9 (s, 1H), 7.8 (s, 1H), 7.2 (s, 1H), 4.0 (s, 6H), 4.00 (s, 1H), 2.6 (s, 3H). ^{13}C NMR (100.61 MHz, $CDCl_3$, ppm): δ 206.2, 165.1, 155.9, 150.4, 137.5, 120.3, 119.7, 67.3, 57.8, 51.6. HRMS: m/*z* 387.1056 (calculated for $[M + Na + H]^+$ 387.1195).

General synthesis of ester precursors [**1**], [**2**] and [**3**]:

ACE glass *vial* containing 4'-(^{t}butyl)-2,2',6'2"-terpyridine, and anhydrous $RuCl_3$ in ethanol (15.00 mL) was refluxed under 120 °C for 12 h. The resulting dark red-turbid solution was filtered using a Buchner funnel to obtain dark maroon solids of $[Ru(tpy^{4'\text{-}^{t}butyl})(Cl)_3]$. This complex was further treated with $AgNO_3$ in a mixture containing 5 mL of ethanol: water ((1:1) *v*:*v*) and 30 mL acetonitrile solution and refluxed under dark for 12 h. The reaction mixture was cooled down and filtered to obtain the crude product. Purification was done by silica gel (60–100 mesh) column chromatography using a solvent mixture of CH_3CN: H_2O: KNO_3 (aqueous) (89: 9: 1 *v*: *v*: *v*). The dark red band was collected, and the counter anion was exchanged using KPF_6, giving $[Ru(tpy^{4'\text{-}^{t}butyl})(CH_3CN)_3](PF_6)_2$ as a red powder. Subsequently, a Schlenk flask containing a mixture of $[Ru(tpy^{4'\text{-}^{t}butyl})(CH_3CN)_3](PF_6)_2$, and $L_1/L_2/L_3$ in ^{n}BuOH was refluxed under 120 °C for 12 h to obtain a dark red solution. Subsequently, the solvent was dried, and crude solids were purified using a 10.00 cm column packed with silica gel (60 – 100 mesh) using an eluent comprising a CH_3CN: H_2O: KNO_3 (aqueous) (89: 9: 1 *v*: *v*: *v*) mixture. The product was obtained as a dark red band (R_f value: 0.60). Further treatment with an excess KPF_6 precipitated the product of [**1**], [**2**] and [**3**].

[**I**]**:** The *tris* acetonitrile complex, $[Ru(tpy^{4'\text{-}^{t}butyl})(CH_3CN)_3](PF_6)_2$ was first obtained by following the general synthesis using $tpy^{4'\text{-}^{t}butyl}$ (0.30 g, 1.03 mmol), $RuCl_3$ (0.22 g, 1.06 mmol), $AgNO_3$ (0.52 g, 3.08 mmol), ethanol (5.00 mL), CH_3CN (30.00 mL) and degassed analytically pure grade of water (5.00 mL) as red solids. Yield: 0.09 g, 42%. ^1H NMR (400.00 MHz, CD_3CN, ppm): δ 8.90 (d, $^3J_{C\text{–}H}$ = 6.3, 2H), 8.51(d, $^3J_{C\text{–}H}$ = 9.5, 2H), 8.36(s, 2H), 8.16(m, 2H), 7.71(m, 2H), 1.94(s, 9H). ^{13}C NMR (100.61 MHz, CD_3CN, ppm): δ 159.3, 156.8, 155.9, 137.5, 130.1, 128.0, 127.4, 125.6, 123.7, 120.6, 37.5, 34.7, 33.2, 29.2. HRMS: m/*z* 593.1600 (calculated for $[M + 2Na + CH_4O + H]^+$) 593.1555.

[**1**]: General procedure for ester precursors was adopted by using $[Ru(tpy^{4'\text{-}^{t}butyl})(CH_3CN)_3](PF_6)_2$ (0.20 g, 0.25 mmol) and L_1 (0.072 g, 0.25 mmol) in ^{n}BuOH. After column chromatography, red solids of $[Ru(L_1)(tpy^{4'\text{-}^{t}butyl})](PF_6)_2$ were obtained. Yield: 0.25 g, 65%. ^1H NMR (400.00 MHz, CD_3CN): δ 9.19 (s, 2H), 8.74 (s, 2H), 8.63 (d, $^3J_{C\text{–}H}$ = 8.1, 2H), 8.58 (d, $^3J_{C\text{–}H}$ = 8.1, 2H), 7.94 (d, $^3J_{C\text{–}H}$ = 8.0, 2H), 7.89 (m, 2H), 7.38 (m, 1H), 7.25 (m, 2H), 7.22 (d, $^3J_{C\text{–}H}$ = 5.5 Hz, 2H), 7.08 (m, 5H), 7.0 (m, 2H), 4.2 (s, 3H), 1.70 (s, 9H) ppm. ^{13}C NMR (100.61 MHz, CD_3CN, ppm): δ 164.0, 158.6, 157.9, 156.0, 154.2, 153.0, 139.4, 138.5, 136.8, 127.3, 126.9, 124.5, 123.9, 121.7, 65.3, 36.3, 30.2, 14.5 ppm. HRMS: m/*z* 753.1497 (calculated for $[M + Na + 4H]^+$) 753.1548. ATR-FTIR (*v*, cm^{-1}): 548.53, 825.39 (P−F stretch), 1239.00, 1126.24, (C−O stretch), 1614.56, 1740.00 (ester C=O stretch), 2883.02 (−CH aliphatic stretch), 2972.55 (−CH aryl stretch).

[**2**]: General procedure for ester precursors was adopted by using the *tris*-acetonitrile precursor $[Ru(tpy^{4'\text{-}^{t}butyl})(CH_3CN)_3](PF_6)_2$ (0.20 g, 0.23 mmol) and L_2 (0.06 g, 0.23 mmol) in ^{n}BuOH. After column chromatography, the ester complex [**2**] was obtained as red solids. Yield: 0.16 g, 67%. ^1H NMR (400.00 MHz, CD_3CN): δ 9.27 (s, 2H), 8.96 (s, 1H), 8.78 (s, 2H), 8.61 (d ($^3J_{C\text{–}H}$ = 7.9 Hz), 3H), 7.92 (m, 3H), 7.58 (m, 1H), 7.31 (d, $^3J_{C\text{–}H}$ = 5.5 Hz, 2H), 7.22 (d, $^3J_{C\text{–}H}$ = 7.6 Hz, 1H), 7.14 (m, 2H), 6.98 (m, 1H), 4.18 (s, 3H), 3.90 (s, 3H), 1.70 (s, 9H), 1.62 (s, 3H) ppm. ^{13}C NMR (100.61 MHz, CD_3CN, ppm): δ 164.2, 163.3, 162.0, 158.5, 157.5, 156.5, 155.0, 154.0, 152.6, 151.4, 138.06, 128.0, 127.2, 124.4, 121.7, 66.4, 35.9, 35.2, 29.6, 23.5 ppm. HRMS: m/*z* 899.2423 (calculated for $[M + C_4H_{11}O + 3Na + H]^+$ 899.2063. ATR-FTIR (*v*, cm^{-1}) 554.00, 819.36 (P−F stretch), 1254.41, 1311.22 (C−O stretch), 1620.14, 1734.00 (ester C=O), 2364.00 (−CH aliphatic stretch), 2958.54 (−CH aryl stretch).

[**3**]: $[Ru(tpy^{4'\text{-}^{t}butyl})(CH_3CN)_3](PF_6)_2$ (0.20 g, 0.20 mmol) was refluxed with L_3 (0.06 g, 0.20 mmol) in ^{n}BuOH and further purified by column chromatography to obtain red solids of $[Ru(L_3)(tpy^{4'\text{-}^{t}butyl})](PF_6)_2$. Yield: 0.16 g, 73%. ^1H NMR (400.00 MHz, CD_3CN): δ 9.39 (s, 2H), 9.08 (s, 2H), 8.77 (s, 2H), 8.61 (d, $^3J_{C\text{–}H}$ = 8.1 Hz, 2H), 7.92 (m, 2H), 7.66 (m, 2H), 7.60 (m, 2H), 7.21 (d, $^3J_{C\text{–}H}$ = 5.6 Hz, 1H), 7.10 (m, 2H), 4.21 (s, 3H), 3.94 (s, 6H), 1.72 (s, 9H) ppm. ^{13}C NMR (100.61 MHz, CD_3CN): δ 163.72, 162.80, 158.69, 158.07, 156.03, 154.12, 153.29, 152.92, 138.86, 138.48, 127.29, 126.75, 124.65, 123.77, 121.57, 53.23, 52.93, 36.34, 30.04 ppm. ATR-FTIR (*v*, cm^{-1}): 523.53, 823.81 (P−F stretch), 1262.21, 1311.26 (C−O stretch), 1620.41, 1716.11 (ester C=O stretch), 2356.05 ($-CH_3$ aliphatic stretch), 2958.94 (−CH aryl stretch). HRMS: m/*z* 943.0882 (calculated for $[M + C_4H_{11}O + Na + H_2O]^+$) 943.1155.

Quantum Chemical Calculations

The dispersion-corrected density functional theory (DFT–D3)[6, 7] calculations were performed for the ruthenium(II) terpyridyl heteroleptic complexes [**S1**] – [**S3**]. *Restricted Kohn-Sham* (RKS) formalism was followed for computing all singlet electronic states, while *unrestricted* (U)-KS formalism was adopted for calculating the electronic states of other spin multiplicities. The geometries of the electronic states of all photosensitizers were optimized without constraints according to the default convergence criteria (5.0×10^{-6} E_h for energy change, 3.0×10^{-4} E_h/Bohr for maximum gradient, 1.0×10^{-4} E_h/Bohr for RMS gradient, 4.0×10^{-3} Bohr and 2.0×10^{-3} Bohr for maximum and RMS displacement, respectively). All computations were carried out utilizing the ORCA program (version 5.0.4),[8, 9] with *Becke,* and the three-parameter *Lee–Yang–Parr* (B3LYP) hybrid functional.[10, 11] The Ahlrichs' split valence triple-ζ def2-TZVPP basis set for the ruthenium atom and double-ζ def2-SVP basis set for all other atoms were employed.[12-17] Additionally, the Stuttgart–Dresden (SDD) relativistic pseudopotential was utilized to describe the Ru-28 core electrons. The RIJCOSX approximation[12] was also used in all DFT–D3 calculations to speed up the computations of the *Coulomb* and *Hartree-Fock* exchange integrals at the default grids. All *non-periodic* calculations were carried out in the acetonitrile phase, modelled *via* a solvation model based on density (SMD).[18] The singlet ground (S_0) states and their singly oxidized doublets were optimized in the vacuum and acetonitrile phases. The ground state geometries of [**S1**] – [**S3**] in the solution phase are listed in Table S1 of the Supporting Information. The $Ru^{2+/3+}$ oxidation potentials for all complexes were calculated *via* the *Born-Haber* cycle that employs the *Gibbs* free energies of their S_0 states and their oxidized forms. Further, the nature of the singly oxidized/reduced doublets with an overall charge of 3+/1+ and doubly oxidized/reduced triplets of the respective charge 4^+/0 was characterized through the *Mulliken* spin densities of the ruthenium center and tpy ligands.

The bonding interactions between the ruthenium center within the [Ru^{2+}–tpy^A] fragment and the coordinating atoms of the tpy donor of the [tpy^D] fragment in the S_0 state were evaluated through the extended transition state-natural orbitals for chemical valence (ETS-NOCV) method.[19, 20] This method decomposes the Ru – N (tpy^D) bond into pairwise bonding interactions. Subtracting the square of the NOCV pair from that of another contributes to a pairwise interaction and gives a deformation density. This deformation density qualitatively illustrates the electron density rearrangement upon metal$_{\text{(Ru)}}$-ligand$_{(\text{tpy}D)}$ bond formations. Charge-displacement[21, 22] (CD) function applied to these deformation densities was evaluated *via* Pycubescd code.[23] For computing the charge-displacement, the cartesian coordinates of the S_0-geometries of [**S1**] – [**S3**] were re-oriented by aligning the ruthenium atom at the origin (0 Å), tpy^D on its right (+ *z*-axis), and tpy^A on its left (– *z*-axis), as depicted by the CD graph-horizontal axis (Supporting Information, Figure S19 and Table S1). The $\Delta q(z)$ curves peaking along the vertical axis of the CD-NOCV graph depict the magnitude of charge displacement (Δq) due to bonding interactions. The upward ($+\Delta q(z)$) and downward ($-\Delta q(z)$) charge displacement arise respectively due to the σ-donation (right to left) and π back-donation (left to right) interactions between the tpy^D and [Ru(II)–tpy^A] fragments.

The geometries of the lowest-lying excited closed-shell singlet (S_1) and the ground open-shell triplet (T_1) electronic states of 2+ charge were relaxed *via* time-dependent (TD)-DFT and ground state optimizations, respectively. TDDFT calculations were also performed on the ground states of all complexes to generate fifty vertical excitations. Electron density difference maps (EDDMs) using the *orca_plot* utility were generated for the relevant singlet excitations to visualize and identify the nature of charge transfer excitations. An inter-fragment charge transfer (IFCT) analysis was performed using Multiwfn 3.6 program[24] to quantify the extent of charge transfer occurring in these excitations. A relaxed one-dimensional potential energy scan (1D-PES) along the Ru – N (tpy acceptor) coordinate was performed on the triplet surface to find the metal-centered states. For the ^{3}PES scan, the Ru – N bond was stretched in steps of 0.03 Å. The nature of all higher- and lower-lying triplet states was characterized by *Mulliken* spin densities. The metal- and ligand-based orbitals and their energies involved in these triplet states were identified by analyzing their corresponding singly-occupied molecular orbitals. All electronic states were characterized as having no negative imaginary frequencies through vibrational frequency computations.

The periodic optimization of the TiO_2 unit cell through the "*vc-relax*" method that allows variation of atomic positions and lattice constants was done using the Quantum Espresso program package (version 6.8)[25] at the PBE[26] level of theory. This calculation was performed *via* the projector-augmented wave method with kinetic energy cutoff for wavefunctions and charge density of 30 Ry and 360 Ry, respectively.[27] The relaxed tetragonal lattice of the TiO_2 unit cell was found to have lattice vectors of $a = b = 3.400$ Å and c = 11.294 Å. Furthermore, the unit cell was extended and cut at the anatase (101) surface. This was then modeled to form a $(TiO_2)_{46}$ cluster and optimized using the ORCA program. The dye – TiO_2 assemblies of all complexes were modeled using the optimized $(TiO_2)_{46}$ cluster, and a constrained optimization was performed in acetonitrile solution at the B3LYP level of theory.[28-33]

Constraints were applied on the *xyz* coordinates of the bottom layers of the relaxed $(TiO_2)_{46}$ cluster, excluding the top two Ti layers and top four O layers. The adsorption energy of stability of the dye – TiO_2 assemblies (E_{ads}) was calculated as $E_{ads} = E_{Dye - TiO2} - (E_{Dye} + E_{TiO2})$.[34-36] The terms $E_{Dye - TiO2}$, E_{Dye} and E_{TiO2} represent the energy of the dye – TiO_2 assembly, free dye and TiO_2 cluster, respectively. The negative value of E_{ads} corresponds to the stable adsorption of ruthenium complexes on the surface of the $(TiO_2)_{46}$ cluster.[34, 35] The partial density of states (PDOS) of the $(TiO_2)_{46}$ cluster and the dye – TiO_2 assemblies of [**S1**] – [**S3**] were computed using the GaussSum program.[37] These dye – TiO_2 assemblies were subjected to TDDFT calculations in the acetonitrile phase to generate fifty vertical singlet excitations. These excitations were visualized through EDDMs, and the extent of charge transfer was computed through the IFCT analysis.

Quantum dynamics simulations were carried out on the dye – $(TiO_2)_{46}$ assemblies of [**S1**] – [**S3**] to evaluate the interfacial electron transfer *via* the IET code[38] with the default extended *Hückel* (EH) parameters. The relevant extended *Hückel* (EH) orbitals involved in the interfacial electron transfer (IET) resemble the tpy^A-localized virtual *Kohn-Sham* orbitals. Simulations were carried out with a time step of 0.1 fs in the vacuum phase at a fixed geometry of the dye – $(TiO_2)_{46}$ assemblies within the periodic boundary conditions (dimensions) of 22.49 × 35.41 × 24.08 Å for [**S1**] – $(TiO_2)_{46}$, 24.73 × 35.19 × 23.33 Å for [**S2**] – $(TiO_2)_{46}$ and 25.25 × 35.61 × 24.62 Å for [**S3**] – $(TiO_2)_{46}$ in type-*a* mode, 25.03 × 32.00 × 22.50 Å for [**S2**] – $(TiO_2)_{46}$ and 23.97 × 32.85 × 22.48 Å for [**S3**] – $(TiO_2)_{46}$ in type-*b* mode of adsorption, using 1 × 1 × 1 *k*-point sampling. Absorbing potentials for Ti^{4+} ions were applied to the Ti atoms in the bottom layer of the $(TiO_2)_{46}$ cluster to prevent the undesired artificial recurrences in the transient electron population. The survival probability obtained through these simulations demonstrates the likelihood of the electron wavepacket localization on the dye at time *t*. The electron injection time was obtained *via* an exponential fit ($f(t) = exp(-t/\tau)$) to the survival probability.

Nuclear Magnetic Resonance (NMR) interpretations (^{1}H and ^{13}C)

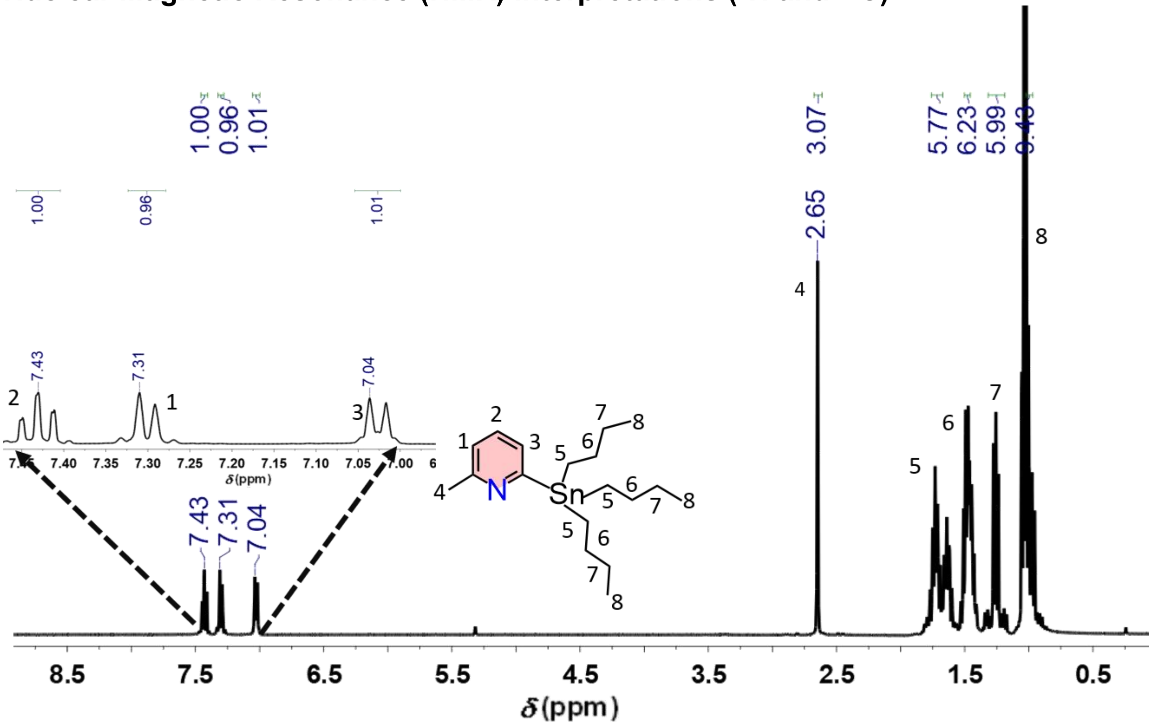

Figure S1. ^{1}H NMR spectrum of (b) in $CDCl_3$, 400.00 MHz.

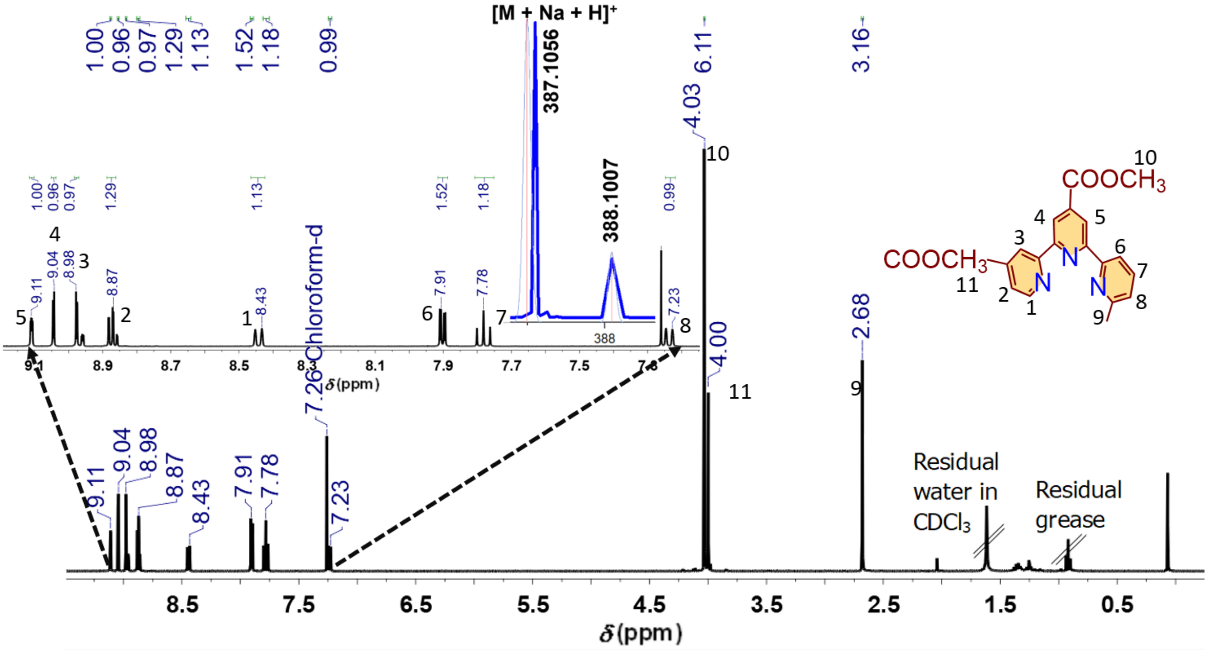

Figure S2. ^{1}H NMR spectrum and HRMS data of (L_2) in $CDCl_3$, 400.00 MHz.

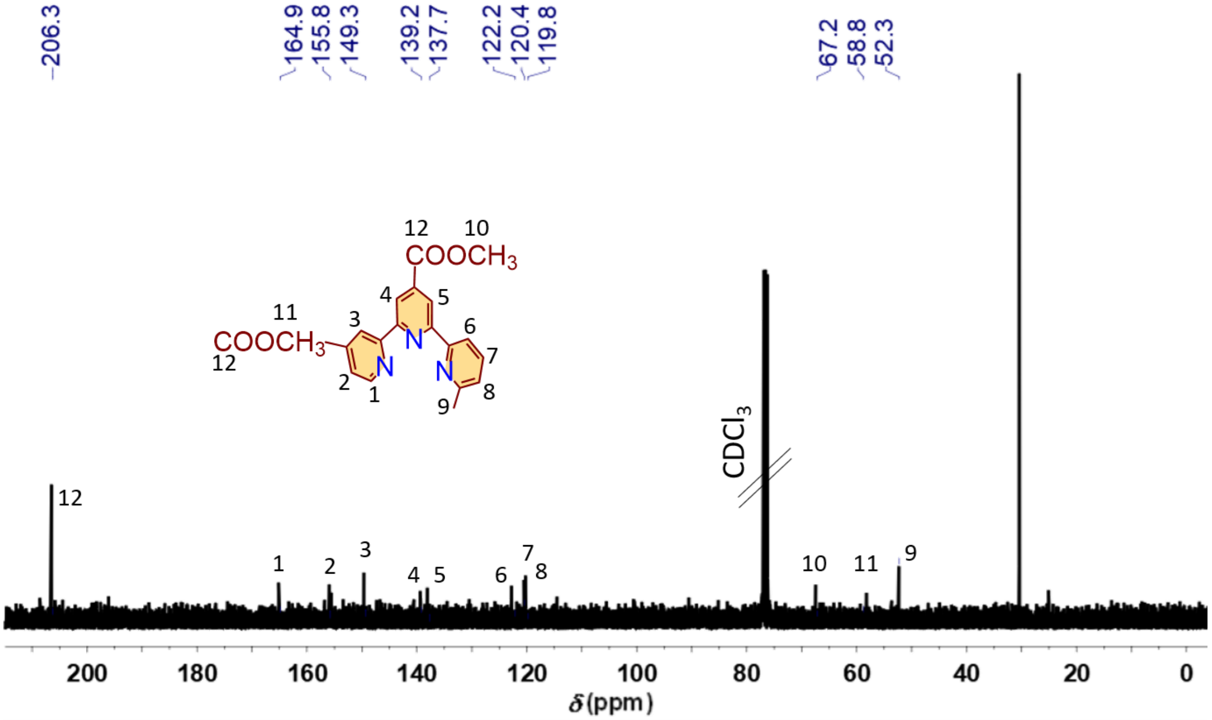

Figure S3. ^{13}C NMR spectrum of (L_2) in CD_3CN, 100.61 MHz.

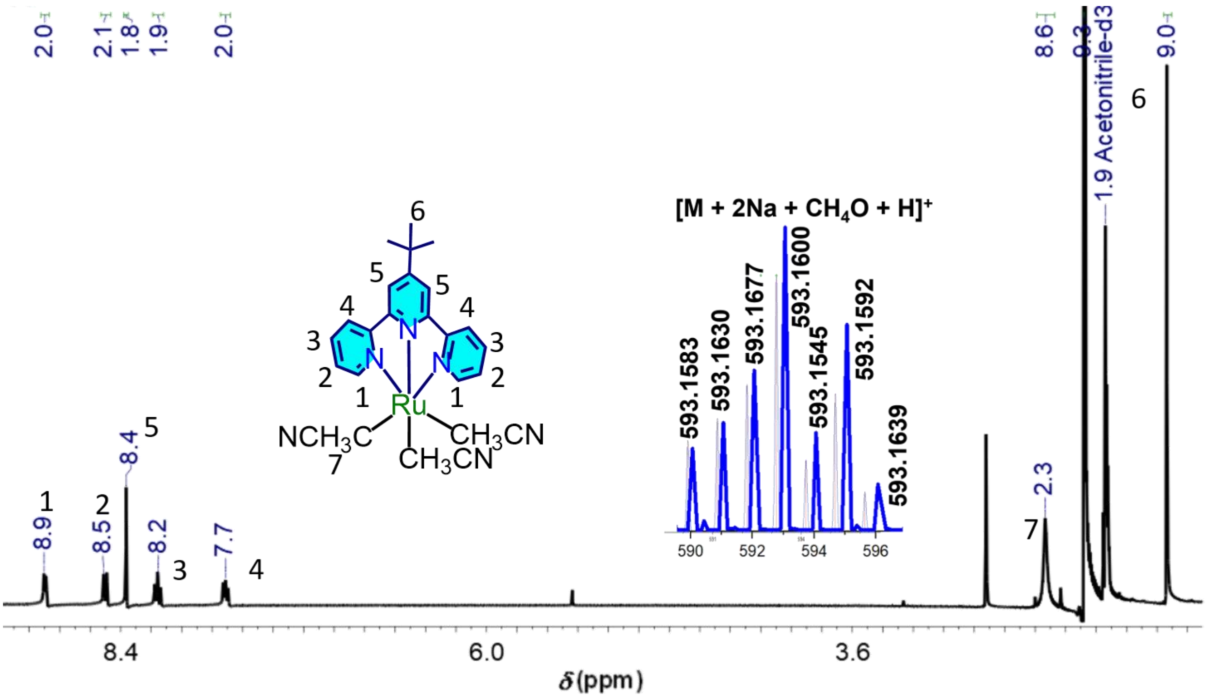

Figure S4. ^{1}H NMR spectrum and HRMS data of (**I**) in CD_3CN, 400.00 MHz.

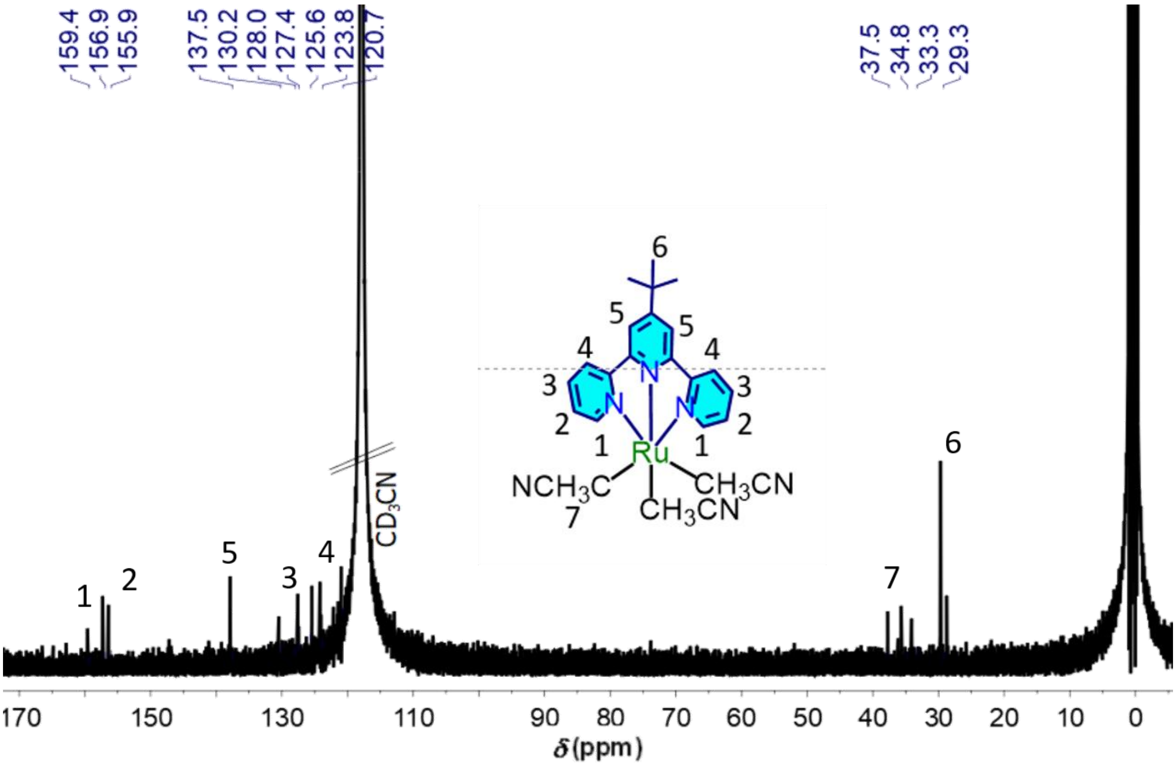

Figure S5. ^{13}C NMR spectrum of (**I**) in CD_3CN, 100.61 MHz.

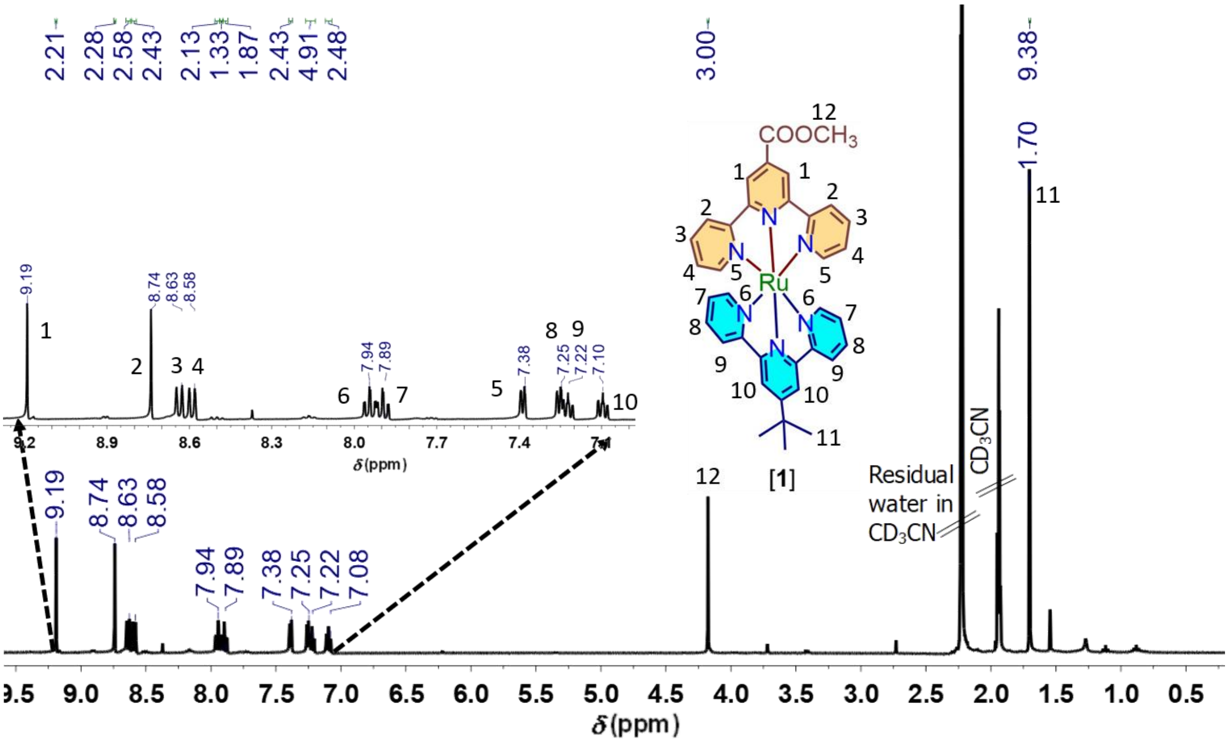

Figure S6. ^{1}H NMR spectrum of [**1**] in CD_3CN, 400.00 MHz.

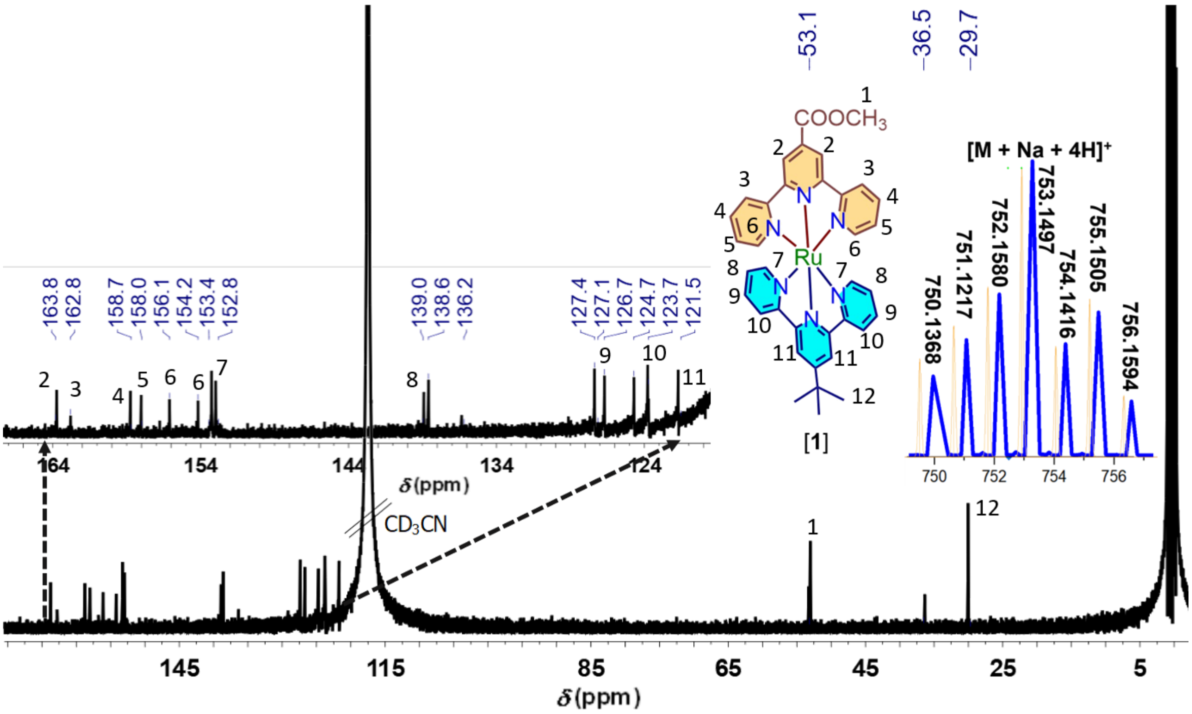

Figure S7. ^{13}C NMR spectrum and HRMS data of [**1**] in CD_3CN, 100.61 MHz.

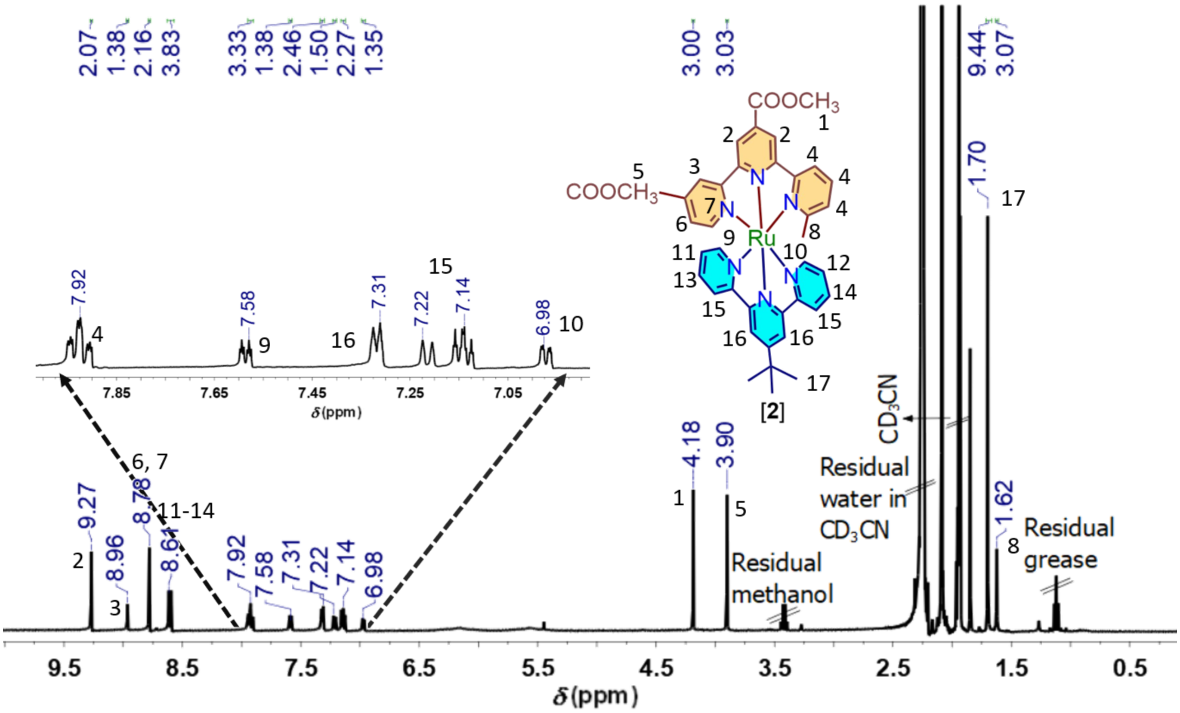

Figure S8. ^{1}H NMR spectrum of [**2**] in CD_3CN, 400.00 MHz.

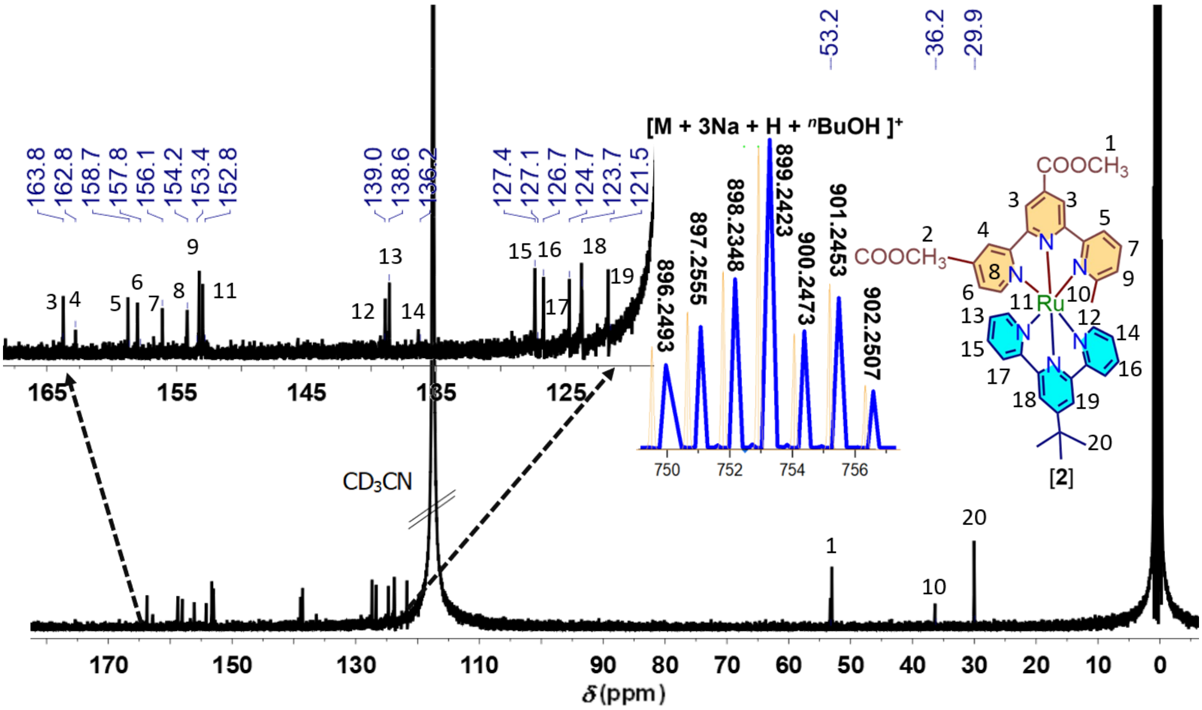

Figure S9. ^{13}C NMR spectrum and HRMS data of [**2**] in CD_3CN, 100.61 MHz.

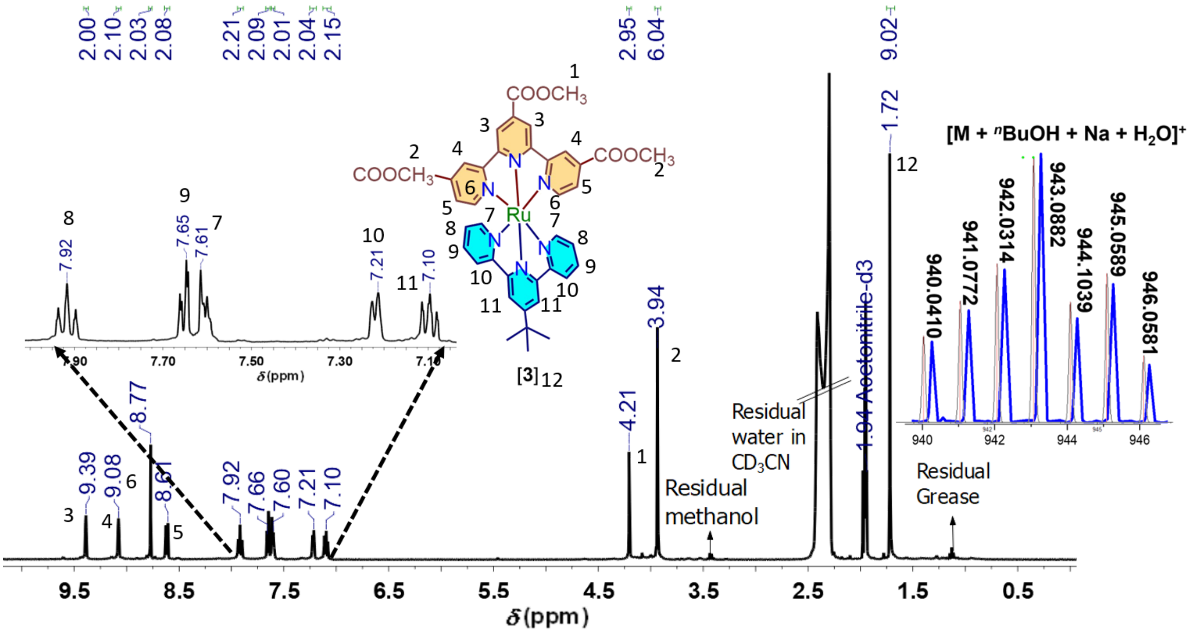

Figure S10. ^{1}H NMR spectrum and HRMS data of [**3**] in CD_3CN, 400.00 MHz.

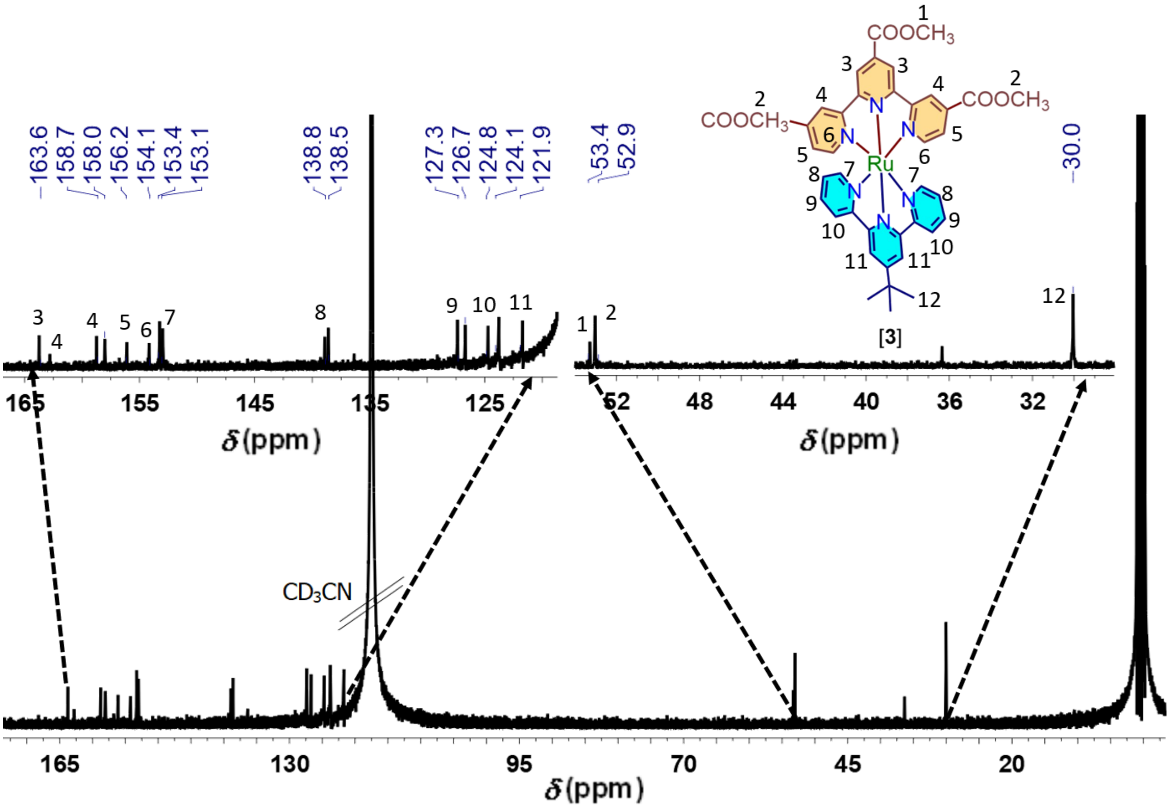

Figure S11. ^{13}C NMR spectrum of [**3**] in CD_3CN, 100.61 MHz.

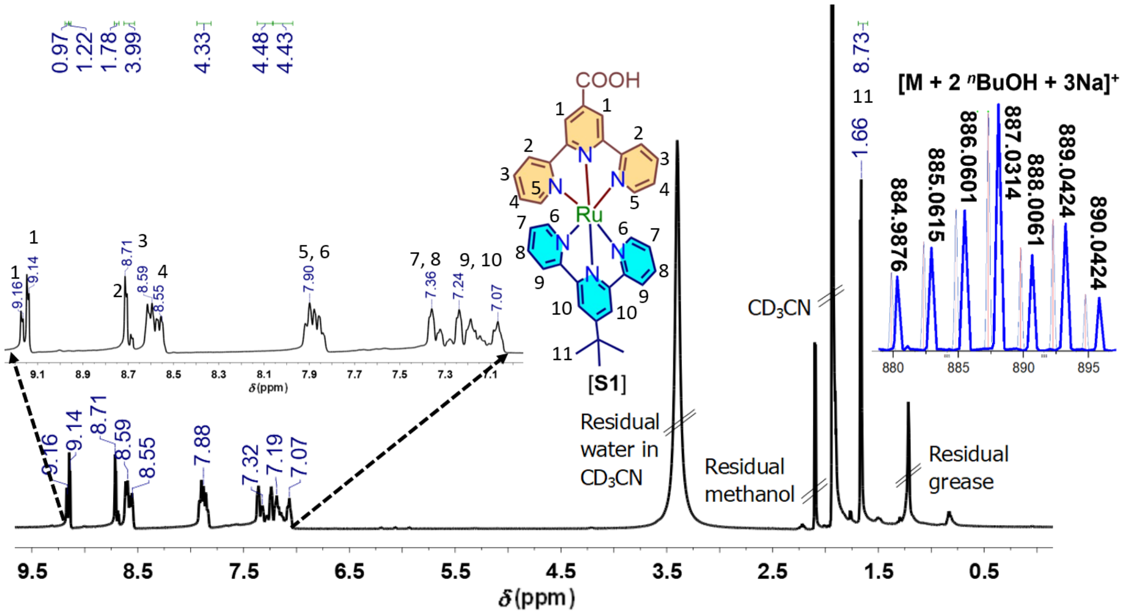

Figure S12. ^{1}H NMR spectrum and HRMS data of [**S1**] in CD_3CN, 400.00 MHz.

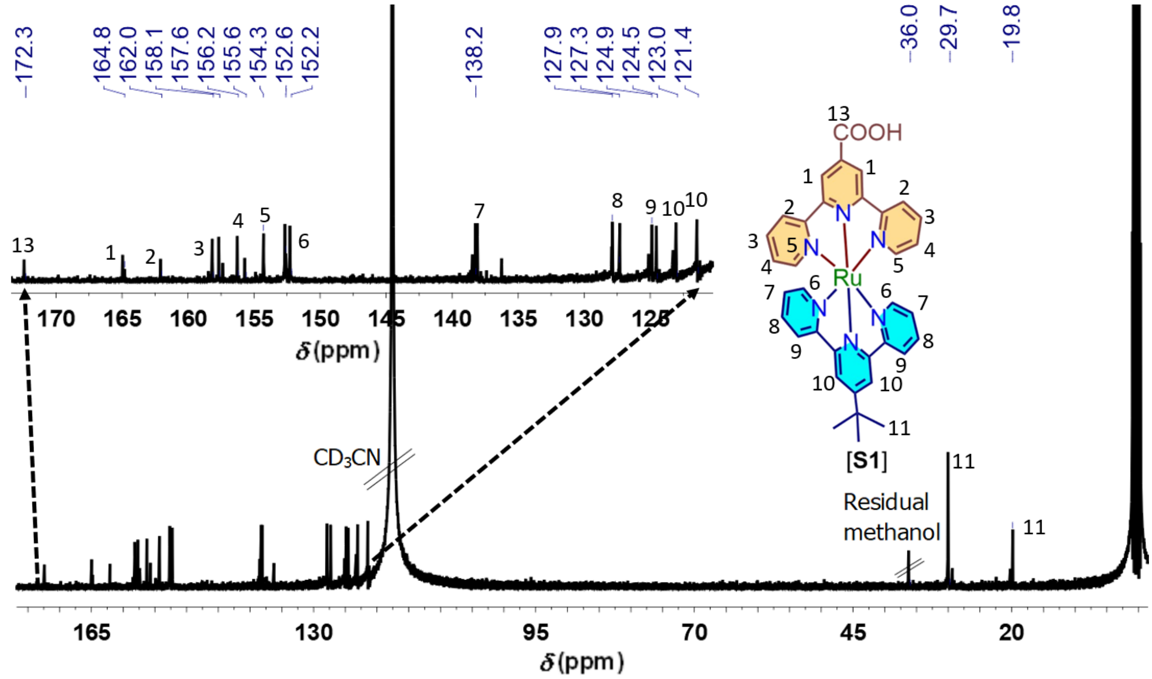

Figure S13. ^{13}C NMR spectrum of [**S1**] in CD_3CN, 100.61 MHz.

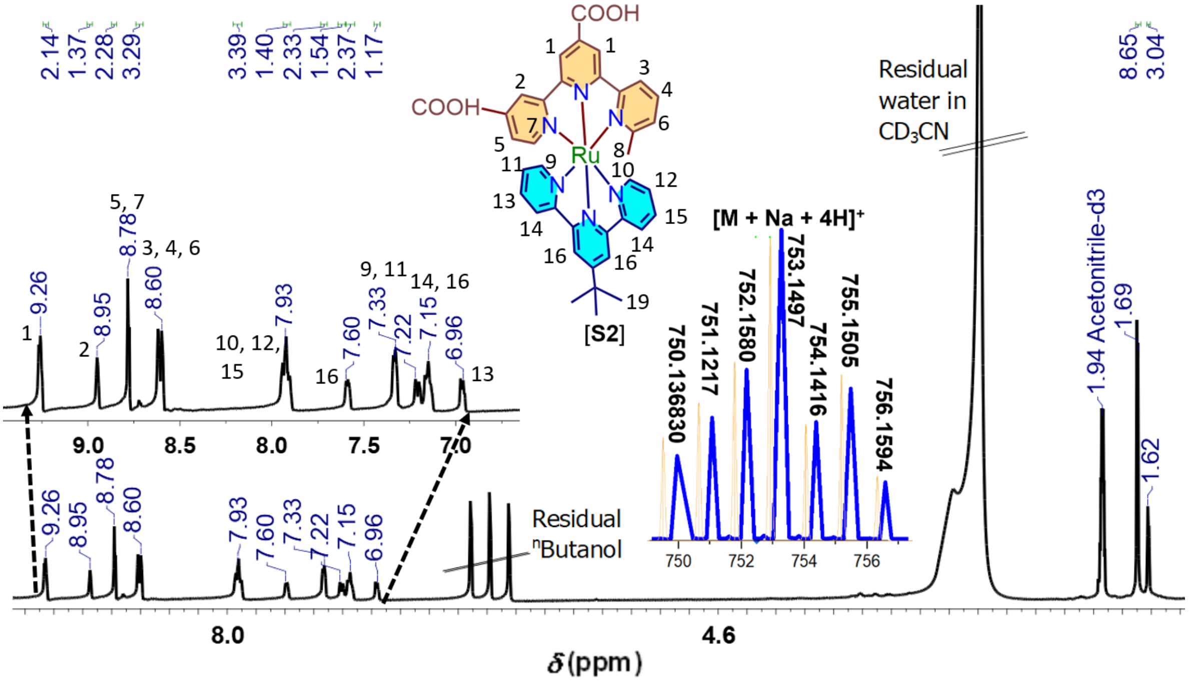

Figure S14. ^{1}H NMR spectrum and HRMS data of [**S2**] in CD_3CN, 400.00 MHz.

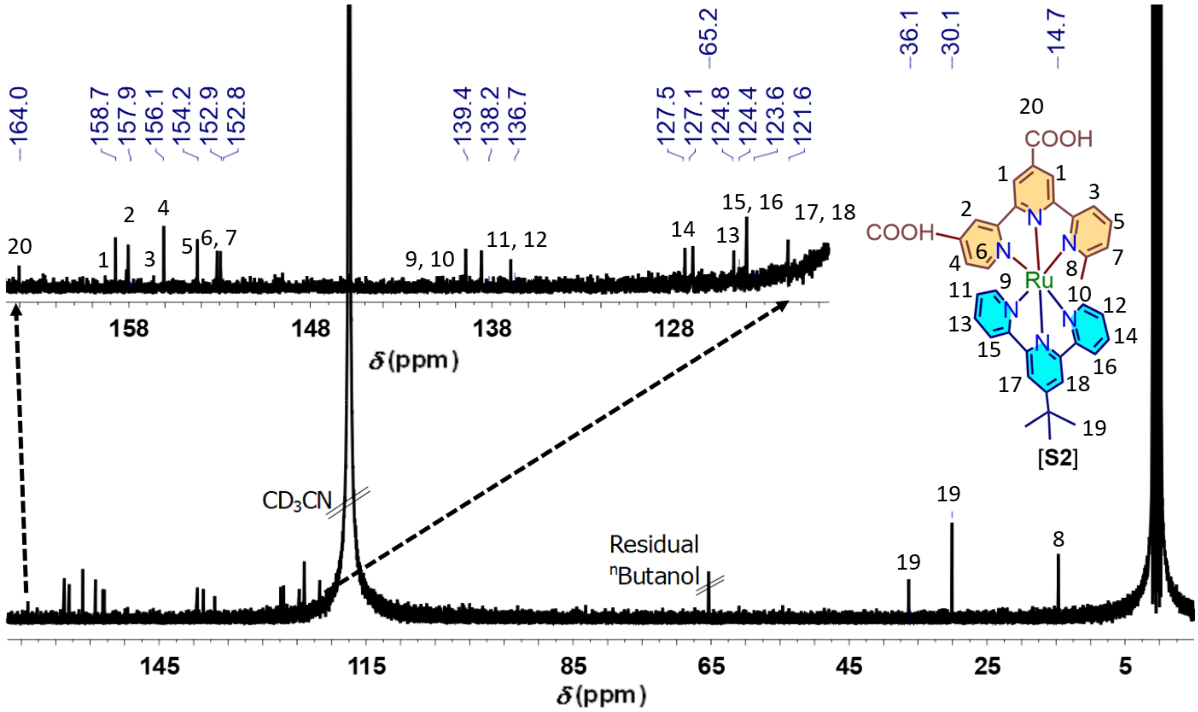

Figure S15. ^{13}C NMR spectrum of [**S2**] in CD_3CN, 100.61 MHz.

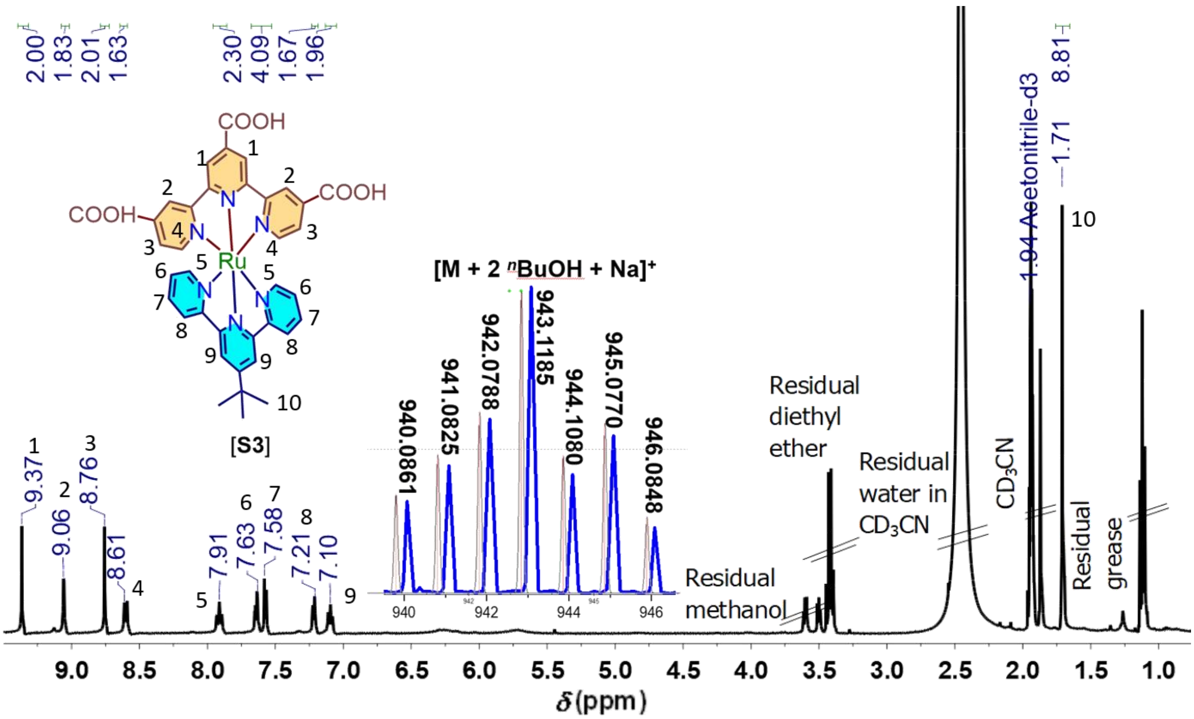

Figure S16. ^{1}H NMR spectrum and HRMS data of [**S3**] in CD_3CN, 400.00 MHz.

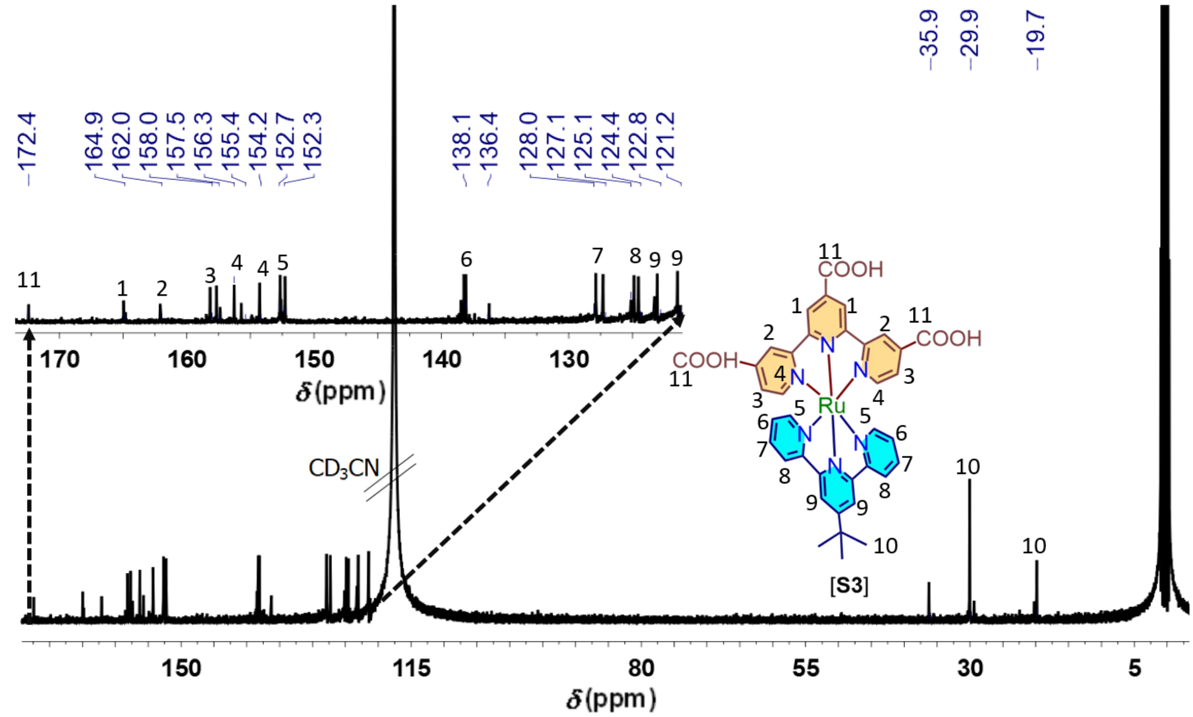

Figure S17. ^{13}C NMR spectrum of [**S3**] in CD_3CN, 100.61 MHz.

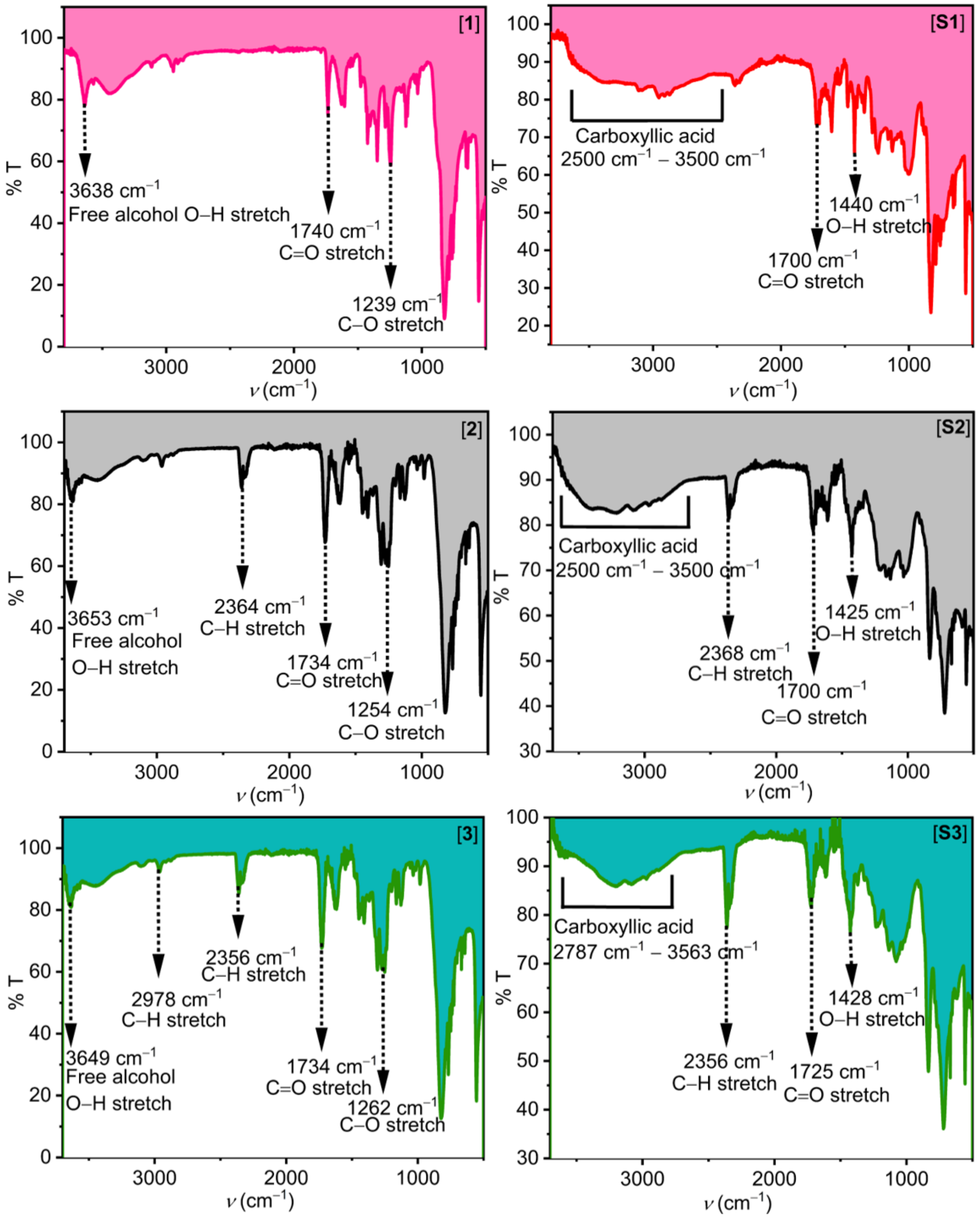

Figure S18. FTIR spectra of ester [**1**] – [**3**] and acid [**S1**] – [**S3**] complexes.

Table S1

Electron transfer between [Tpy^2–Ru^{II}] and [tpy^1] fragments of [**S1**] – [**S3**] obtained from the charge displacement analysis.

[**S1**]				[**S2**]				[**S3**]			
σ-interaction											
ρ_1		ρ_5		ρ_1		ρ_4		ρ_1		ρ_4	
N(sp^2) → Ru(d_{z2})		N(sp^2) → Ru($d_{x2\text{-}y2}$)		N(sp^2) → Ru(d_{z2})		N(sp^2) → Ru($d_{x2\text{-}y2}$)		N(sp^2) → Ru(d_{z2})		N(sp^2) → Ru($d_{x2\text{-}y2}$)	
Ru – N^{1a}	Ru – N$^{1b,b'}$	Ru – N^{1a}	Ru – N$^{1b,b'}$	Ru – N^{1a}	Ru – N$^{1b,b'}$	Ru – N^{1a}	Ru – N$^{1b,b'}$	Ru – N^{1a}	Ru – N$^{1b,b'}$	Ru – N^{1a}	Ru – N$^{1b,b'}$
0.271	0.206	0.207	0.318	0.265	0.203	0.190	0.300	0.273	0.205	0.124	0.238
π-interaction											
ρ_2: Ru(d_{yz}) → N(π_y)											
0.300				0.277				0.292			

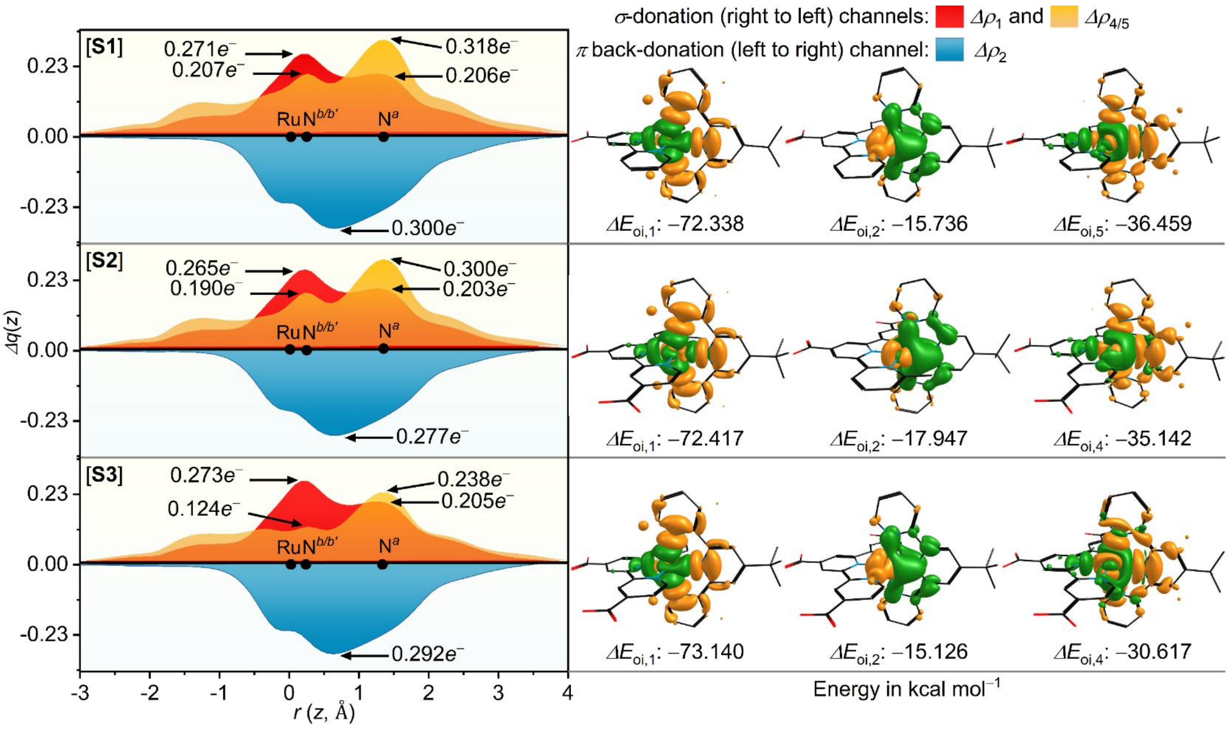

Figure S19. Charge displacement curves and natural orbitals for chemical valence (NOCV)-deformation density isosurfaces of contour 0.001. Orbital interaction (oi) energies (ΔE_{oi}, kcal mol^{-1}) relative to NOCV pair, $\Delta\rho_i$ (i = 1, 2 and 4/5) contribution of fragments [tpy^A–Ru(**II**)]$\cdots$tpy^D of [**S1**] – [**S3**].

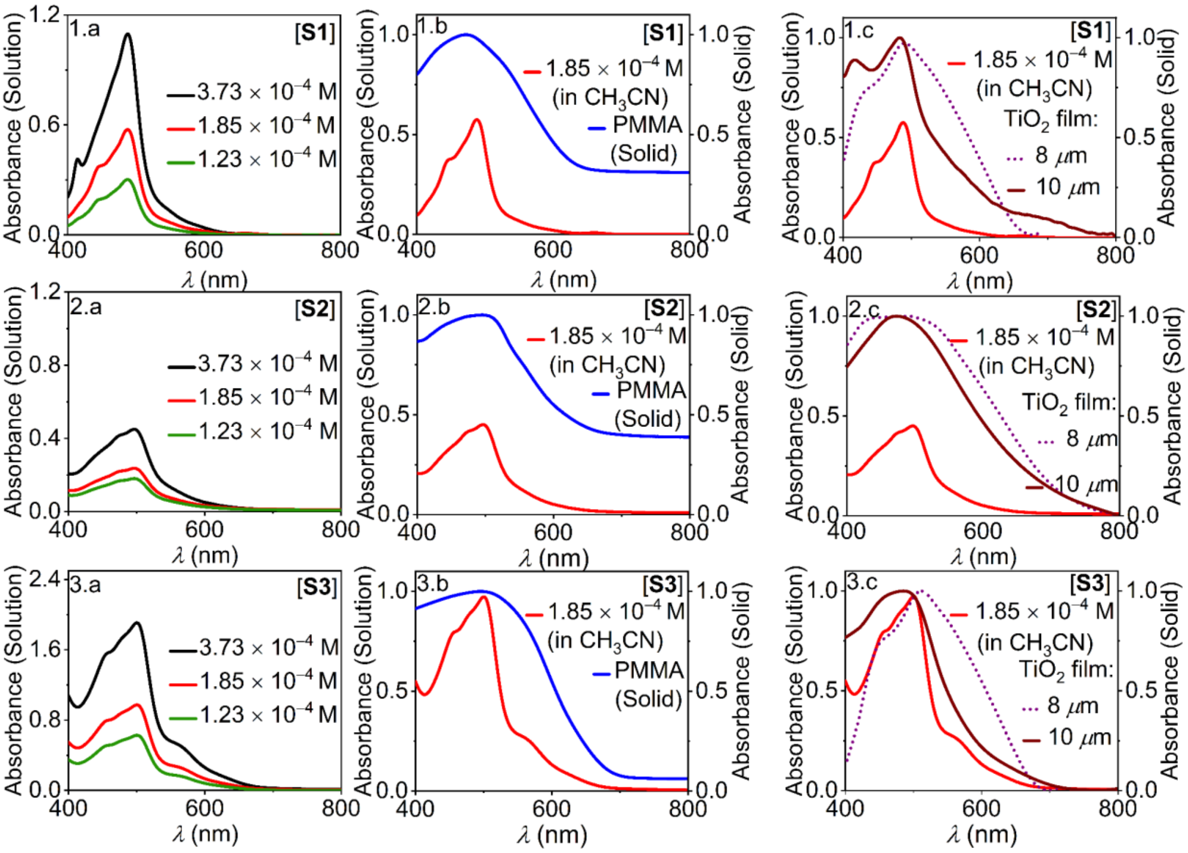

Figure S20. (a) Absorbance of [**S1**] – [**S3**] measured in acetonitrile solution and solid state.

All complexes show ^{1}MLLCT excitations in acetonitrile solution and in dye-TiO_2/PMMA assemblies where, PMMA refers to polymethyl methacrylate.

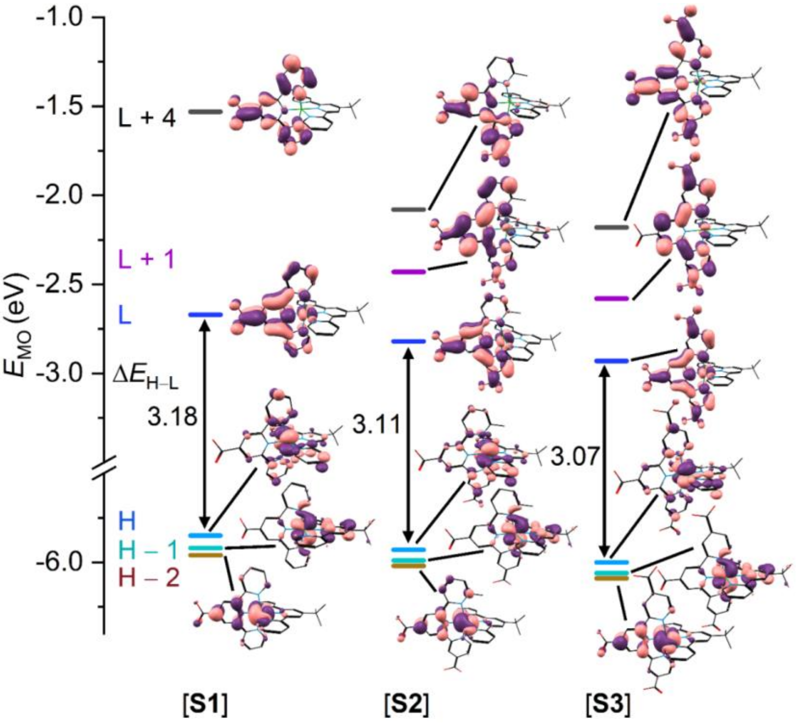

Figure S20. (b) Doubly-occupied/unoccupied *Kohn-Sham* molecular orbitals (contour: 0.03) of complexes [**S1**] – [**S3**] in the acetonitrile (SMD) phase.

Table S2

TDDFT transition energies (in nm) along with oscillator strengths (f), orbital contributions and excitation character of the selected visible-light transitions (including those with $f > 0.02$) charge transfer (CT) excitations of complexes [**S1**] – [**S3**] in the acetronitrile (SMD) phase. The HOMO and LUMO orbitals are represented by abbreviations H and L, respectively.

(a) [**S1**]

Excited State	λ (nm)	Oscillator strength (f)	Excitation (Maximum orbital contribution)	Atom/Ligand %										Excitation character
				From					To					
				COOH^a	$\text{Tpy}_{acceptor}$	Ru	tpy_{donor}	^{t}Bu	COOH^a	$\text{Tpy}_{acceptor}$	Ru	tpy_{donor}	^{t}Bu	
S_1	549.86	0.000	H → L (98%)	–	16	68	16	–	10	78	11	02	–	^{1}MLLCT
S_4	467.67	0.021	H – 2 → L (52%)	02	22	69	08	–	10	78	11	02	–	^{1}MLLCT
			H → L + 2 (30%)	–	16	68	16	–	–	77	01	21	–	^{1}MLLCT
S_{16}	330.56	0.027	H – 2 → L + 4 (34%)	02	22	69	08	–	15	85	–	–	–	^{1}MLLCT
			H → L + 5 (46%)	–	16	68	16	–	–	50	–	50	–	^{1}MLLCT
			H – 1 → L + 5 (14%)	–	08	71	20	01	–	50	–	50	–	^{1}MLLCT
S_{29}	300.51	0.024	H – 3 → L + 1 (51%)	–	07	01	92	–	–	09	07	84	01	^{1}ILCT/^{1}LLCT
			H – 4 → L + 1 (20%)	–	92	02	06	–	–	09	07	84	01	^{1}LLCT
			H → L + 6 (12%)	–	16	68	16	–	–	–	01	99	–	^{1}MLLCT
S_{32}	295.67	0.030	H – 4 → L + 1 (69%)	–	92	02	06	–	–	09	07	84	01	^{1}LLCT
			H – 3 → L + 1 (11%)	–	07	01	92	–	–	09	07	84	01	^{1}ILCT/^{1}LLCT
S_{34}	292.66	0.020	H – 2 → L + 10 (73%)	02	22	69	08	–	–	16	65	19	–	^{1}MC
			H – 2 → L + 13 (14%)	02	22	69	08	–	–	22	59	18	–	^{1}MC
S_{38}	272.39	0.025	H – 4 → L + 2 (38%)	–	92	02	06	–	–	77	01	21	–	^{1}ILCT/^{1}LLCT
			H – 6 → L (25%)	–	98	02	01	–	10	78	11	02	–	^{1}ILCT/^{1}LLCT
			H – 4 → L + 3 (23%)	–	92	02	06	–	–	14	03	83	01	^{1}LLCT
S_{40}	269.65	0.052	H – 3 → L + 3 (42%)	–	07	01	92	–	–	14	03	83	01	^{1}ILCT/^{1}LLCT
			H → L + 8 (25%)	–	16	68	16	–	–	46	07	47	–	^{1}MLLCT
S_{45}	256.69	0.038	H – 6 → L (65%)	–	98	02	01	–	10	78	11	02	–	^{1}ILCT/^{1}LLCT
			H – 4 → L + 2 (14%)	–	92	02	06	–	–	77	01	21	–	^{1}ILCT/^{1}LLCT

(b) [**S2**]

Excited State	λ (nm)	Oscillator strength (f)	Excitation (Maximum orbital contribution)	Atom/Ligand %										Excitation character
				From					To					
				$\text{COOH}^{a\|b}$	$\text{Tpy}_{acceptor}$	Ru	tpy_{donor}	^{t}Bu	$\text{COOH}^{a\|b}$	$\text{Tpy}_{acceptor}$	Ru	tpy_{donor}	^{t}Bu	
S_1	556.90	0.000	H → L (46%)	–|01	16	66	16	–	05|06	77	10	02	–	^{1}MLLCT
			H – 1 → L (43%)	–	08	71	20	01	05|06	77	10	02	–	^{1}MLLCT
S_3	485.58	0.015	H – 2 → L (52%)	01|–	20	70	08	–	05|06	77	10	02	–	^{1}MLLCT
			H → L (14%)	–|01	16	66	16	–	05|06	77	10	02	–	^{1}MLLCT
			H → L + 1 (14%)	–|01	16	66	16	–	03|03	85	03	07	–	^{1}MLLCT
S_{32}	296.95	0.034	H – 1 → L + 8 (42%)	–	08	71	20	01	04|–	90	02	05	–	^{1}MLLCT
			H – 3 → L + 2 (26%)	–	02	02	96	–	–	02	07	89	01	^{1}ILCT/^{1}LLCT
			H → L + 6 (12%)	–|01	16	66	16	–	–	–	01	99	–	^{1}MLLCT
S_{43}	271.45	0.022	H – 3 → L + 3 (47%)	–	02	02	96	–	0|01	08	03	87	01	^{1}ILCT/^{1}LLCT
			H → L + 7 (12%)	–|01	16	66	16	–	04|01	20	04	71	–	^{1}MLLCT
	264.26	0.057	H – 5 → L (38%)	–|01	95	02	03	–	05|06	77	10	02	–	^{1}ILCT/^{1}LLCT

S_{46}			H – 4 → L + 4 (20%)	–	97	02	01	–	06|13	76	–	05	–	^{1}ILCT/^{1}LLCT
			H – 4 → L + 1 (15%)	–	97	02	01	–	03|03	85	03	07	–	^{1}ILCT/^{1}LLCT
S_{50}	253.45	0.028	H – 5 → L + 1 (86%)	–|01	95	02	03	–	03|03	85	03	07	–	^{1}ILCT/^{1}LLCT

*Subscripts *a* and *b* for carboxylic acid corresponds to its linkage to the central and peripheral pyridine rings of terpyridine (tpy$_{acceptor}$).

(c) [**S3**]

				Atom/Ligand %										
				From					To					
Excited State	λ (nm)	Oscillator strength (f)	Excitation (Maximum orbital contribution)	COOH$^{a\|b\|}_{b'}$	Tpy$_{acceptor}$	Ru	tpy$_{donor}$	^{t}Bu	COOH$^{a\|b\|}_{b'}$	Tpy$_{acceptor}$	Ru	tpy$_{donor}$	^{t}Bu	Excitation character
S_1	570.32	0.001	H → L (49%)	–|01|01	16	66	17	–	04|04|04	76	10	02	–	^{1}MLLCT
			H – 1 → L (48%)	–	07	71	20	01	04|04|04	76	10	02	–	^{1}MLLCT
S_3	495.71	0.013	H – 2 → L (62%)	02|–|–	22	69	08	–	04|04|04	76	10	02	–	^{1}MLLCT
			H → L + 1 (33%)	–|01|01	16	66	17	–	–|04|04	86	03	04	–	^{1}MLLCT
S_8	436.27	0.037	H – 1 → L + 2 (44%)	–	07	71	20	01	–	01	07	91	01	^{1}MLLCT
			H → L + 1 (38%)	–|01|01	16	66	17	–	–|04|04	86	03	04	–	^{1}MLLCT
			H – 2 → L (11%)	02|–|–	22	69	08	–	04|04|04	76	10	02	–	^{1}MLLCT
S_{13}	384.92	0.020	H → L + 4 (85%)	–|01|01	16	66	17	–	12|07|07	72	01	–	–	^{1}MLLCT
S_{20}	327.07	0.048	H – 4 → L (84%)	–	95	02	03	–	04|04|04	76	10	02	–	^{1}ILCT/^{1}LLCT
S_{30}	301.49	0.025	H – 2 → L + 7 (86%)	02|–|–	22	69	08	–	14|–|–	84	01	–	–	^{1}MLLCT
S_{31}	297.47	0.036	H – 3 → L + 2 (48%)	–	03	02	95	–	–	01	07	91	01	^{1}ILCT/^{1}LLCT
			H → L + 6 (30%)	–|01|01	16	66	17	–	–	–	01	98	–	^{1}MLLCT
S_{32}	292.86	0.032	H – 2 → L + 10 (73%)	02|–|–	22	69	08	–	–	15	64	21	–	^{1}MC
			H – 2 → L + 14 (10%)	02|–|–	22	69	08	–	–	23	59	17	–	^{1}MC
S_{44}	271.33	0.031	H – 3 → L + 3 (54%)	–	03	02	95	–	–	03	03	93	01	^{1}ILCT/^{1}LLCT
			H – 4 → L + 3 (15%)	–	95	02	03	–	–	03	03	93	01	^{1}LLCT
			H → L + 8 (13%)	–|01|01	16	66	17	–	–|01|01	03	04	92	–	^{1}MLLCT

*Subscripts *a*, *b* and *b’* for carboxylic acid corresponds to its linkage to the central and peripheral pyridine rings of terpyridine (tpy$_{acceptor}$).

Table S3

Electron density difference maps (EDDMs, contour: 0.001) of complexes [**S1**] – [**S3**] depicting relevant singlet electronic excitations in the UV-Visible range in the acetonitrile (SMD) phase. The charge flows from the blue to orange region.

	[**S1**]	
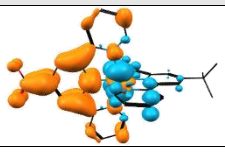	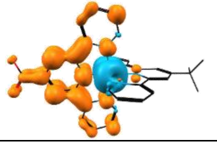	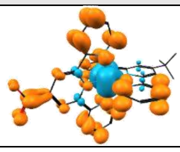
$S_0 \rightarrow S_1$ (549.9 nm, f = 4.8E – 05)	$S_0 \rightarrow S_4$ (467.7 nm, f = 0.021)	$S_0 \rightarrow S_{16}$ (330.6 nm, f = 0.027)
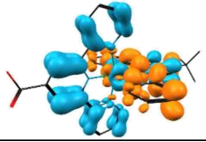	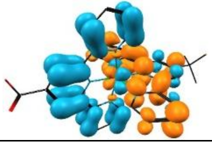	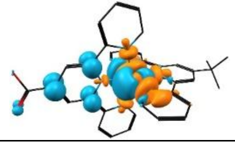
$S_0 \rightarrow S_{29}$ (300.5 nm, f = 0.024)	$S_0 \rightarrow S_{32}$ (295.7 nm, f = 0.030)	$S_0 \rightarrow S_{34}$ (292.7 nm, f = 0.020)

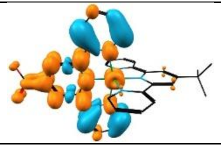

$S_0 \rightarrow S_{38}$ (272.4 nm, *f* = 0.025)

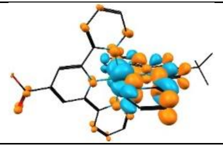

$S_0 \rightarrow S_{40}$ (269.6 nm, *f* = 0.052)

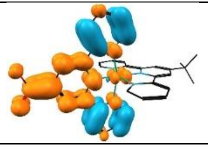

$S_0 \rightarrow S_{45}$ (256.7 nm, *f* = 0.038)

[**S2**]

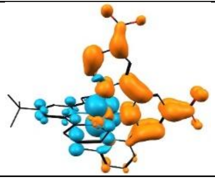

$S_0 \rightarrow S_1$ (556.9 nm, *f* = 3.2E – 04)

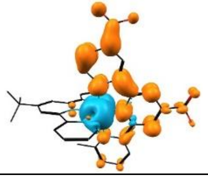

$S_0 \rightarrow S_3$ (485.6 nm, *f* = 0.015)

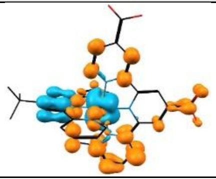

$S_0 \rightarrow S_{32}$ (296.9 nm, *f* = 0.034)

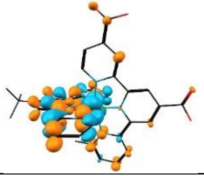

$S_0 \rightarrow S_{43}$ (271.4 nm, *f* = 0.022)

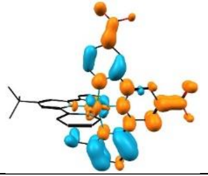

$S_0 \rightarrow S_{46}$ (264.3 nm, *f* = 0.057)

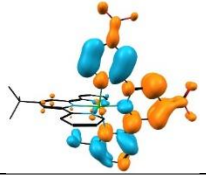

$S_0 \rightarrow S_{50}$ (253.4 nm, *f* = 0.028)

[**S3**]

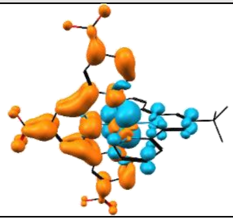

$S_0 \rightarrow S_1$ (570.3 nm, *f* = 0.001)

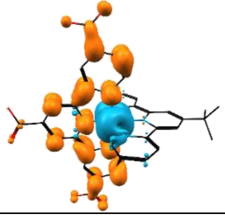

$S_0 \rightarrow S_3$ (495.7 nm, *f* = 0.013)

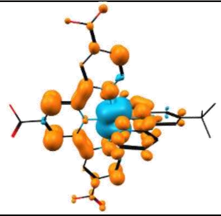

$S_0 \rightarrow S_8$ (436.3 nm, *f* = 0.037)

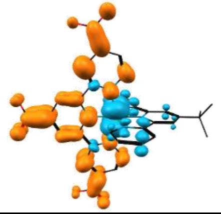

$S_0 \rightarrow S_{13}$ (384.9 nm, *f* = 0.020)

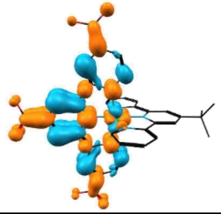

$S_0 \rightarrow S_{20}$ (327.1 nm, *f* = 0.048)

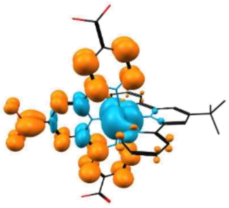

$S_0 \rightarrow S_{30}$ (301.5 nm, *f* = 0.025)

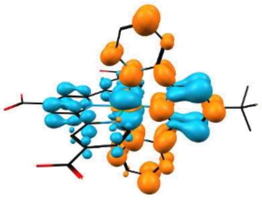

$S_0 \rightarrow S_{31}$ (297.5 nm, *f* = 0.036)

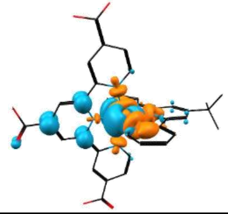

$S_0 \rightarrow S_{32}$ (292.2 nm, *f* = 0.032)

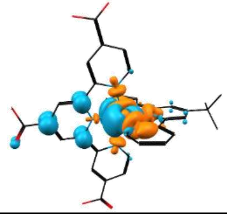

$S_0 \rightarrow S_{44}$ (271.3 nm, *f* = 0.031)

Table S4

Inter-fragment charge transfer (IFCT) analysis of relevant excitations of [**S1**] in the acetonitrile (SMD) phase. Electron transfer greater than value of 0.05 are highlighted in the following tables.

(a) S_1 state

[**S1**]		Acceptor								
Donor			Tpy^2				Tpy^1			
		COOH	Py^{2a}	Py^{2b}	Py$^{2b'}$	Ru	Py^{1a}	Py^{1b}	Py$^{1b'}$	^{t}Bu
COOH		–	–	–	–	–	–	–	–	–
Tpy^2	Py^{2a}	–	–	–	–	–	–	–	–	–
	Py^{2b}	–	0.03	–	–	–	–	–	–	–
	Py$^{2b'}$	–	0.03	–	–	–	–	–	–	–
Ru		0.06	0.33	0.09	0.09	–	–	–	–	–

Tpy^1	Py^{1a}	–	0.01	–	–	–	–	–	–	–
	Py^{1b}	–	0.03	–	–	–	–	–	–	–
	Py$^{1b'}$	–	0.03	–	0.01	–	–	–	–	–
^{t}Bu		–	–	–	–	–	–	–	–	–

(b) S_4 state

[**S1**]		Acceptor								
Donor			Tpy^2				Tpy^1			
		COOH	Py^{2a}	Py^{2b}	Py$^{2b'}$	Ru	Py^{1a}	Py^{1b}	Py$^{1b'}$	^{t}Bu
COOH		–	–	–	–	–	–	–	–	–
Tpy^2	Py^{2a}	–	–	0.01	–	–	–	–	–	–
	Py^{2b}	–	0.01	–	–	–	–	–	–	–
	Py$^{2b'}$	–	0.01	–	–	–	–	–	–	–
Ru		0.03	0.32	0.11	0.11	–	–	0.02	0.01	–
Tpy^1	Py^{1a}	–	–	–	–	–	–	–	–	–
	Py^{1b}	–	–	–	–	–	–	–	–	–
	Py$^{1b'}$	–	–	–	–	–	–	–	–	–
^{t}Bu		–	–	–	–	–	–	–	–	–

(c) S_{16} state

[**S1**]		Acceptor								
Donor			Tpy^2				Tpy^1			
		COOH	Py^{2a}	Py^{2b}	Py$^{2b'}$	Ru	Py^{1a}	Py^{1b}	Py$^{1b'}$	^{t}Bu
COOH		–	–	–	–	–	–	–	–	–
Tpy^2	Py^{2a}	–	–	0.01	–	–	–	0.01	0.01	–
	Py^{2b}	–	–	–	–	–	–	–	–	–
	Py$^{2b'}$	–	0.01	0.01	–	–	–	–	–	–
Ru		0.04	–	0.17	0.11	–	–	0.10	0.10	–
Tpy^1	Py^{1a}	–	–	0.01	–	–	–	–	–	–
	Py^{1b}	–	–	–	–	–	–	–	–	–
	Py$^{1b'}$	–	–	0.01	–	–	–	–	–	–
^{t}Bu		–	–	–	–	–	–	–	–	–

(d) S_{29} state

[**S1**]		Acceptor								
Donor			Tpy^2				Tpy^1			
		COOH	Py^{2a}	Py^{2b}	Py$^{2b'}$	Ru	Py^{1a}	Py^{1b}	Py$^{1b'}$	^{t}Bu
COOH		–	–	–	–	–	–	–	–	–
Tpy^2	Py^{2a}	–	–	–	–	–	–	–	–	–
	Py^{2b}	–	–	–	–	–	0.01	0.01	–	–
	Py$^{2b'}$	–	–	–	–	–	0.01	0.01	–	–
Ru		–	–	–	–	–	0.04	0.04	0.03	–
Tpy^1	Py^{1a}	–	–	–	–	0.02	–	0.10	0.08	–
	Py^{1b}	–	–	–	–	0.01	0.06	–	0.05	–
	Py$^{1b'}$	–	–	–	–	0.01	0.06	0.07	–	–
^{t}Bu		–	–	–	–	–	–	–	–	–

(e) S_{32} state

[**S1**]		Acceptor								
Donor			Tpy^2				Tpy^1			
		COOH	Py^{2a}	Py^{2b}	Py$^{2b'}$	Ru	Py^{1a}	Py^{1b}	Py$^{1b'}$	^{t}Bu
COOH		–	–	–	–	–	–	–	–	–
Tpy^2	Py^{2a}	–	–	–	–	0.02	0.12	0.12	0.09	–
	Py^{2b}	–	–	–	–	0.01	0.08	0.08	0.06	–
	Py$^{2b'}$	–	–	–	–	0.01	0.08	0.08	0.08	–
Ru		–	–	–	–	–	0.02	0.04	0.01	–
Tpy^1	Py^{1a}	–	–	–	–	–	–	–	–	–

	Py^{1b}	–	–	–	–	–	–	–	–	–
	Py$^{1b'}$	–	–	–	–	–	–	–	–	–
^{t}Bu		–	–	–	–	–	–	–	–	–

(f) S$_{34}$ state

[**S1**]		Acceptor								
Donor			Tpy^{2}				Tpy^{1}			
		COOH	Py^{2a}	Py^{2b}	Py$^{2b'}$	Ru	Py^{1a}	Py^{1b}	Py$^{1b'}$	^{t}Bu
COOH		–	–	–	–	–	–	–	–	–
Tpy^{2}	Py^{2a}	–	–	0.01	0.01	0.08	–	–	–	–
	Py^{2b}	–	–	–	–	0.01	–	–	–	–
	Py$^{2b'}$	–	–	–	–	0.01	–	–	–	–
Ru		–	0.01	0.08	0.07	–	–	0.03	0.03	–
Tpy^{1}	Py^{1a}	–	–	–	–	0.01	–	–	–	–
	Py^{1b}	–	–	–	–	0.02	–	–	–	–
	Py$^{1b'}$	–	–	–	–	0.02	–	–	–	–
^{t}Bu		–	–	–	–	–	–	–	–	–

(g) S$_{38}$ state

[**S1**]		Acceptor								
Donor			Tpy^{2}				Tpy^{1}			
		COOH	Py^{2a}	Py^{2b}	Py$^{2b'}$	Ru	Py^{1a}	Py^{1b}	Py$^{1b'}$	^{t}Bu
COOH		–	–	–	–	–	–	–	–	–
Tpy^{2}	Py^{2a}	–	–	0.04	0.04	0.01	–	–	–	–
	Py^{2b}	–	0.13	–	0.05	0.02	–	–	–	–
	Py$^{2b'}$	–	0.13	–	–	0.02	–	–	–	–
Ru		–	0.01	0.01	–	–	–	–	–	–
Tpy^{1}	Py^{1a}	–	0.02	–	0.01	–	–	–	–	–
	Py^{1b}	–	0.02	–	–	–	–	–	–	–
	Py$^{1b'}$	–	0.02	–	–	–	–	–	–	–
^{t}Bu		–	–	–	–	–	–	–	–	–

(h) S$_{40}$ state

[**S1**]		Acceptor								
Donor			Tpy^{2}				Tpy^{1}			
		COOH	Py^{2a}	Py^{2b}	Py$^{2b'}$	Ru	Py^{1a}	Py^{1b}	Py$^{1b'}$	^{t}Bu
COOH		–	–	–	–	–	–	–	–	–
Tpy^{2}	Py^{2a}	–	–	–	–	–	0.03	0.01	0.02	–
	Py^{2b}	–	–	–	–	–	0.02	0.01	0.01	–
	Py$^{2b'}$	–	–	–	–	–	0.02	0.01	0.01	–
Ru		–	0.01	0.01	0.01	–	0.07	0.04	0.04	–
Tpy^{1}	Py^{1a}	–	–	0.01	0.01	–	–	0.03	0.03	–
	Py^{1b}	–	–	0.01	0.01	–	0.04	–	0.03	–
	Py$^{1b'}$	–	–	0.01	0.01	–	0.04	0.02	–	–
^{t}Bu		–	–	–	–	–	–	–	–	–

(i) S$_{45}$ state

[**S1**]		Acceptor								
Donor			Tpy^{2}				Tpy^{1}			
		COOH	Py^{2a}	Py^{2b}	Py$^{2b'}$	Ru	Py^{1a}	Py^{1b}	Py$^{1b'}$	^{t}Bu
COOH		–	–	–	–	–	–	–	–	–
Tpy^{2}	Py^{2a}	–	–	0.02	0.02	0.01	–	–	–	–
	Py^{2b}	0.02	0.18	–	0.06	0.03	–	–	–	–
	Py$^{2b'}$	0.02	0.18	0.06	–	0.03	–	–	–	–
Ru		–	0.01	–	–	–	–	–	–	–
Tpy^{1}	Py^{1a}	–	–	–	–	–	–	–	–	–
	Py^{1b}	–	–	–	–	–	–	–	–	–

Py$^{1b'}$	–	–	–	–	–	–	–	–	–
^{t}Bu	–	–	–	–	–	–	–	–	–

Table S5

Inter-fragment charge transfer (IFCT) analysis of relevant excitations of [**S2**] in the acetonitrile (SMD) phase. Electron transfer greater than value of 0.05 are highlighted in the following tables.

a) S$_1$ state

[**S2**]		Acceptor									
Donor			Tpy^{2}					Tpy^{1}			
		COOH^{2a}	COOH^{2b}	Py^{2a}	Py^{2b}	Py$^{2b'}$	Ru	Py^{1a}	Py^{1b}	Py$^{1b'}$	^{t}Bu
COOH^{2a}		–	–	–	–	–	–	–	–	–	–
COOH^{2b}		–	–	–	–	–	–	–	–	–	–
Tpy^{2}	Py^{2a}	–	–	–	–	–	–	–	–	–	–
	Py^{2b}	–	–	0.01	–	–	–	–	–	–	–
	Py$^{2b'}$	0.01	0.03	0.01	0.01	–	–	–	–	–	–
Ru		–	–	0.24	0.22	0.06	–	–	–	–	–
Tpy^{1}	Py^{1a}	–	–	0.02	0.01	–	–	–	–	–	–
	Py^{1b}	–	–	0.01	–	–	–	–	–	–	–
	Py$^{1b'}$	–	–	0.02	0.02	–	–	–	–	–	–
^{t}Bu		–	–	–	–	–	–	–	–	–	–

b) S$_3$ state

[**S2**]		Acceptor									
Donor			Tpy^{2}					Tpy^{1}			
		COOH^{2a}	COOH^{2b}	Py^{2a}	Py^{2b}	Py$^{2b'}$	Ru	Py^{1a}	Py^{1b}	Py$^{1b'}$	^{t}Bu
COOH^{2a}		–	–	–	–	–	–	–	–	–	–
COOH^{2b}		–	–	–	–	–	–	–	–	–	–
Tpy^{2}	Py^{2a}	–	–	–	0.03	0.01	–	–	–	–	–
	Py^{2b}	–	–	0.01	–	–	–	–	–	–	–
	Py$^{2b'}$	–	–	0.01	0.01	–	–	–	–	–	–
Ru		0.02	0.03	0.23	0.21	0.06	–	0.01	0.02	0.01	–
Tpy^{1}	Py^{1a}	–	–	–	–	–	–	–	–	–	–
	Py^{1b}	–	–	0.01	0.01	–	–	–	–	–	–
	Py$^{1b'}$	–	–	0.01	0.02	–	–	–	–	–	–
^{t}Bu		–	–	–	–	–	–	–	–	–	–

c) S$_{32}$ state

[**S2**]		Acceptor									
Donor			Tpy^{2}					Tpy^{1}			
		COOH^{2a}	COOH^{2b}	Py^{2a}	Py^{2b}	Py$^{2b'}$	Ru	Py^{1a}	Py^{1b}	Py$^{1b'}$	^{t}Bu
COOH^{2a}		–	–	–	–	–	–	–	–	–	–
COOH^{2b}		–	–	–	–	–	–	–	–	–	–
Tpy^{2}	Py^{2a}	–	–	–	–	–	–	–	–	–	–
	Py^{2b}	–	–	–	–	–	–	–	–	–	–
	Py$^{2b'}$	–	–	–	–	–	–	–	–	–	–
Ru		0.02	–	0.02	0.07	0.13	–	–	0.07	0.06	–
Tpy^{1}	Py^{1a}	–	–	–	0.02	0.04	0.01	–	0.02	0.02	–
	Py^{1b}	–	–	–	0.01	0.02	–	–	–	0.01	–
	Py$^{1b'}$	–	–	–	0.01	0.02	–	–	0.01	–	–
^{t}Bu		–	–	–	–	–	–	–	–	–	–

d) S$_{43}$ state

[**S2**]		Acceptor									
Donor			Tpy^{2}					Tpy^{1}			
		COOH^{2a}	COOH^{2b}	Py^{2a}	Py^{2b}	Py$^{2b'}$	Ru	Py^{1a}	Py^{1b}	Py$^{1b'}$	^{t}Bu
COOH^{2a}		–	–	–	–	–	–	–	–	–	–
COOH^{2b}		–	–	–	–	–	–	–	–	–	–

Tpy^2	Py^{2a}	–	–	–	–	–	–	–	–	–	–
	Py^{2b}	–	–	–	–	–	–	0.01	–	–	–
	Py$^{2b'}$	–	–	–	–	–	–	0.01	0.01	0.01	–
Ru		–	–	–	–	0.01	–	0.05	0.03	0.04	–
Tpy^1	Py^{1a}	–	–	0.01	0.01	0.02	–	–	0.05	0.07	–
	Py^{1b}	–	–	0.01	–	0.01	–	0.05	–	0.04	–
	Py$^{1b'}$	–	–	0.01	–	0.02	–	0.06	0.03	–	–
^{t}Bu		–	–	–	–	–	–	–	–	–	–

e) S_{46} state

[**S2**]		Acceptor									
Donor				Tpy^2				Tpy^1			
		COOH^{2a}	COOH^{2b}	Py^{2a}	Py^{2b}	Py$^{2b'}$	Ru	Py^{1a}	Py^{1b}	Py$^{1b'}$	^{t}Bu
COOH^{2a}		–	–	–	–	–	–	–	–	–	–
COOH^{2b}		–	–	–	–	–	–	–	–	–	–
Tpy^2	Py^{2a}	–	–	–	0.04	0.03	0.01	–	–	–	–
	Py^{2b}	–	–	–	–	0.04	0.02	–	–	–	–
	Py$^{2b'}$	0.01	0.01	0.10	0.09	–	0.03	–	–	–	–
Ru		–	–	0.02	0.01	0.01	–	–	–	–	–
Tpy^1	Py^{1a}	–	–	0.01	–	–	–	–	–	–	–
	Py^{1b}	–	–	–	–	–	–	–	–	–	–
	Py$^{1b'}$	–	–	0.01	–	–	–	–	–	–	–
^{t}Bu		–	–	–	–	–	–	–	–	–	–

f) S_{50} state

[**S2**]		Acceptor									
Donor				Tpy^2				Tpy^1			
		COOH^{2a}	COOH^{2b}	Py^{2a}	Py^{2b}	Py$^{2b'}$	Ru	Py^{1a}	Py^{1b}	Py$^{1b'}$	^{t}Bu
COOH^{2a}		–	–	–	–	–	–	–	–	–	–
COOH^{2b}		–	–	–	–	–	–	–	–	–	–
Tpy^2	Py^{2a}	–	–	–	0.02	–	0.01	–	–	–	–
	Py^{2b}	0.01	0.01	0.20	–	0.06	–	–	–	–	–
	Py$^{2b'}$	0.01	0.01	0.16	0.06	–	–	–	–	–	–
Ru		–	–	0.01	–	–	–	–	–	–	–
Tpy^1	Py^{1a}	–	–	–	–	–	–	–	–	–	–
	Py^{1b}	–	–	–	–	–	–	–	–	–	–
	Py$^{1b'}$	–	–	–	–	–	–	–	–	–	–
^{t}Bu		–	–	–	–	–	–	–	–	–	–

Table S6

Inter-fragment charge transfer (IFCT) analysis of relevant excitations of [**S3**] in the acetonitrile (SMD) phase. Electron transfer greater than value of 0.05 are highlighted in the following tables.

(a) S_1 state

[**S3**]		Acceptor										
Donor					Tpy^2				Tpy^1			
		COOH^{2a}	COOH^{2b}	COOH$^{2b'}$	Py^{2a}	Py^{2b}	Py$^{2b'}$	Ru	Py^{1a}	Py^{1b}	Py$^{1b'}$	^{t}Bu
COOH^{2a}		–	–	–	–	–	–	–	–	–	–	–
COOH^{2b}		–	–	–	–	–	–	–	–	–	–	–
COOH$^{2b'}$		–	–	–	–	–	–	–	–	–	–	–
Tpy^2	Py^{2a}	–	–	–	–	–	–	–	–	–	–	–
	Py^{2b}	–	–	–	0.01	–	0.01	–	–	–	–	–
	Py$^{2b'}$	–	–	–	0.01	–	–	–	–	–	–	–
Ru		0.02	0.02	0.02	0.20	0.15	0.16	–	–	–	–	–
Tpy^1	Py^{1a}	–	–	–	0.03	0.02	0.02	0.01	–	–	–	–
	Py^{1b}	–	–	–	–	–	–	–	–	–	–	–
	Py$^{1b'}$	–	–	–	–	0.01	–	–	–	–	–	–
^{t}Bu		–	–	–	–	–	–	–	–	–	–	–

(b) S$_3$ state

[**S1**]		Acceptor										
Donor					Tpy^2				Tpy^1			
		COOH^{2a}	COOH^{2b}	COOH$^{2b'}$	Py^{2a}	Py^{2b}	Py$^{2b'}$	Ru	Py^{1a}	Py^{1b}	Py$^{1b'}$	^{t}Bu
COOH^{2a}		–	–	–	–	–	–	–	–	–	–	–
COOH^{2b}		–	–	–	–	–	–	–	–	–	–	–
COOH$^{2b'}$		–	–	–	–	–	–	–	–	–	–	–
Tpy^2	Py^{2a}	–	–	–	–	0.02	0.02	–	–	–	–	–
	Py^{2b}	–	–	–	0.01	–	0.01	–	–	–	–	–
	Py$^{2b'}$	–	–	–	0.01	0.01	–	–	–	–	–	–
Ru		0.01	0.02	0.02	0.20	0.16	0.16	–	–	–	–	–
Tpy^1	Py^{1a}	–	–	–	–	–	–	–	–	–	–	–
	Py^{1b}	–	–	–	0.01	0.01	0.01	–	–	–	–	–
	Py$^{1b'}$	–	–	–	0.01	0.01	0.01	–	–	–	–	–
^{t}Bu		–	–	–	–	–	–	–	–	–	–	–

(c) S$_8$ state

[**S3**]		Acceptor										
Donor					Tpy^2				Tpy^1			
		COOH^{2a}	COOH^{2b}	COOH$^{2b'}$	Py^{2a}	Py^{2b}	Py$^{2b'}$	Ru	Py^{1a}	Py^{1b}	Py$^{1b'}$	^{t}Bu
COOH^{2a}		–	–	–	–	–	–	–	–	–	–	–
COOH^{2b}		–	–	–	–	–	–	–	–	–	–	–
COOH$^{2b'}$		–	–	–	–	–	–	–	–	–	–	–
Tpy^2	Py^{2a}	–	–	–	–	–	–	–	–	–	–	–
	Py^{2b}	–	–	–	–	–	–	–	–	–	–	–
	Py$^{2b'}$	–	–	–	–	–	–	–	–	–	–	–
Ru		–	0.01	0.01	0.13	0.10	0.10	–	0.11	0.10	0.07	–
Tpy^1	Py^{1a}	–	–	–	0.01	0.01	0.01	–	–	0.01	–	–
	Py^{1b}	–	–	–	–	–	–	–	–	–	–	–
	Py$^{1b'}$	–	–	–	–	–	–	–	–	–	–	–
^{t}Bu		–	–	–	–	–	–	–	–	–	–	–

(d) S$_{13}$ state

[**S3**]		Acceptor										
Donor					Tpy^2				Tpy^1			
		COOH^{2a}	COOH^{2b}	COOH$^{2b'}$	Py^{2a}	Py^{2b}	Py$^{2b'}$	Ru	Py^{1a}	Py^{1b}	Py$^{1b'}$	^{t}Bu
COOH^{2a}		–	–	–	–	–	–	–	–	–	–	–
COOH^{2b}		–	–	–	–	–	–	–	–	–	–	–
COOH$^{2b'}$		–	–	–	–	–	–	–	–	–	–	–
Tpy^2	Py^{2a}	–	–	–	–	0.01	0.01	–	–	–	–	–
	Py^{2b}	–	–	–	0.01	–	0.01	–	–	–	–	–
	Py$^{2b'}$	–	–	–	0.01	0.01	–	–	–	–	–	–
Ru		0.06	0.05	0.05	0.15	0.14	0.15	–	–	–	–	–
Tpy^1	Py^{1a}	–	–	–	–	–	–	–	–	–	–	–
	Py^{1b}	–	–	–	0.01	0.01	0.01	–	–	–	–	–
	Py$^{1b'}$	–	–	–	0.01	0.01	0.01	–	–	–	–	–
^{t}Bu		–	–	–	–	–	–	–	–	–	–	–

(e) S$_{20}$ state

[**S3**]		Acceptor										
Donor					Tpy^2				Tpy^1			
		COOH^{2a}	COOH^{2b}	COOH$^{2b'}$	Py^{2a}	Py^{2b}	Py$^{2b'}$	Ru	Py^{1a}	Py^{1b}	Py$^{1b'}$	^{t}Bu
COOH^{2a}		–	–	–	–	–	–	–	–	–	–	–
COOH^{2b}		–	–	–	–	–	–	–	–	–	–	–
COOH$^{2b'}$		–	–	–	–	–	–	–	–	–	–	–
Tpy^2	Py^{2a}	–	0.01	0.01	–	0.08	0.08	0.03	–	–	–	–
	Py^{2b}	0.01	–	–	0.07	–	0.05	0.02	–	–	–	–

	Py$^{2b'}$	0.01	–	–	0.07	0.05	–	0.02	–	–	–	–
Ru		–	–	–	0.02	0.01	0.01	–	–	–	–	–
Tpy^1	Py^{1a}	–	–	–	–	–	–	–	–	–	–	–
	Py^{1b}	–	–	–	–	–	–	–	–	–	–	–
	Py$^{1b'}$	–	–	–	–	–	–	–	–	–	–	–
^{t}Bu		–	–	–	–	–	–	–	–	–	–	–

(f) S$_{30}$ state

[**S3**]		Acceptor										
Donor					Tpy^2				Tpy^1			
		COOH^{2a}	COOH^{2b}	COOH$^{2b'}$	Py^{2a}	Py^{2b}	Py$^{2b'}$	Ru	Py^{1a}	Py^{1b}	Py$^{1b'}$	^{t}Bu
COOH^{2a}		–	–	–	–	–	–	–	–	–	–	–
COOH^{2b}		–	–	–	–	–	–	–	–	–	–	–
COOH$^{2b'}$		–	–	–	–	–	–	–	–	–	–	–
Tpy^2	Py^{2a}	0.01	–	–	–	0.04	0.04	–	–	–	–	–
	Py^{2b}	–	–	–	0.07	–	0.02	–	–	–	–	–
	Py$^{2b'}$	–	–	–	–	0.01	–	–	–	–	–	–
Ru		0.08	–	–	0.08	0.02	0.02	–	–	0.02	0.02	–
Tpy^1	Py^{1a}	–	–	–	–	–	–	–	–	–	–	–
	Py^{1b}	–	–	–	–	0.01	0.01	–	–	–	–	–
	Py$^{1b'}$	–	–	–	–	0.01	0.01	–	–	–	–	–
^{t}Bu		–	–	–	–	–	–	–	–	–	–	–

(g) S$_{31}$ state

[**S3**]		Acceptor										
Donor					Tpy^2				Tpy^1			
		COOH^{2a}	COOH^{2b}	COOH$^{2b'}$	Py^{2a}	Py^{2b}	Py$^{2b'}$	Ru	Py^{1a}	Py^{1b}	Py$^{1b'}$	^{t}Bu
COOH^{2a}		–	–	–	–	–	–	–	–	–	–	–
COOH^{2b}		–	–	–	–	–	–	–	–	–	–	–
COOH$^{2b'}$		–	–	–	–	–	–	–	–	–	–	–
Tpy^2	Py^{2a}	–	–	–	–	–	–	–	0.02	0.02	0.02	–
	Py^{2b}	–	–	–	–	–	–	–	0.01	0.02	0.01	–
	Py$^{2b'}$	–	–	–	–	–	–	–	0.01	0.02	0.01	–
Ru		–	–	–	–	–	–	–	0.06	0.09	0.08	–
Tpy^1	Py^{1a}	–	–	–	–	–	–	0.01	–	0.08	0.06	–
	Py^{1b}	–	–	–	–	–	–	0.01	0.03	–	0.04	–
	Py$^{1b'}$	–	–	–	–	–	–	0.01	0.03	0.05	–	–
^{t}Bu		–	–	–	–	–	–	–	–	–	–	–

(h) S$_{32}$ state

[**S3**]		Acceptor										
Donor					Tpy^2				Tpy^1			
		COOH^{2a}	COOH^{2b}	COOH$^{2b'}$	Py^{2a}	Py^{2b}	Py$^{2b'}$	Ru	Py^{1a}	Py^{1b}	Py$^{1b'}$	^{t}Bu
COOH^{2a}		–	–	–	–	–	–	–	–	–	–	–
COOH^{2b}		–	–	–	–	–	–	–	–	–	–	–
COOH$^{2b'}$		–	–	–	–	–	–	–	–	–	–	–
Tpy^2	Py^{2a}	–	–	–	–	–	–	0.07	–	0.02	0.01	–
	Py^{2b}	–	–	–	–	–	–	0.01	–	–	–	–
	Py$^{2b'}$	–	–	–	–	–	–	0.01	–	–	–	–
Ru		–	–	–	0.01	0.01	0.01	–	0.03	0.09	0.08	–
Tpy^1	Py^{1a}	–	–	–	–	–	–	0.02	–	–	–	–
	Py^{1b}	–	–	–	–	–	–	0.02	–	–	–	–
	Py$^{1b'}$	–	–	–	–	–	–	0.02	–	–	–	–
^{t}Bu		–	–	–	–	–	–	–	–	–	–	–

(i) S$_{44}$ state

[**S3**]		Acceptor										
Donor		COOH^{2a}				Tpy^2		Ru		Tpy^1		^{t}Bu

			COOH^{2b}	COOH$^{2b'}$	Py^{2a}	Py^{2b}	Py$^{2b'}$		Py^{1a}	Py^{1b}	Py$^{1b'}$	
COOH^{2a}		–	–	–	–	–	–	–	–	–	–	–
COOH^{2b}		–	–	–	–	–	–	–	–	–	–	–
COOH$^{2b'}$		–	–	–	–	–	–	–	–	–	–	–
Tpy^2	Py^{2a}	–	–	–	–	–	–	–	0.01	–	–	–
	Py^{2b}	–	–	–	–	–	–	–	0.02	0.01	0.01	–
	Py$^{2b'}$	–	–	–	–	–	–	–	0.02	0.01	0.01	–
Ru		–	–	–	–	–	–	–	0.04	0.02	0.03	–
Tpy^1	Py^{1a}	–	–	–	–	–	–	0.01	–	0.06	0.08	–
	Py^{1b}	–	–	–	–	–	–	–	0.08	–	0.06	–
	Py$^{1b'}$	–	–	–	–	–	–	–	0.08	0.04	–	–
^{t}Bu		–	–	–	–	–	–	–	–	–	–	–

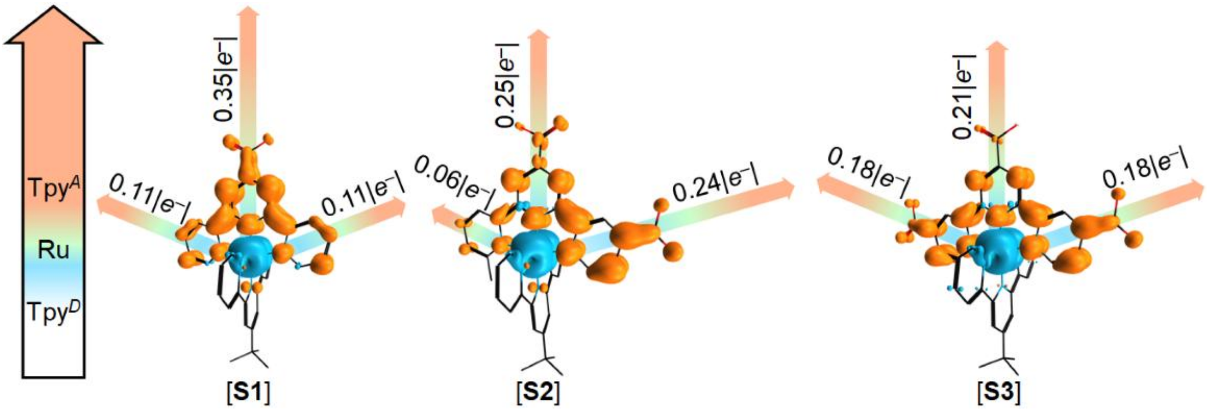

Figure S21. Inter-fragment charge transfer (Ru → tpy^A) along with electron density difference maps (blue and orange regions correspond to charge loss and accumulation).

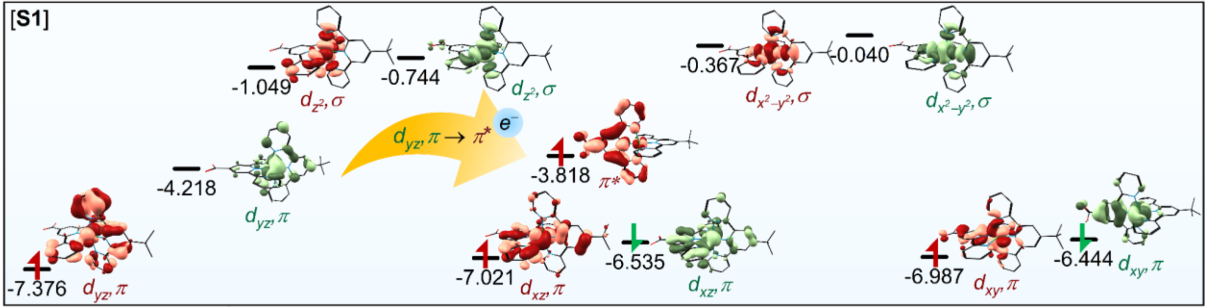

^{3}MLLCT singly occupied and unoccupied molecular orbitals with energy in eV

(a) Ruthenium and ligand-based singly occupied/unoccupied of [**S1**] in its ^{3}MLLCT state.

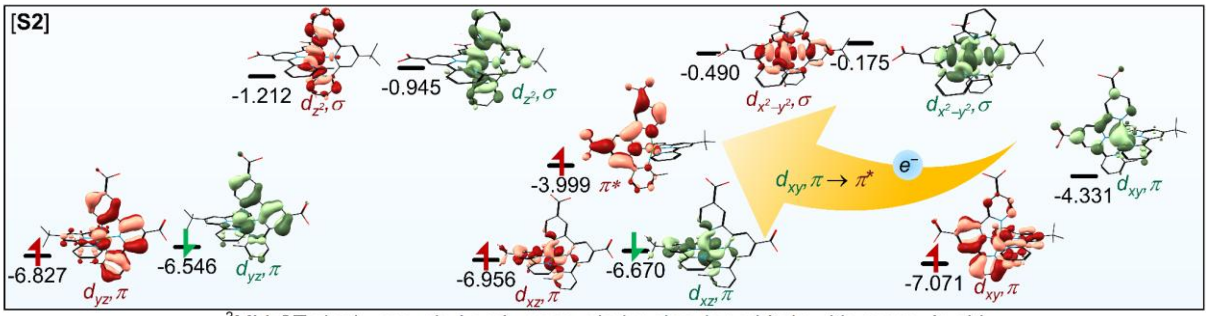

^{3}MLLCT singly occupied and unoccupied molecular orbitals with energy in eV

(b) Ruthenium and ligand-based singly occupied/unoccupied of [**S2**] in its ^{3}MLLCT state.

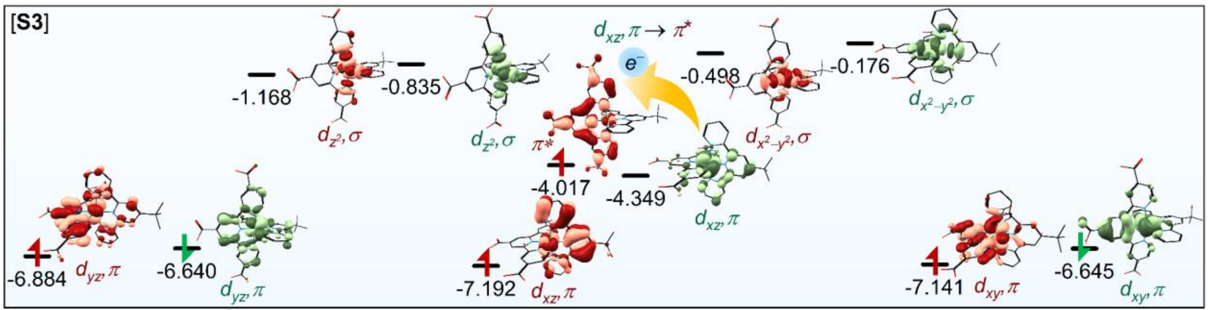

^{3}MLLCT singly occupied and unoccupied molecular orbitals with energy in eV

(c) Ruthenium and ligand-based singly occupied/unoccupied molecular orbitals of [**S3**] in its ^{3}MLLCT state.

Figure S22. ^{3}MLLCT state singly occupied/unoccupied molecular orbitals (contour: 0.03) of (a) [**S1**], (b) [**S2**] and (c) [**S3**] in the acetonitrile (SMD) phase. The red and green colours of orbitals correspond to the orbitals belonging to the *α*- and *β*-electrons, respectively.

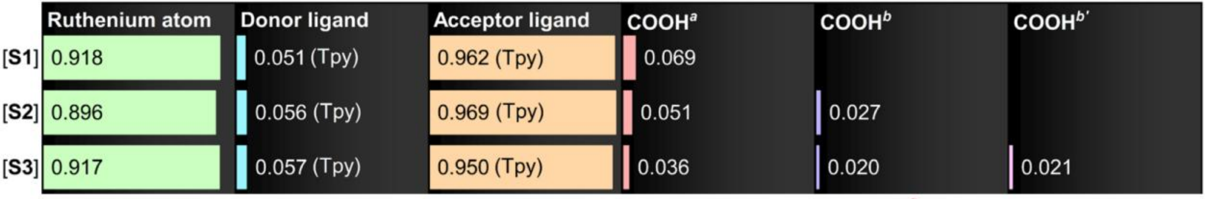

	Ruthenium atom	Donor ligand	Acceptor ligand	COOH^a	COOH^b	COOH$^{b'}$
[**S1**]	0.918	0.051 (Tpy)	0.962 (Tpy)	0.069		
[**S2**]	0.896	0.056 (Tpy)	0.969 (Tpy)	0.051	0.027	
[**S3**]	0.917	0.057 (Tpy)	0.950 (Tpy)	0.036	0.020	0.021

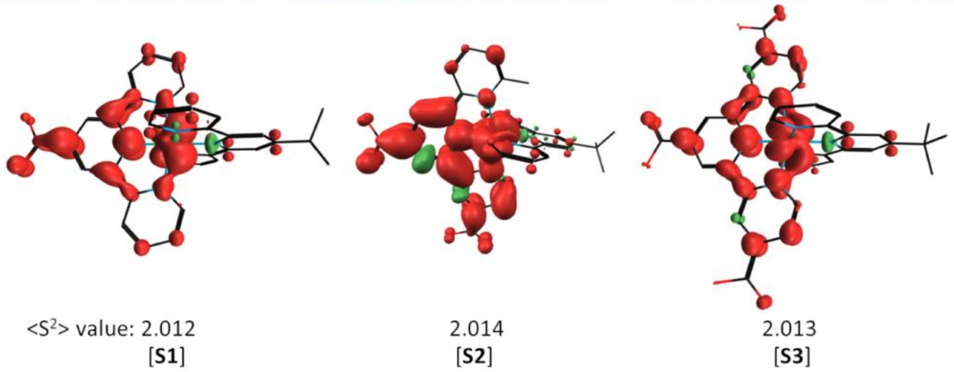

(a) ^{3}MLLCT state: *Mulliken* spin density plots (contour: 0.003) and expectation value for ground triplet states (<S^2>).

	Ruthenium atom	Donor ligand	Acceptor ligand
[**S1**]	1.705	0.117	0.178
(Ist ^{3}MC) [**S2**]	1.571	0.255	0.174
(IInd ^{3}MC)	1.712	0.117	0.170
[**S3**]	1.722	0.111	0.167

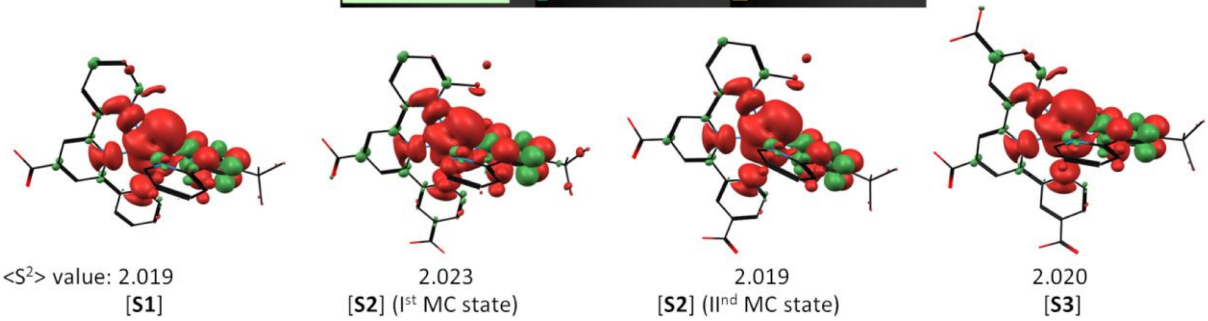

(b) ^{3}MC state: *Mulliken* spin density plot (contour: 0.001) and expectation value for ground triplet states (<S^2>).

Figure S23. *Mulliken* spin density plots and expectation values of (a) ^{3}MLLCT state and, (b) ^{3}MC state. The red and green regions indicate orbitals belonging to the *α*- and *β*-electrons, respectively. The donor and acceptor ligands correspond to the tpy^1 and tpy^2 ligands of [**S1**] – [**S3**], respectively.

Table S7

(a) Relaxed triplet potential energy surface (^{3}PES) scan curve for all complexes along the Ru–N^a bond of central pyridine ring of tpy acceptor (tpy^2), starting from the optimized ^{3}MLLCT state in the acetonitrile (SMD) phase.

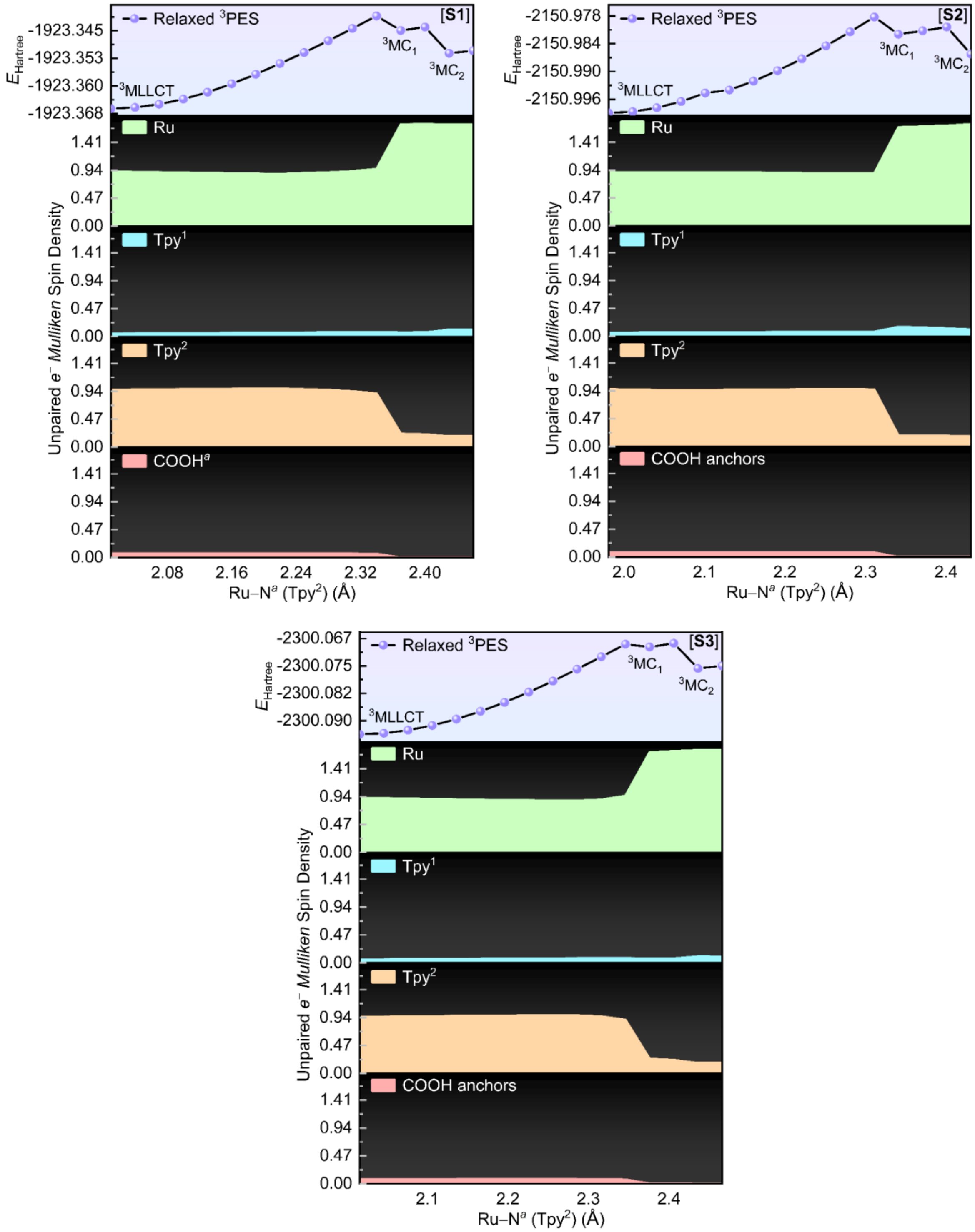

(b) Δ-SCF energies of the optimized excited ^{1}MLLCT state and ground ^{3}MLLCT and ^{3}MC states with their nuclear coordinates vs those of S_0 states in the acetonitrile phase(SMD) along with potential energy scan and ruthenium-spin density.

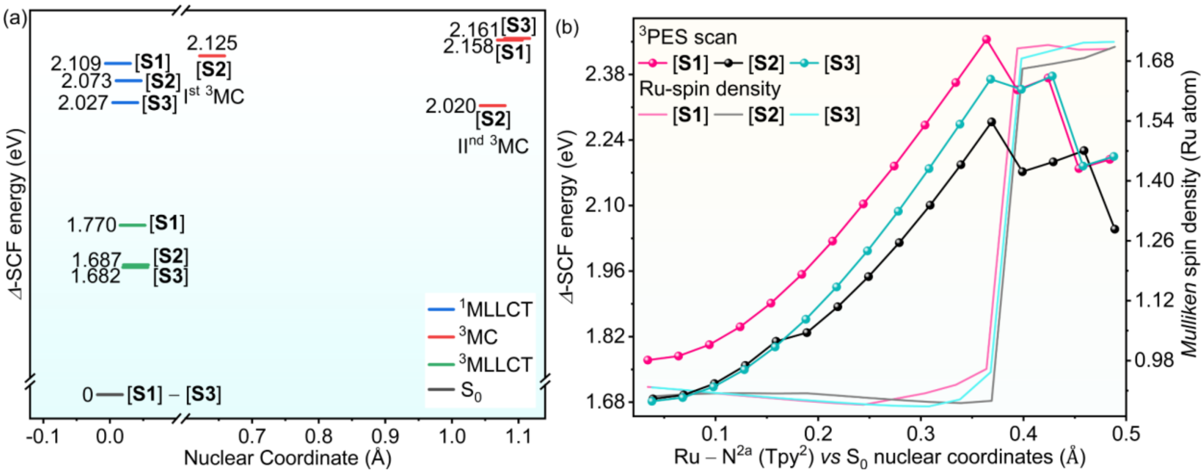

Table S8

Mulliken spin density of triplet electronic states along with their energy (in eV) obtained from the relaxed potential energy surface (^{3}PES) scan and those obtained from optimization of the local minima found in the ^{3}PES.

		Electronic state		Δ-SCF energy (eV)	
	Local minima	After relaxed-^{3}PES scan	After optimization	Initially relaxed ^{3}MLLCT state	Optimized minima (obtained from scan)
[S1]	13	^{3}MC	^{3}MLLCT	1.770	1.770
	15	^{3}MC			2.158
[S2]	13	^{3}MC		1.687	2.125
	16	^{3}MC			2.020
[S3]	13	^{3}MC	^{3}MLLCT	1.682	1.682
	15	^{3}MC			2.161

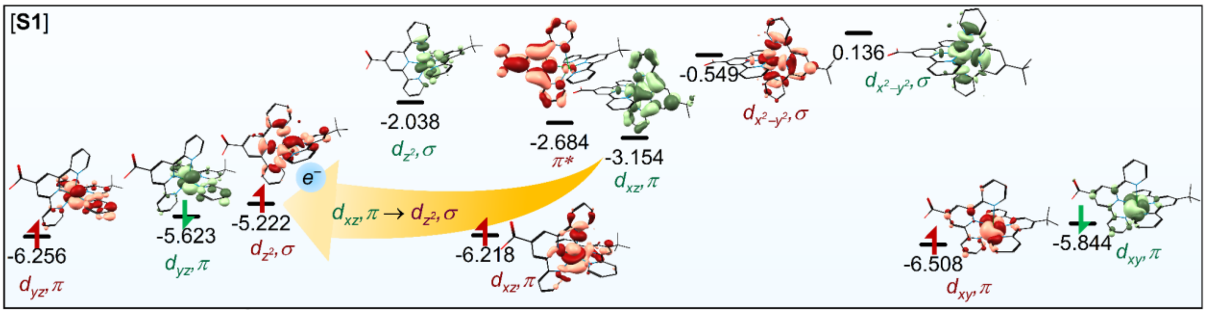

^{3}MC singly occupied and unoccupied molecular orbitals with energy in eV

(a) Ru-based singly occupied/unoccupied molecular orbitals of [**S1**] in its ^{3}MC state.

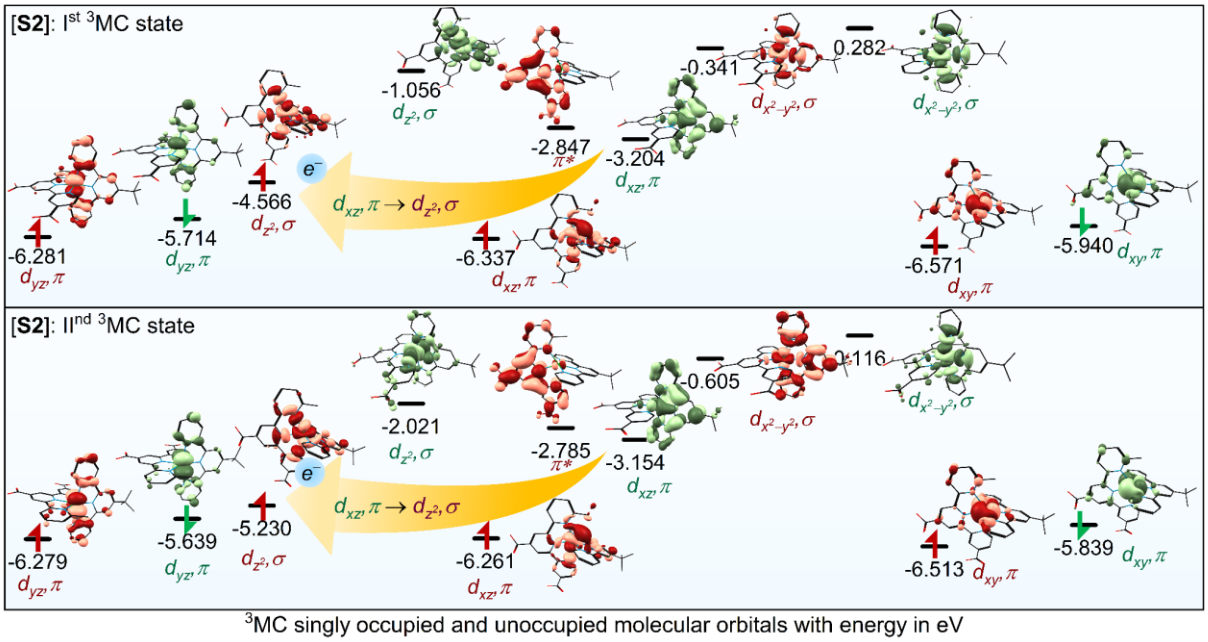

(b) Ru-based singly occupied/unoccupied molecular orbitals of [**S2**] in its ^{3}MC state.

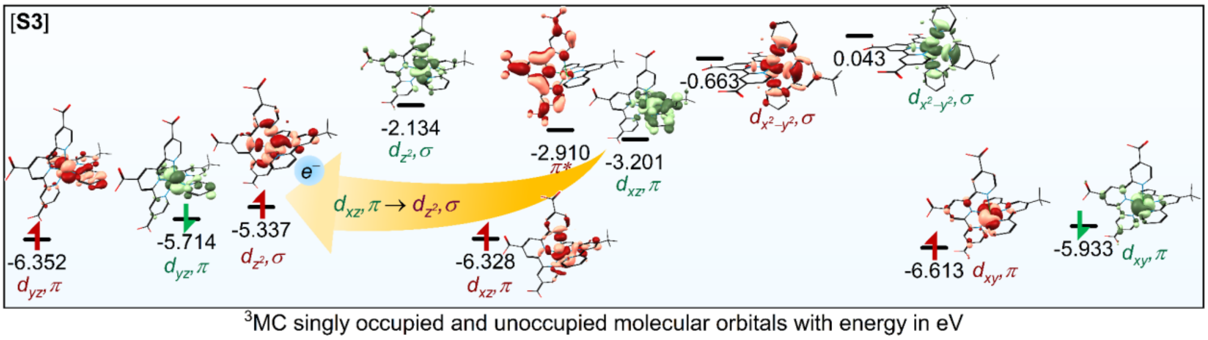

(c) Ru-based singly occupied/unoccupied molecular orbitals of [**S3**] in its ^{3}MC state.

Figure S24. ^{3}MC state singly occupied/unoccupied molecular orbitals (contour: 0.03) of (a) [**S1**], (b) [**S2**] and (c) [**S3**] in the acetronitrile (SMD) phase. The red and green colours of orbitals correspond to the orbitals belonging to the α- and β-electrons, respectively.

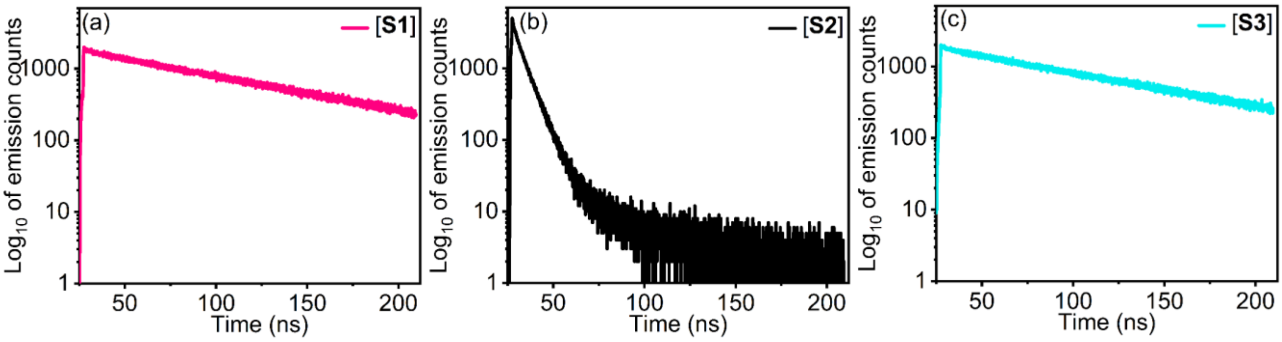

Figure S25. Lifetime Values of [**S1**] – [**S3**].

Table S9

DFT-computed geometrical features of the *push-pull* [Ru(tpy^{D})(tpy^{A})]$^{2+}$-based complexes [**S1**] – [**S3**] in the acetonitrile (SMD) phase.

(a) Metal-ligand geometrical parameters, including bond lengths (in Å) and angles in degrees.

(tpy^{D} group)	–C(CH$_3$)$_3$											
(Tpy^{A} groups)	COOH	2COOH	3COOH	COOH	2COOH	3COOH	COOH	2COOH	3COOH	COOH	2COOH	3COOH
Complex	[**S1**]	[**S2**]	[**S3**]	[**S1**]	[**S2**]	[**S3**]	[**S1**]	[**S2**]	[**S3**]	[**S1**]	[**S2**]	[**S3**]
States	S$_0$			^{1}MLLCT			^{3}MLLCT			^{3}MC		
Ru – N^{Da}	1.992	1.992	1.995	1.978	1.966	1.971	1.989	2.022	1.986	1.986	1.966 (1.989)	1.988
Ru – N^{Db}	2.079	2.080	2.080	2.076	2.079	2.080	2.071	2.074	2.081	2.107	2.085 (2.109)	2.109
Ru – N$^{Db'}$				2.083	2.085	2.085		2.076	2.091	2.111	2.087 (2.114)	2.111
Ru – N^{Aa}	1.975	1.980	1.974	2.068	2.030	2.025	2.010	1.981	2.016	2.352	2.196 (2.340)	2.356
Ru – N^{Ab}	2.076	2.061	2.069	2.069	2.077	2.065	2.077	2.081	2.066	2.213	2.471 (2.602)	2.597
Ru – N$^{Ab'}$		2.139			2.123	2.064	2.093	2.137	2.065	2.595	2.167 (2.239)	2.204
∠N^{Db} – Ru – N$^{Db'}$	157.88	157.85	157.75	159.95	160.42	160.18	159.43	154.67	159.55	158.33	159.29 (158.17)	158.24
∠N^{Ab} – Ru – N$^{Ab'}$	158.97	158.55	159.14	154.38	154.66	154.51	154.38	159.18	154.66	137.45	144.03 (138.25)	137.32

*The nitrogen atoms-N^{a}, N^{b} and N$^{b'}$ corresponds to the metal-coordinating N atoms of the inner and outer pyridine rings of the tpy ligand.

*The geometrical features of the second ^{3}MC state of [**S2**] is in parenthesis.

(b) Geometrical features of [**S1**] – [**S3**] in all electronic states.

Electronic States	[**S1**]	[**S2**]	[**S3**]
R-value			
S$_0$	2.047	**2.055**	2.045
^{1}MLLCT	2.048	**2.060**	2.048
^{3}MLLCT	2.052	**2.062**	2.051
^{3}MC	2.227	2.162 **2.232**	2.228
Octahedricity (*O*)-value (Ideal value = 0)			
S$_0$	10.788	**10.888**	10.778
^{1}MLLCT	11.090	**11.143**	11.125
^{3}MLLCT	11.205	**11.248**	11.148
^{3}MC	16.018	14.163 15.883	**16.070**

*The *R*-value is the average of all metal-ligand bond distances.

*The *O*-value corresponds to the mean absolute deviation of the set of all metal-ligand angles from the ideal bond angles of the octahedral structure.

The computed ground state (S$_0$) geometries of [**S1**] – [**S3**] in acetonitrile solution exhibit a *pseudo*-octahedral coordination of terpyridine (tpy) ligands around the ruthenium (II) center with ∠N–Ru–N bite angles in the range of 157.75° – 159.14°. In the solution phase, the tpy donor (tpy^{D}) and acceptor (tpy^{A}) ligands bind *meridionally* to the ruthenium center, in an orthogonal fashion. Further, these optimized solvated ground state geometries are also comparable to related complexes in the solid state.[39-42] The rigid tpy backbone favors shorter Ru–N$^{\text{central pyridine}}$ and relatively longer Ru–N$^{\text{peripheral pyridine}}$ bonds. Moreover, the Ru–N$^{\text{central pyridine}}$ bond at the acceptor end (tpy^{A}) is relatively shorter than that at the donor end (tpy^{D}). This Ru–N bond shortening at the acceptor end is most pronounced in [**S3**], featuring three carboxylate anchors.

Table S10

(a) Thermodynamic *Born-Haber* cycle-computed ground state oxidation potential of complexes [**S1**] – [**S3**] in the acetonitrile (SMD) phase. The table also lists excited state oxidation potentials and driving force of interfacial electron injection and dye regeneration.

	[**S1**]	[**S2**]	[**S3**]
${}^{a}G^{\circ}_{vac}$ (Ru^{2+})	–1922.675	–2150.262	–2299.365
${}^{a}G^{\circ}_{vac}$ (Ru^{3+})	–1922.241	–2149.829	–2298.930
${}^{b}\Delta G^{\circ\,ox\,(Ru^{2+}/Ru^{3+})}_{vac}$	0.434	0.433	0.435
${}^{a}G^{\circ}_{solv}$ (Ru^{2+})	–1922.902	–2150.494	–2299.604
${}^{a}G^{\circ}_{solv}$ (Ru^{3+})	–1922.708	–2150.297	–2299.405
${}^{c/d}\Delta G^{\circ}_{solvation}$ (Ru^{2+})	–0.228	–0.232	–0.239
${}^{c/d}\Delta G^{\circ}_{solvation}$ (Ru^{3+})	–0.467	–0.468	–0.475
${}^{e}\Delta\Delta G^{\circ\,ox\,(Ru^{2+}/Ru^{3+})}_{solvation}$	–0.239	–0.236	–0.235
${}^{f}\Delta G^{\circ\,ox\,(Ru^{2+}/Ru^{3+})}_{solv}$	0.194	0.197	0.199
${}^{g\,DFT}E^{\circ(Ru^{2+}/Ru^{3+})}$ (V *vs* SCE)	1.096	1.176	1.235
ΔE_{calc} (eV)	2.109	2.073	2.027
${}^{DFT}E^{\circ(Ru^{2+*}/Ru^{3+})}$ (V *vs* SCE)	–1.012	–0.897	–0.792
${}^{h}D_{inj}$ (V *vs* SCE)	0.312	0.197	0.092
${}^{i}D_{reg}$ (V *vs* SCE)	0.896	0.976	1.035
${}^{j\,Exp.}E^{\circ(Ru^{2+*}/Ru^{3+})}$ (V *vs* SCE)	–1.23	–1.04	–0.87

[a]Gibbs free energy (G°_{vac}) of the singlet ground state of complexes and their oxidized doublet forms.

${}^{b}\Delta G^{\circ\,ox\,(Ru^{2+}/Ru^{3+})}_{vac} = G^{\circ Ru^{3+}}_{vac} - G^{\circ Ru^{2+}}_{vac}$

${}^{c}\Delta G^{\circ Ru^{2+}}_{solvation} = G^{\circ Ru^{2+}}_{solv} - G^{\circ Ru^{2+}}_{vac}$

${}^{d}\Delta G^{\circ Ru^{3+}}_{solvation} = G^{\circ Ru^{3+}}_{solv} - G^{\circ Ru^{3+}}_{vac}$

${}^{e}\Delta\Delta G^{\circ\,ox\,(Ru^{2+}/Ru^{3+})}_{solvation} = \Delta G^{\circ Ru^{3+}}_{solvation} - \Delta G^{\circ Ru^{2+}}_{solvation}$

${}^{f}\Delta G^{\circ\,ox\,(Ru^{2+}/Ru^{3+})}_{solv} = \Delta G^{\circ\,ox\,(Ru^{2+}/Ru^{3+})}_{vac} + \Delta\Delta G^{\circ\,ox\,(Ru^{2+}/Ru^{3+})}_{solvation}$

${}^{g\,DFT}E^{\circ(Ru^{2+}/Ru^{3+})}$(*vs* SCE) = 27.2114 ($\Delta G^{\circ\,ox\,(Ru^{2+}/Ru^{3+})}_{solv}$) – 4.1888 V

${}^{h}D_{inj} = |{}^{DFT}E^{\circ(Ru^{2+*}/Ru^{3+})} - E^{TiO_2}_{CB}| = |{}^{DFT}E^{\circ(Ru^{2+}/Ru^{3+})} - \Delta E_{calc} - E^{TiO_2}_{CB}|$ where, $E^{TiO_2}_{CB}$ = –0.7 V *vs* SCE

${}^{i}D_{reg} = |E^{I_3^-/I^-} - {}^{DFT}E^{\circ(Ru^{2+}/Ru^{3+})}|$ where, $E^{I_3^-/I^-}$ = 0.2 V *vs* SCE

${}^{j\,Exp.}E^{\circ(Ru^{2+*}/Ru^{3+})} = {}^{Exp.}E^{\circ(Ru^{2+}/Ru^{3+})} - E_{0-0}$. E_{0-0} = 1240/λ_{int}, where λ_{int} corresponds to the intersection point of absorption and emission curves.[16, 43-45]

(b) Singly unoccupied (*β*) and occupied (*α*) orbitals (contour: 0.03) of the singly oxidized and reduced doublets of complexes, respectively.

	Charge depletion (*β*-MO)	Charge accumulation (*α*-MO)
[S1]	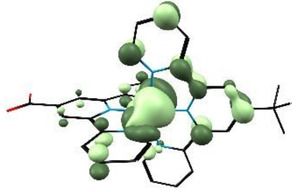	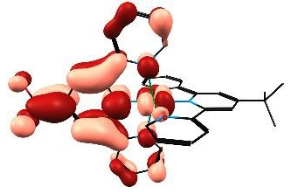
	(Ru-66%)	(Tpy^2-88%)
[S2]	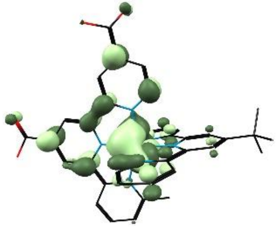	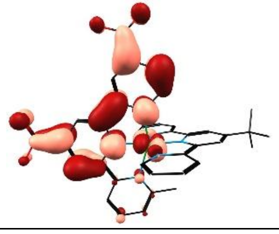

	(Ru-61%)	(Tpy^{2}-89%)
[S3]	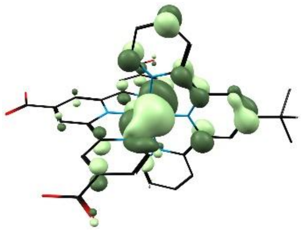 (Ru-66%)	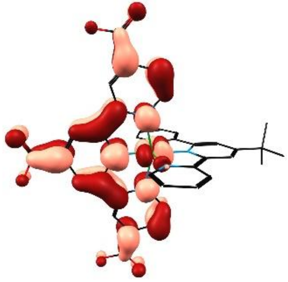 (Tpy^{2}-89%)

(b) Singly unoccupied (β) and occupied (α) orbitals (contour: 0.03) of the singly oxidized and reduced doublets of complexes, respectively.

(c) Spin density plot (contour: 0.001) of doubly oxidized and singly and doubly reduced triplets of [**S1**] – [**S3**].

	Doubly oxidized (Ru^{4+}) state	Singly reduced (Tpy^{-}) state	Doubly reduced (Tpy^{2-}) state
[**S1**]	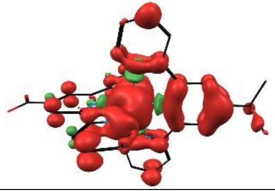	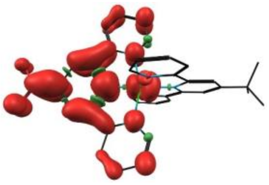	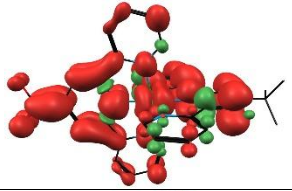
[**S2**]	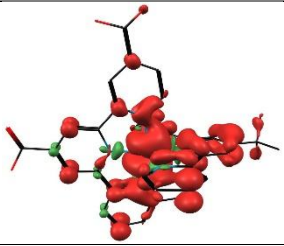	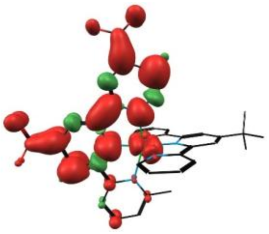	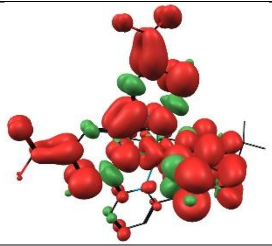
[**S3**]	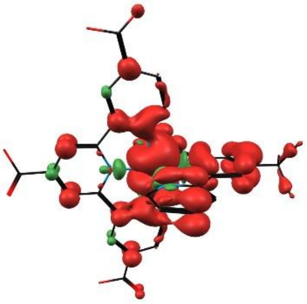	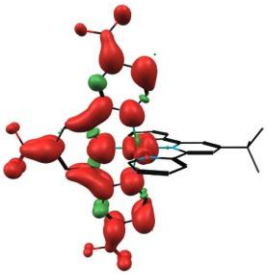	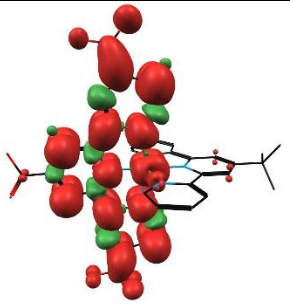

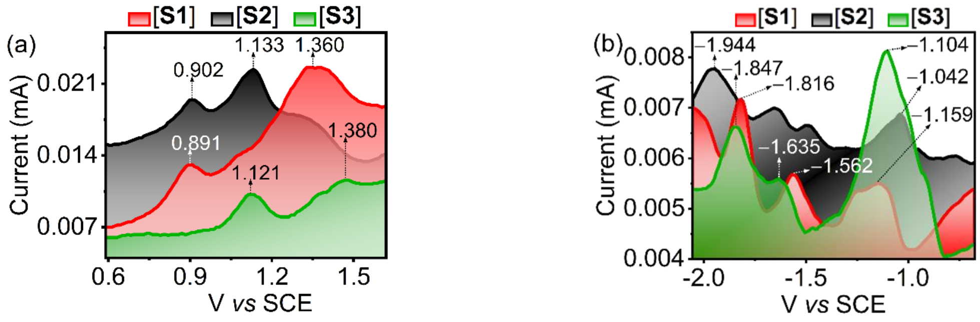

Figure S26. Differential pulse voltammogram of [**S1**] – [**S3**]: (a) oxidation and (b) reduction peak currents.

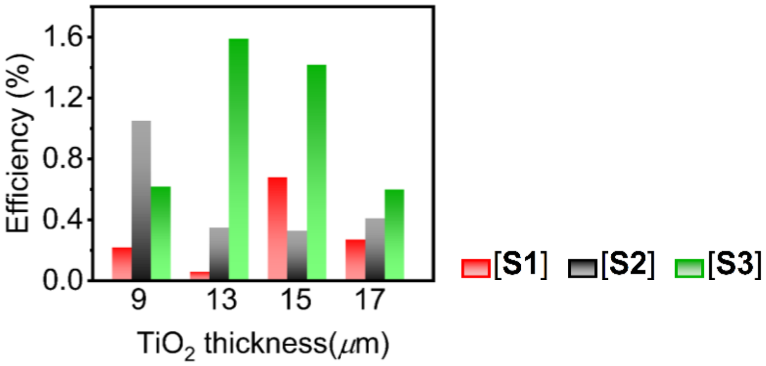

Figure S27. Illustration of efficiency of ruthenium photosensitizers *versus* TiO$_2$ thickness of 9, 13, 15, and 17 μm, respectively.

Table S11

Photovoltaic and electrochemical impedance spectroscopy (after fitting experimental values with an equivalent circuit) data of devices sensitized with **[S1]** – **[S3]** with an active area of 0.36 cm^2

(a). Photovoltaic data.

Dye	TiO$_2$ film (μm)	Dye load (mM)	J_{max} (mA cm^{-2})	J_{sc} (mA cm^{-2})	V_{max} (V)	V_{oc} (V)	*FF*	η (%)
[S1]	9	0.50	0.79±0.024	0.93±0.031	0.27±0.033	0.54±0.002	0.44±0.021	0.22±0.028
	13	0.40	0.15±0.025	0.22±0.033	0.42±0.021	0.55±0.003	0.52±0.012	0.06±0.023
	15	0.40	1.78±0.030	1.80±0.034	0.38±0.041	0.48±0.005	0.78±0.013	0.68±0.022
	17	0.40	0.60±0.045	0.70±0.032	0.45±0.039	0.55±0.004	0.70±0.022	0.27±0.015
[S2]	9	0.40	2.95±0.036	3.21±0.033	0.36±0.027	0.47±0.003	0.69±0.015	1.05±0.033
	13	0.30	1.00±0.026	1.17±0.036	0.35±0.028	0.43±0.002	0.70±0.022	0.35±0.002
	15	0.20	1.19±0.031	1.48±0.055	0.28±0.025	0.38±0.005	0.59±0.011	0.33±0.001
	17	0.20	1.10±0.033	1.28±0.007	0.37±0.030	0.46±0.004	0.69±0.002	0.41±0.003
[S3]	9	0.30	1.74±0.022	2.07±0.009	0.36±0.002	0.48±0.003	0.62±0.033	0.62±0.022
	13	0.40	3.98±0.024	4.40±0.009	0.40±0.013	0.52±0.007	0.69±0.010	1.59±0.004
	15	0.20	4.04±0.025	4.61±0.013	0.35±0.055	0.49±0.006	0.63±0.007	1.42±0.023
	17	0.40	1.43±0.026	1.55±0.020	0.42±0.002	0.52±0.002	0.75±0.023	0.60±0.031

J_{sc} represents short circuit current density; V_{OC} corresponds to open circuit potential; *FF* denotes fill factor; PCE signifies the photon conversion efficiency.

(b). Electrochemical impedance spectroscopy data.

Dye	TiO$_2$ film (μm)	Dye load (mM)	ω_{max} (mA cm^{-2})	τ_e (ms)	R_{CT} (Ω)($\times 10^2$)	D_{eff} ($\times 10^{-3}$ cm^2 s^{-1})	L_n (μm)
[**S1**]	9	0.50	62.50	16.00	4.02	0.56	29.00
	13	0.40	27.00	37.00	35.74	3.13	10.70
	15	0.40	339.32	2.95	8.75	0.78	8.80
	17	0.40	62.50	16.02	22.81	0.12	10.90
[**S2**]	9	0.40	62.50	16.00	7.08	1.89	55.00
	13	0.30	3.73	268.00	2.15	0.05	38.00
	15	0.20	62.50	16.00	6.99	3.53	7.50
	17	0.20	268.62	3.72	11.90	0.15	12.20
[**S3**]	9	0.30	90.50	52.00	1.42	0.10	23.00
	13	0.40	20.00	52.00	1.40	0.18	31.00
	15	0.20	2.03, 2424.00	492.61, 0.41	0.27, 2.26	0.53, 23.70	16.29, 31.00
	17	0.40	51.79	19.30	220.83	1.23	49.00

R_{CT} represents charge transfer resistance; ω_{max} denotes the peak frequency of the bode plot; τ_e signifies electron lifetime at the photoanode in milliseconds; D_{eff} represents the effective electron diffusion coefficient; L_n refers to the effective diffusion length of the electron.

Table S12

Photovoltaic and electrochemical impedance spectroscopy (after fitting experimental values with an equivalent circuit) data of devices sensitized with **N3** dye with an active area of 0.36 cm^2

(a) Photovoltaic data

Dye	TiO$_2$ film (μm)	Dye load (mM)	J_{max} (mA cm^{-2})	J_{sc} (mA cm^{-2})	V_{max} (V)	V_{oc} (V)	*FF*	η (%)
N3	9	0.55	16.00±0.044	16.83±0.003	0.33±0.004	0.56±0.012	0.53±0.020	4.97±0.030
	13	0.56	7.66±0.002	7.72±0.030	0.72±0.002	0.80±0.002	0.68±0.002	4.07±0.022
	15	0.55	11.66±0.002	12.00±0.024	0.53±0.002	0.67±0.014	0.58±0.018	4.66±0.001
	17	0.50	8.67±0.022	9.97±0.013	0.39±0.024	0.57±0.006	0.59±0.002	3.35±0.004

(b) Electrochemical impedance spectroscopy data

Dye	TiO$_2$ film (μm)	Dye load (mM)	ω_{max} (Hz)	τ_e (ms)	R_{CT} (Ω) ($\times 10^2$)	D_{eff} ($\times 10^{-3}$ cm^{2}s^{-1})	L_n (μm)
N3	9	0.55	84.36	11.85	2.19	0.67	28.21
	13	0.56	44.36	22.54	2.19	7.36	128.95
	15	0.55	69.90	14.30	2.08	0.62	29.80
	17	0.50	40.04	12.56	3.33	0.80	35.05

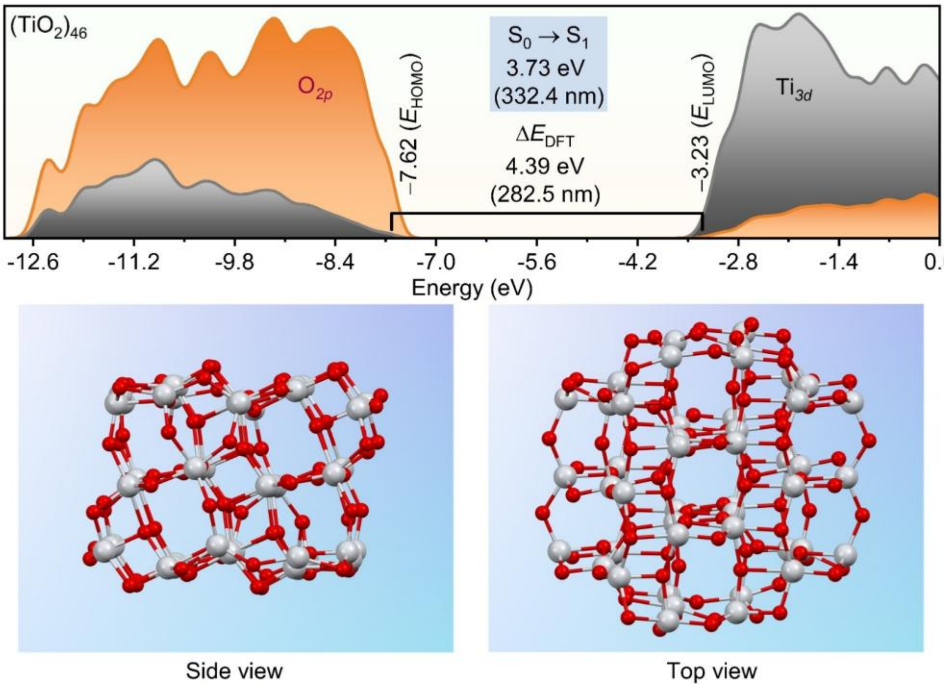

(a) Partial density of states of the optimized $(TiO_2)_{46}$ cluster in acetonitrile phase (SMD).

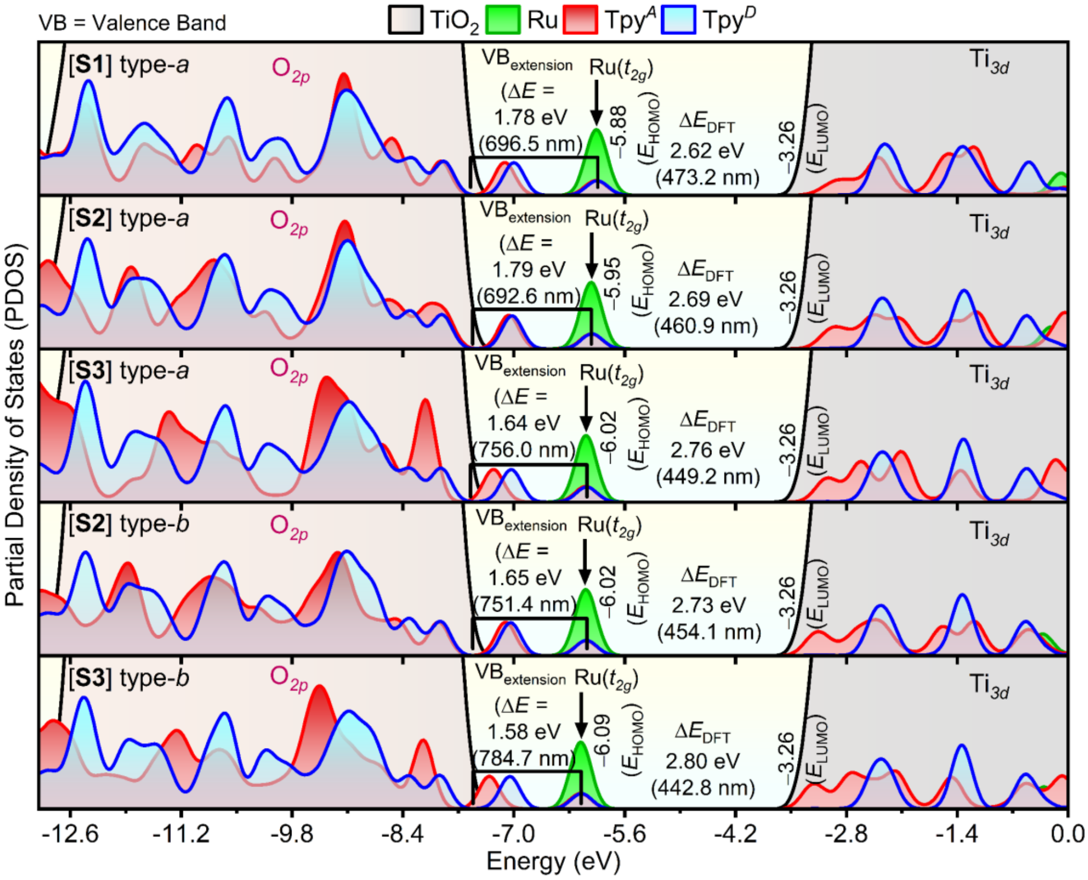

(b) Partial density of states of the optimized dye – $(TiO_2)_{46}$ assemblies of [**S1**] – [**S3**] in acetonitrile phase (SMD).

Figure S28. Partial density of states of (a) $(TiO_2)_{46}$ cluster and (b) dye – $(TiO_2)_{46}$ assemblies of [**S1**] – [**S3**].

Table S13

Electron-density difference maps (contour: 0.001) of the relevant charge transfer states (with oscillator strength, $f \geq 0.02$) obtained from TDDFT featuring excitation from ruthenium center to the anchoring tpy^A mixed with Ti-based vacant *3d* levels.

<table>
<tr><th colspan="4">[S1] <i>type-a</i></th></tr>
<tr>
<td>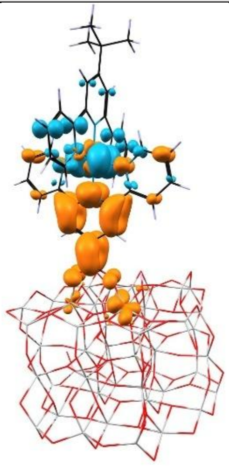</td>
<td>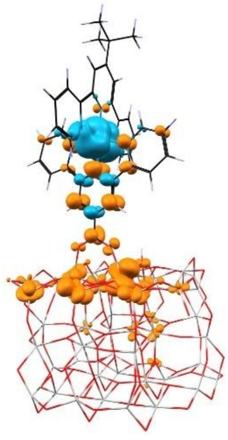</td>
<td>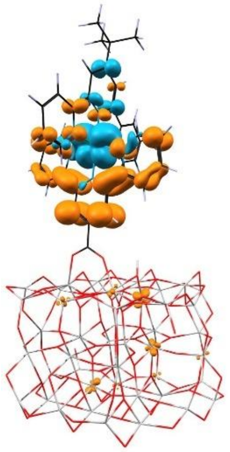</td>
<td>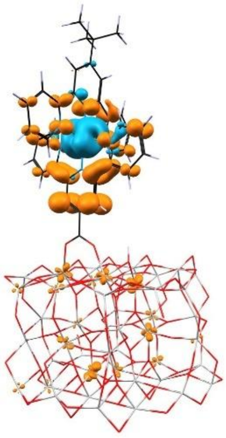</td>
</tr>
<tr>
<td>S_1
(H → L+6 (13%),
(H → L+10 (22%)</td>
<td>S_{11}
(H–2 → L+1 (11%),
(H–2 → L+6 (30%)
(H–2 → L+10 (11%)</td>
<td>S_{38}
(H–1 → L+41 (60%),
(H–1 → L+43 (10%)</td>
<td>S_{39}
(H–1 → L+43 (49%),
(H → L+53 (13%)</td>
</tr>
<tr><th colspan="4">[S2] <i>type-a</i></th></tr>
<tr>
<td>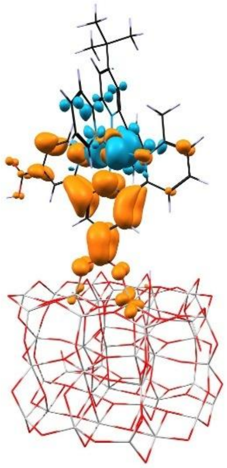</td>
<td>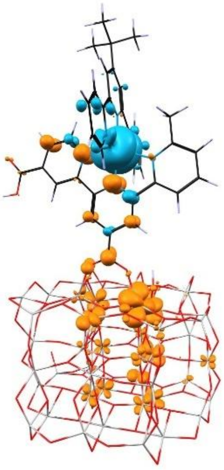</td>
<td>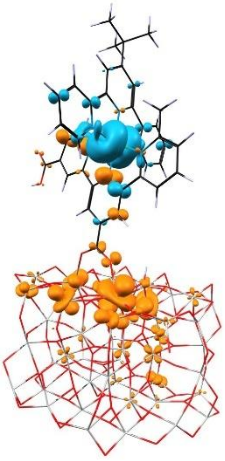</td>
<td>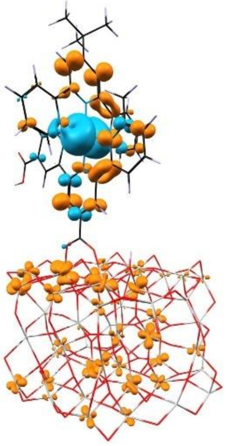</td>
</tr>
<tr>
<td>S_1
(H → L+6 (12%),
(H → L+8 (15%)</td>
<td>S_4
(H → L (25%),
(H → L+1 (20%)
(H → L+3 (10%)</td>
<td>S_5
(H → L+1 (37%),
(H–1 → L+6 (11%)</td>
<td>S_{49}
(H–2 → L+12 (28%),
(H → L+50 (11%)</td>
</tr>
<tr><th colspan="4">[S2] <i>type-b</i></th></tr>
<tr>
<td>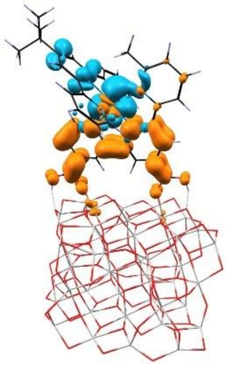</td>
<td>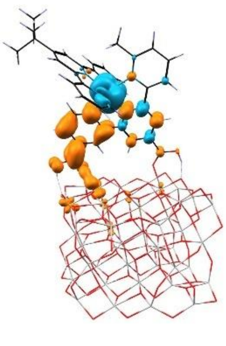</td>
<td>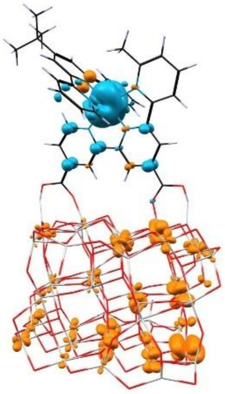</td>
<td>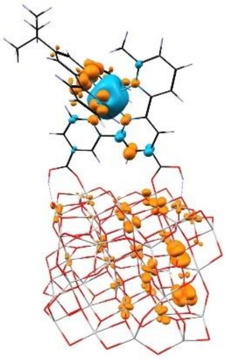</td>
</tr>
</table>

S_1
(H−1 → L (14%),
(H−1 → L+1 (41%),
(H−1 → L+3 (18%)

S_3
(H−2 → L (16%),
(H−2 → L+1 (22%),
(H → L (11%),
(H → L+1 (14%)

S_{31}
(H−1 → L+37 (11%),
(H → L+9 (23%),
(H → L+10 (37%)

S_{32}
(H–1 → L+37 (28%),
(H → L+10 (15%)

[**S3**] *type-a*

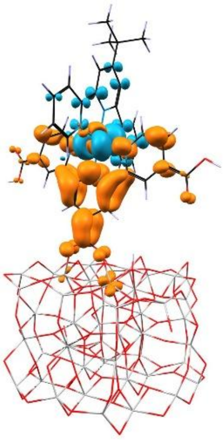

S_1
(H → L+5 (24%),
(H → L+8 (11%)

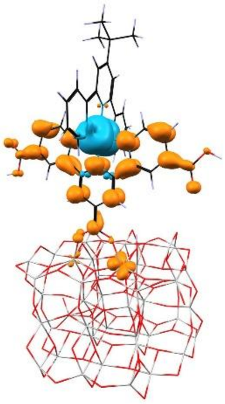

S_3
(H−2 → L (11%),
(H−2 → L+5 (16%),
(H → L+26 (12%),
(H → L+27 (14%)

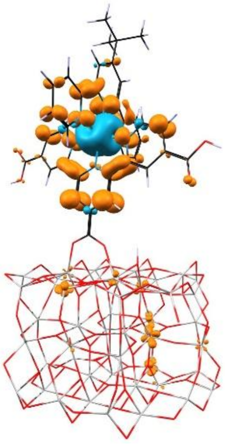

S_{30}
(H−1 → L+39 (38%),
(H → L+26 (14%),
(H → L+27 (18%)

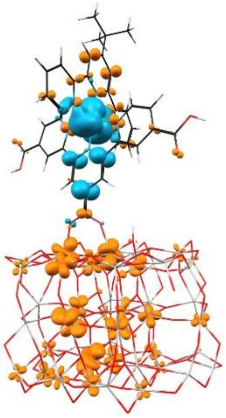

S_{42}
(H–2 → L+10 (10%),
(H–2 → L+12 (25%),
(H → L+50 (11%)

[**S3**] *type-b*

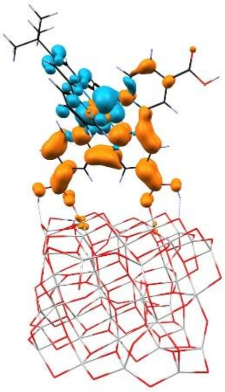

S_1
(H−1 → L (14%),
(H−1 → L+1 (29%)
(H−1 → L+3 (13%),
(H → L+1 (16%)

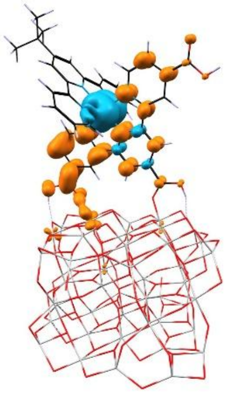

S_3
(H−2 → L (23%),
(H−2 → L+1 (32%),
(H → L+16 (12%)

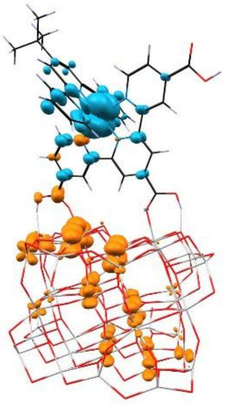

S_4
(H → L (63%)

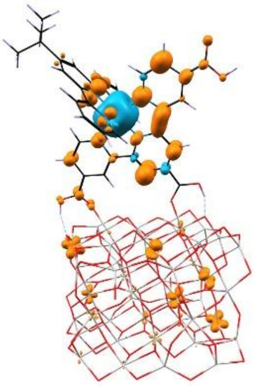

S_{23}
(H–1 → L+37 (25%),
(H → L+16 (15%)

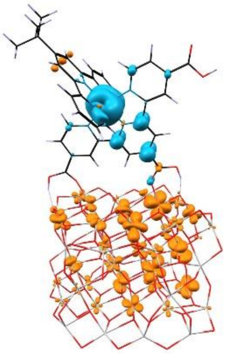

S_{43}
(H−2 → L+11 (48%)

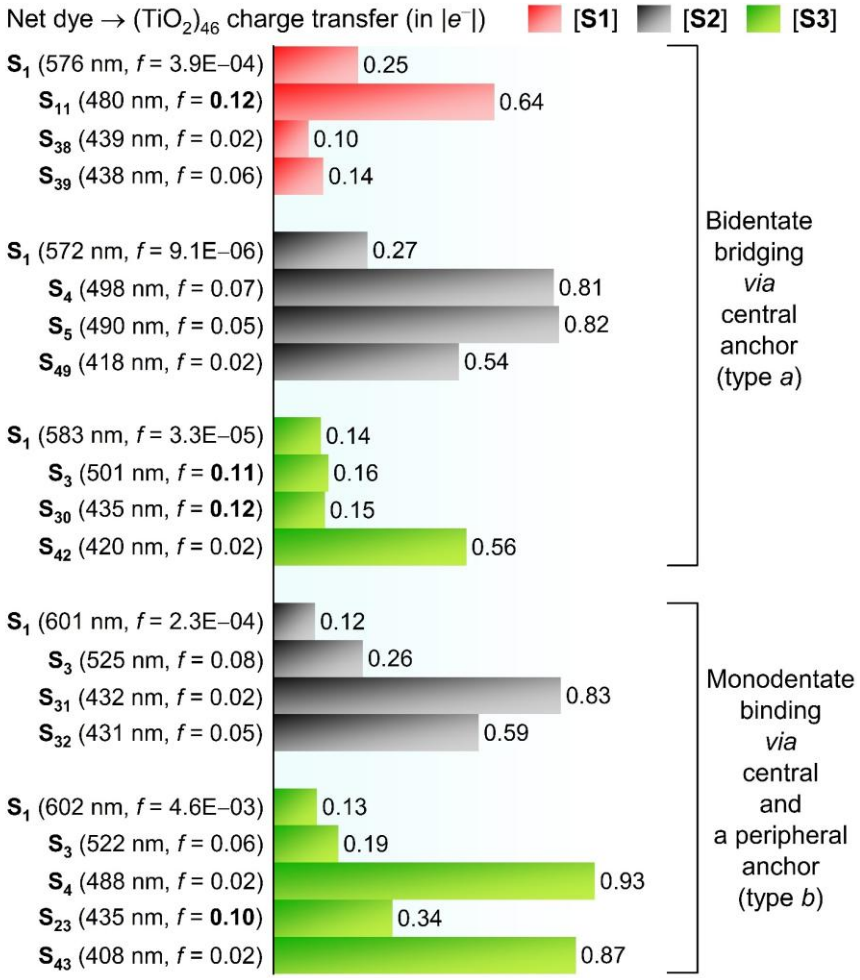

Figure S29. Inter-fragment charge transfer analysis for the dominant electronic excitations ($f \geq 0.02$) of dye – $(TiO_2)_{46}$ assemblies of [**S1**] – [**S3**] in acetonitrile phase(SMD).

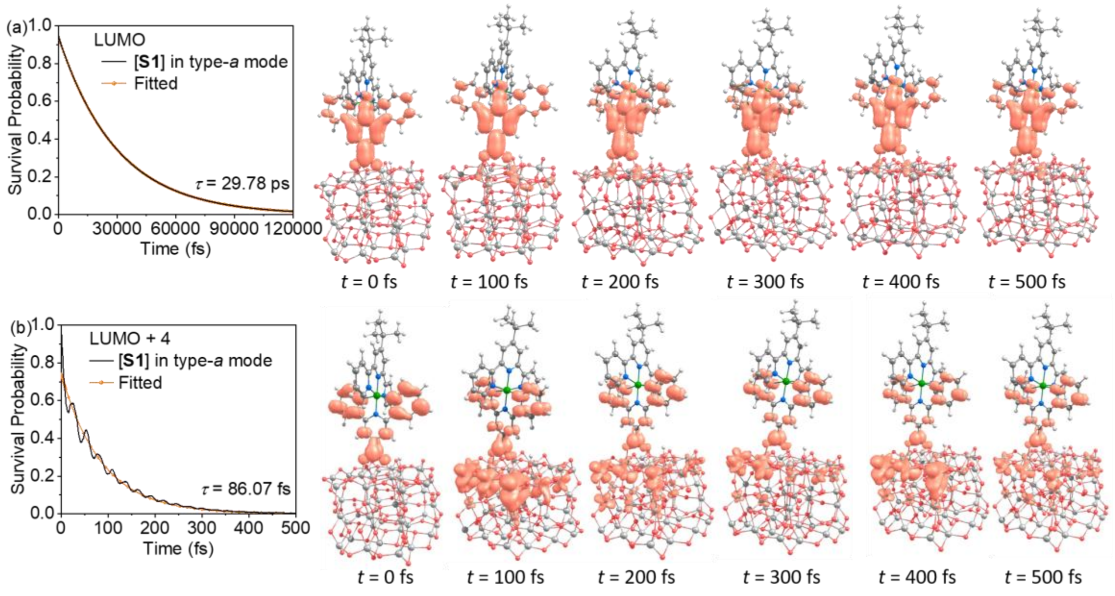

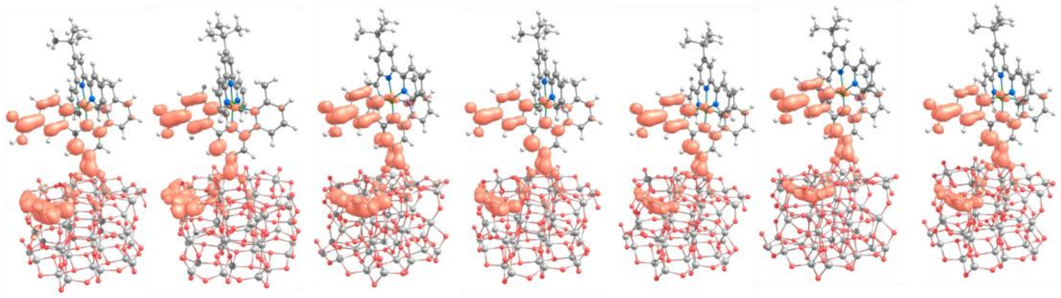

t = 3000 fs *t* = 4000 fs *t* = 5000 fs *t* = 6000 fs *t* = 7000 fs *t* = 8000 fs *t* = 9000 fs

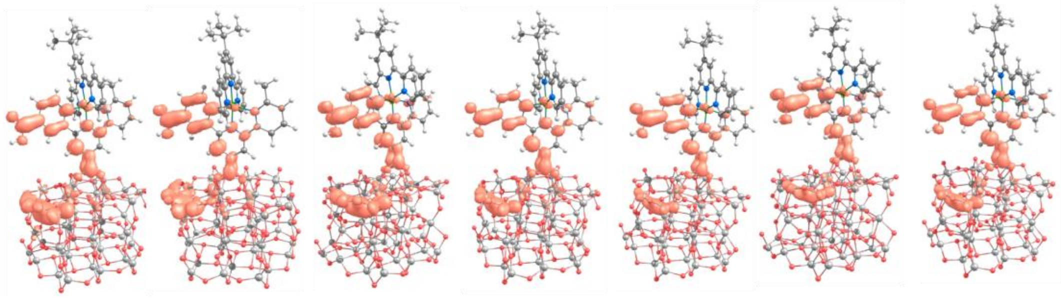

t = 3000 fs *t* = 4000 fs *t* = 5000 fs *t* = 6000 fs *t* = 7000 fs *t* = 8000 fs *t* = 9000 fs

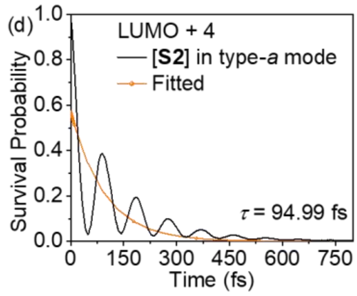

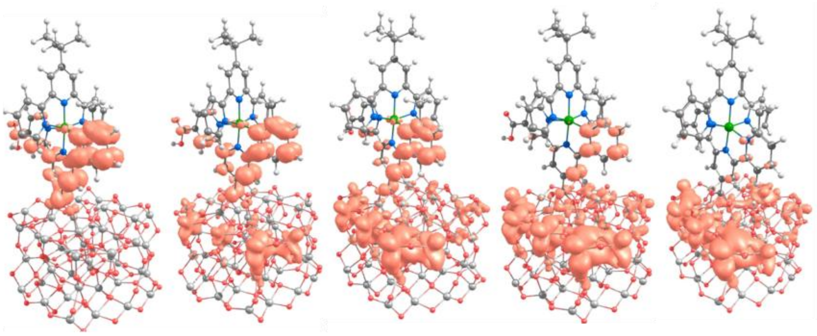

t = 0 fs *t* = 100 fs *t* = 200 fs *t* = 300 fs *t* = 400 fs

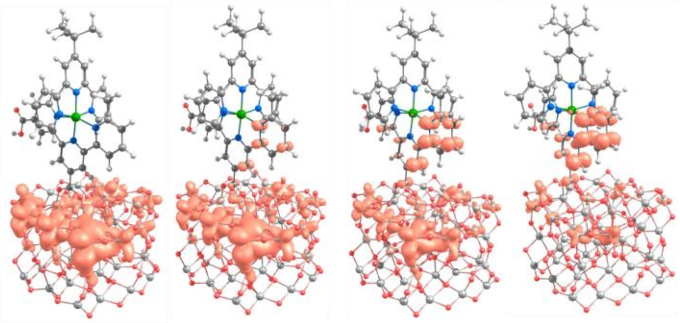

t = 500 fs *t* = 600 fs *t* = 700 fs *t* = 800 fs

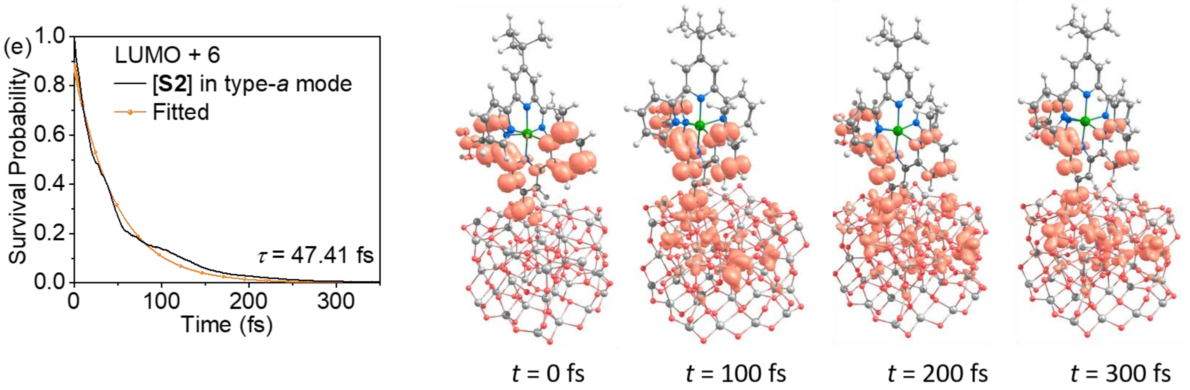
(e)
LUMO + 6
[S2] in type-a mode
Fitted
τ = 47.41 fs
Survival Probability
1.0
0.8
0.6
0.4
0.2
0.0
0
100
200
300
Time (fs)
t = 0 fs
t = 100 fs
t = 200 fs
t = 300 fs

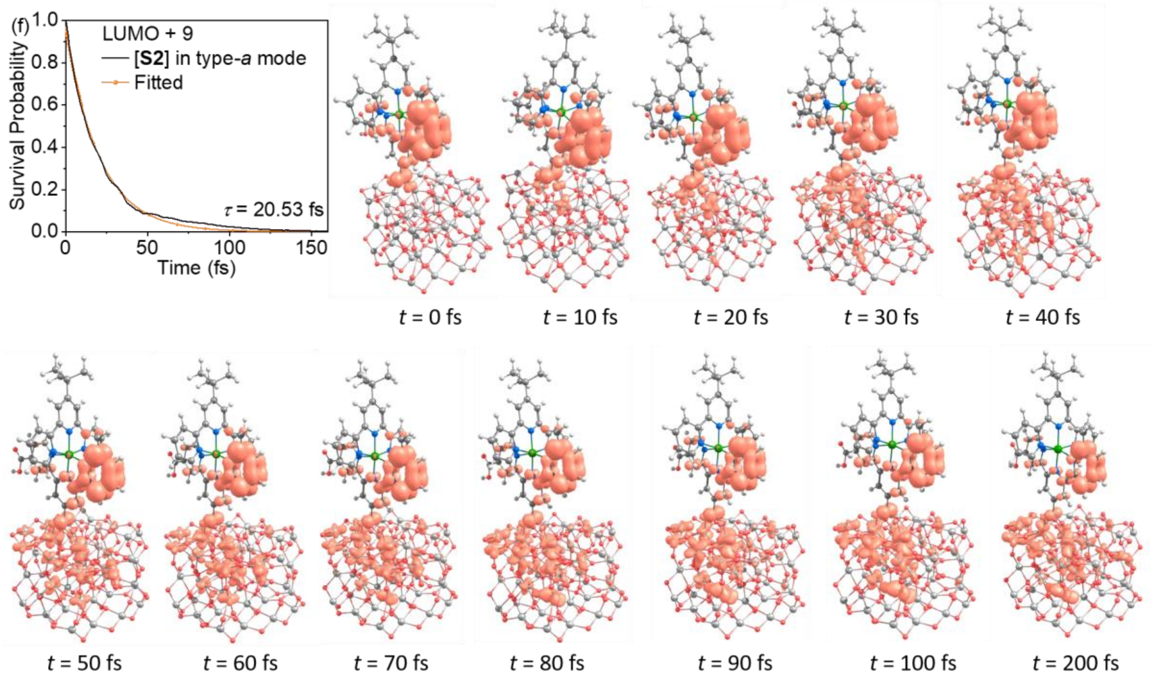
(f)
LUMO + 9
[S2] in type-a mode
Fitted
τ = 20.53 fs
Survival Probability
1.0
0.8
0.6
0.4
0.2
0.0
0
50
100
150
Time (fs)
t = 0 fs
t = 10 fs
t = 20 fs
t = 30 fs
t = 40 fs
t = 50 fs
t = 60 fs
t = 70 fs
t = 80 fs
t = 90 fs
t = 100 fs
t = 200 fs

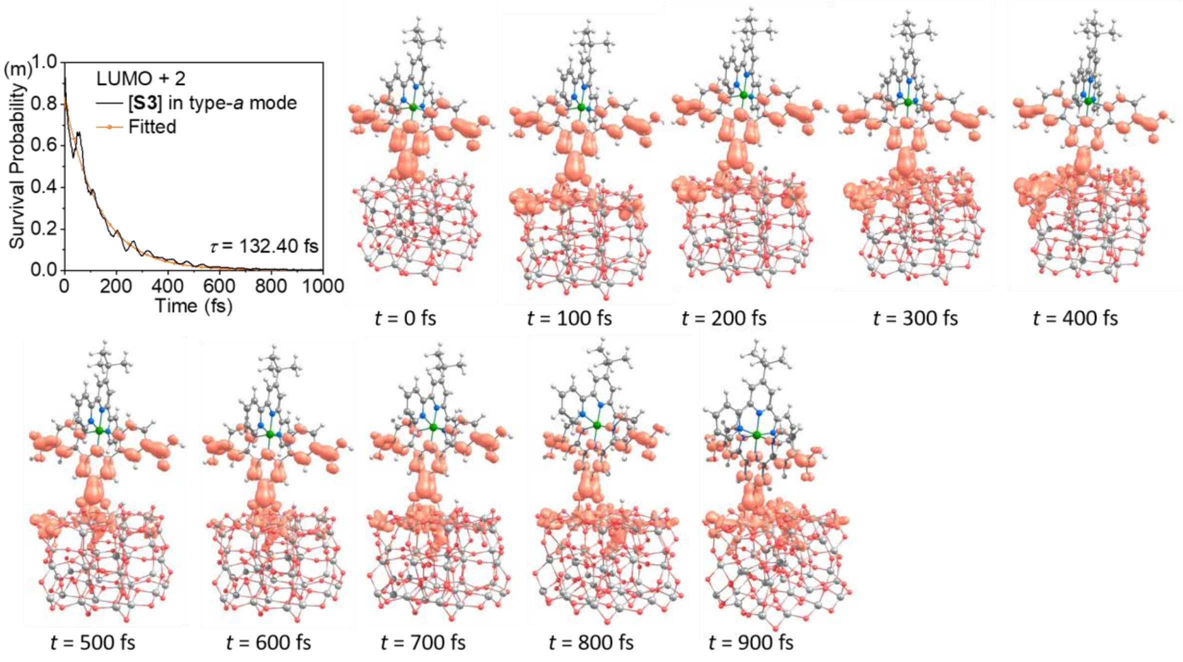
(m)
LUMO + 2
[S3] in type-a mode
Fitted
τ = 132.40 fs
Survival Probability
1.0
0.8
0.6
0.4
0.2
0.0
0
200
400
600
800
1000
Time (fs)
t = 0 fs
t = 100 fs
t = 200 fs
t = 300 fs
t = 400 fs
t = 500 fs
t = 600 fs
t = 700 fs
t = 800 fs
t = 900 fs

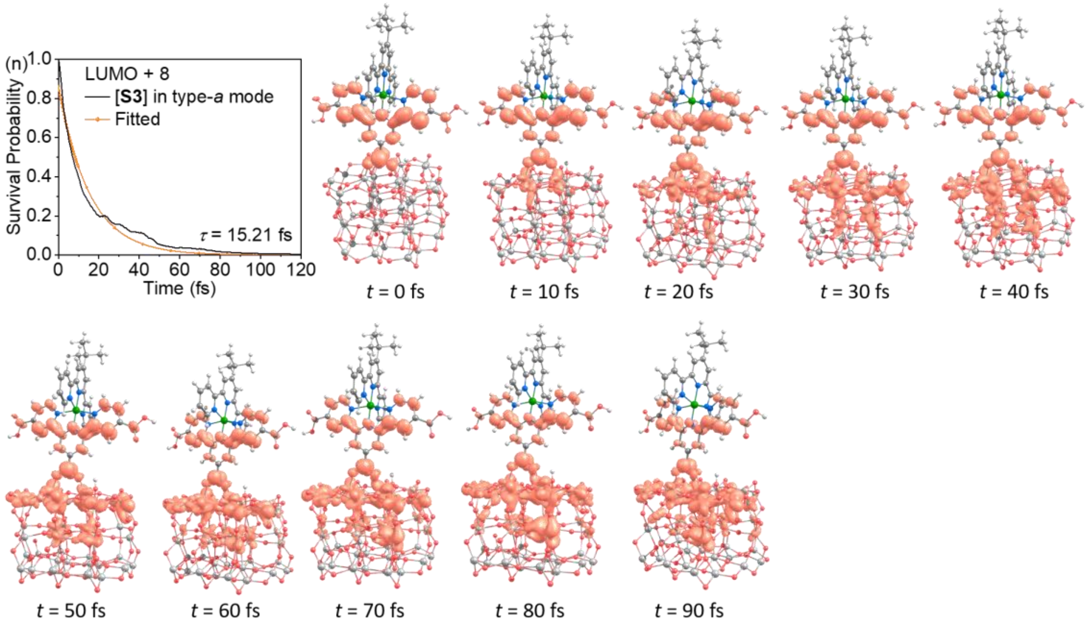
(n)
LUMO + 8
[S3] in type-a mode
Fitted
τ = 15.21 fs
Survival Probability
1.0
0.8
0.6
0.4
0.2
0.0
0 20 40 60 80 100 120
Time (fs)
t = 0 fs
t = 10 fs
t = 20 fs
t = 30 fs
t = 40 fs
t = 50 fs
t = 60 fs
t = 70 fs
t = 80 fs
t = 90 fs

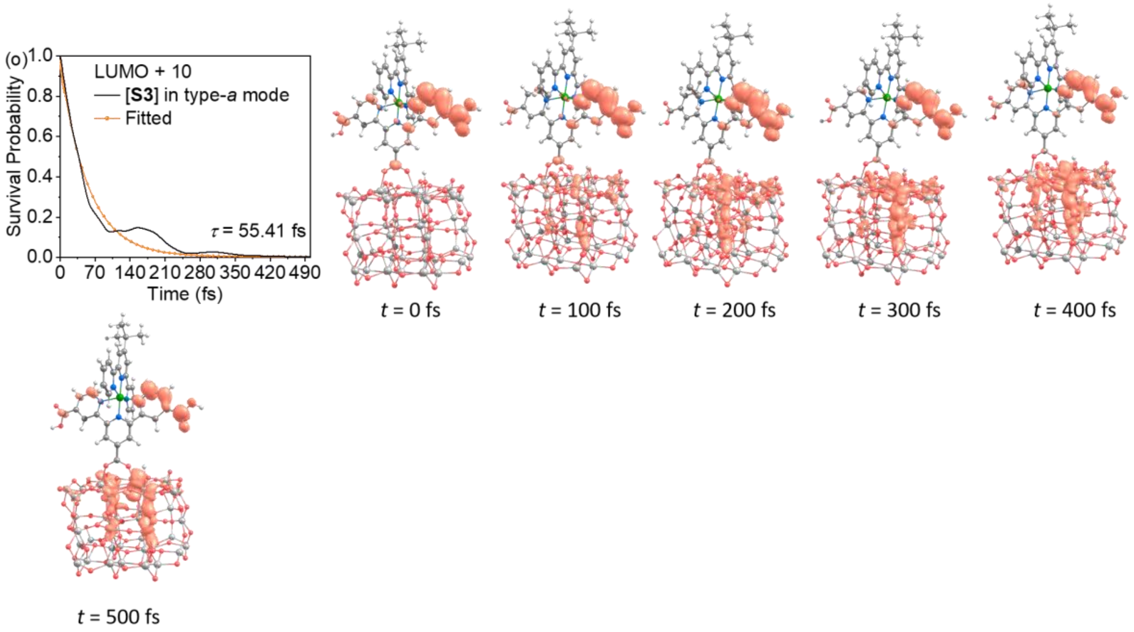
(o)
LUMO + 10
[S3] in type-a mode
Fitted
τ = 55.41 fs
Survival Probability
1.0
0.8
0.6
0.4
0.2
0.0
0 70 140 210 280 350 420 490
Time (fs)
t = 0 fs
t = 100 fs
t = 200 fs
t = 300 fs
t = 400 fs
t = 500 fs

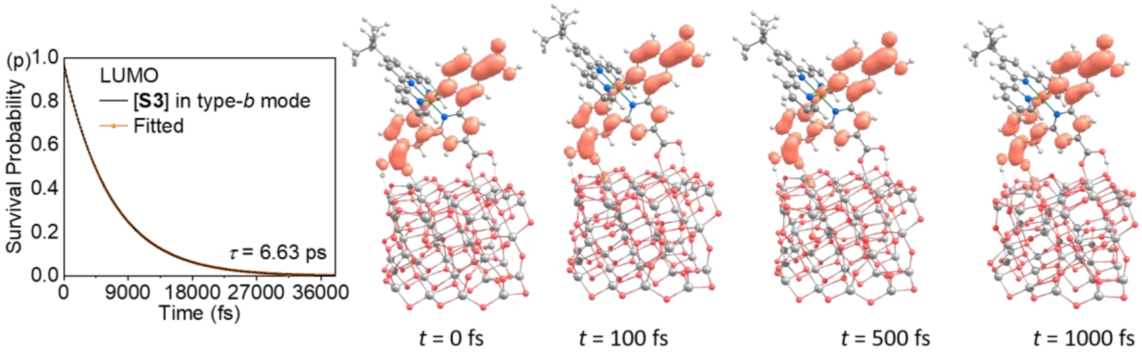
(p)
LUMO
[S3] in type-b mode
Fitted
τ = 6.63 ps
Survival Probability
1.0
0.8
0.6
0.4
0.2
0.0
0 9000 18000 27000 36000
Time (fs)
t = 0 fs
t = 100 fs
t = 500 fs
t = 1000 fs

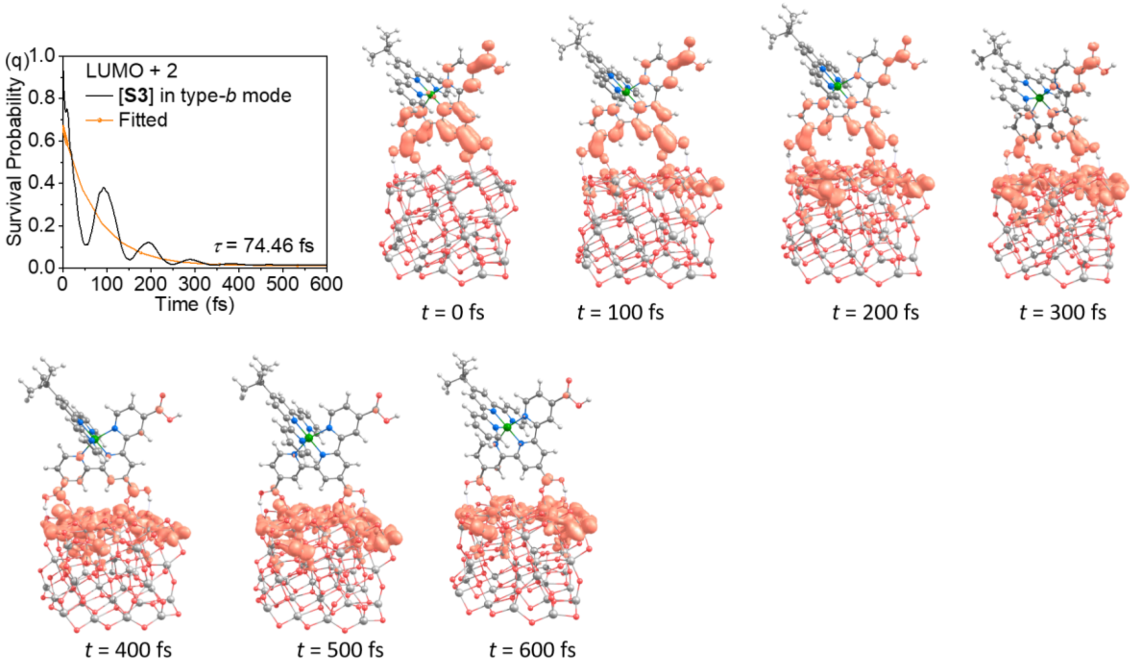
(q)
LUMO + 2
[S3] in type-b mode
Fitted
τ = 74.46 fs
Survival Probability
0.0
0.2
0.4
0.6
0.8
1.0
0
100
200
300
400
500
600
Time (fs)
t = 0 fs
t = 100 fs
t = 200 fs
t = 300 fs
t = 400 fs
t = 500 fs
t = 600 fs

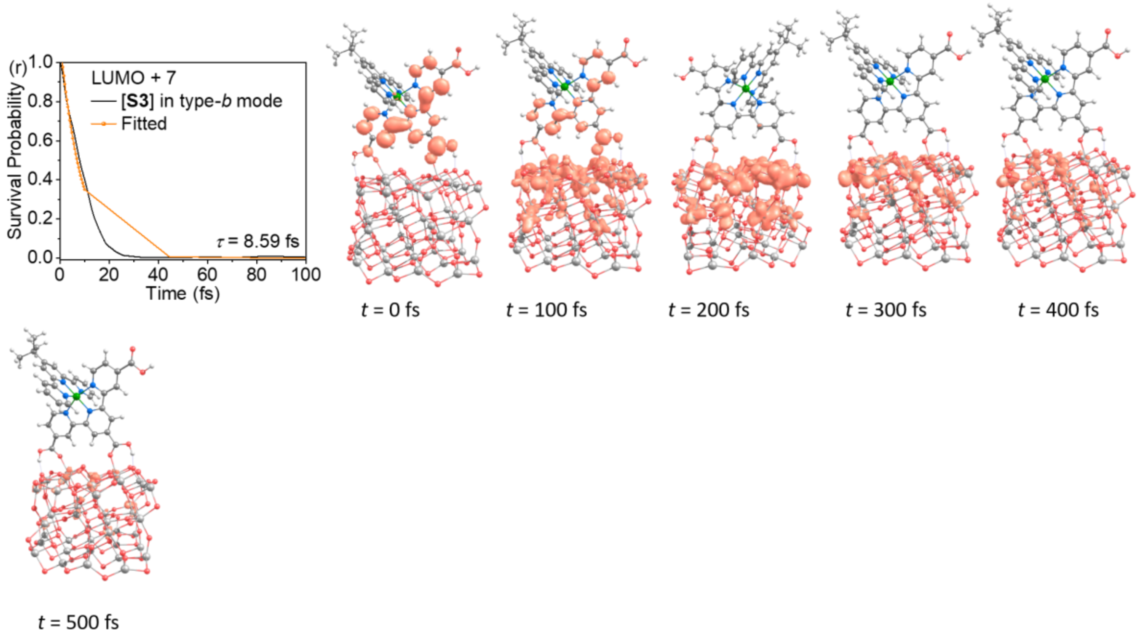
(r)
LUMO + 7
[S3] in type-b mode
Fitted
τ = 8.59 fs
Survival Probability
0.0
0.2
0.4
0.6
0.8
1.0
0
20
40
60
80
100
Time (fs)
t = 0 fs
t = 100 fs
t = 200 fs
t = 300 fs
t = 400 fs
t = 500 fs

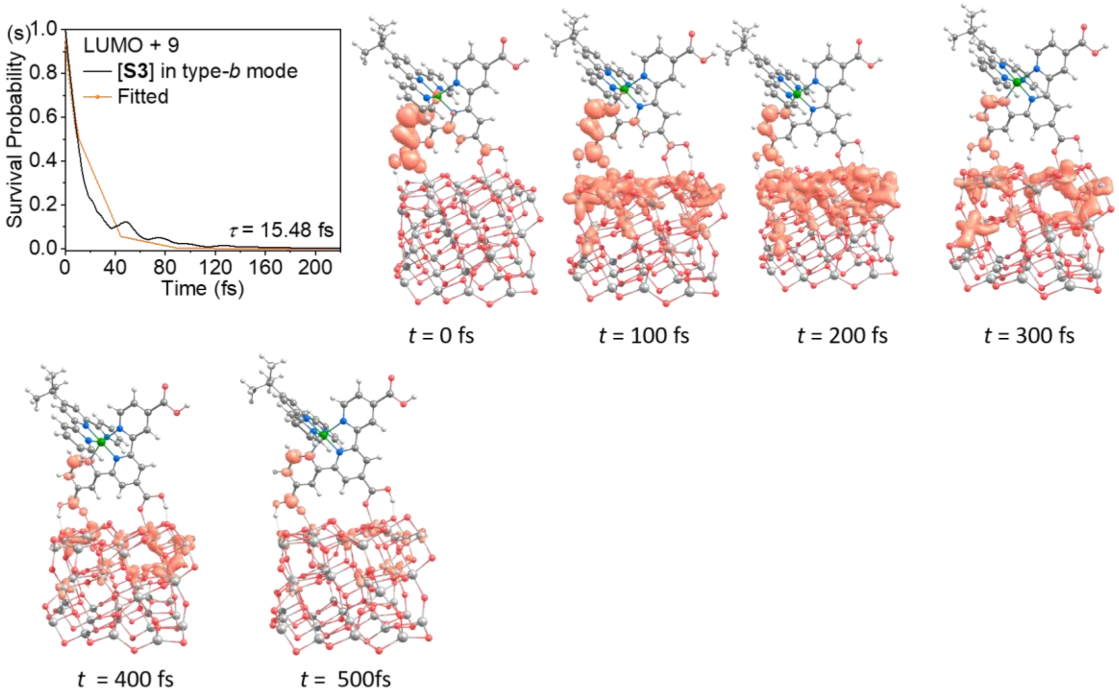

t = 0 fs *t* = 100 fs *t* = 200 fs *t* = 300 fs

t = 400 fs *t* = 500fs

Figure S30. Interfacial electron transfer (IET) dynamics in the dye – $(TiO_2)_{46}$ assemblies of [**S1**] – [**S3**].

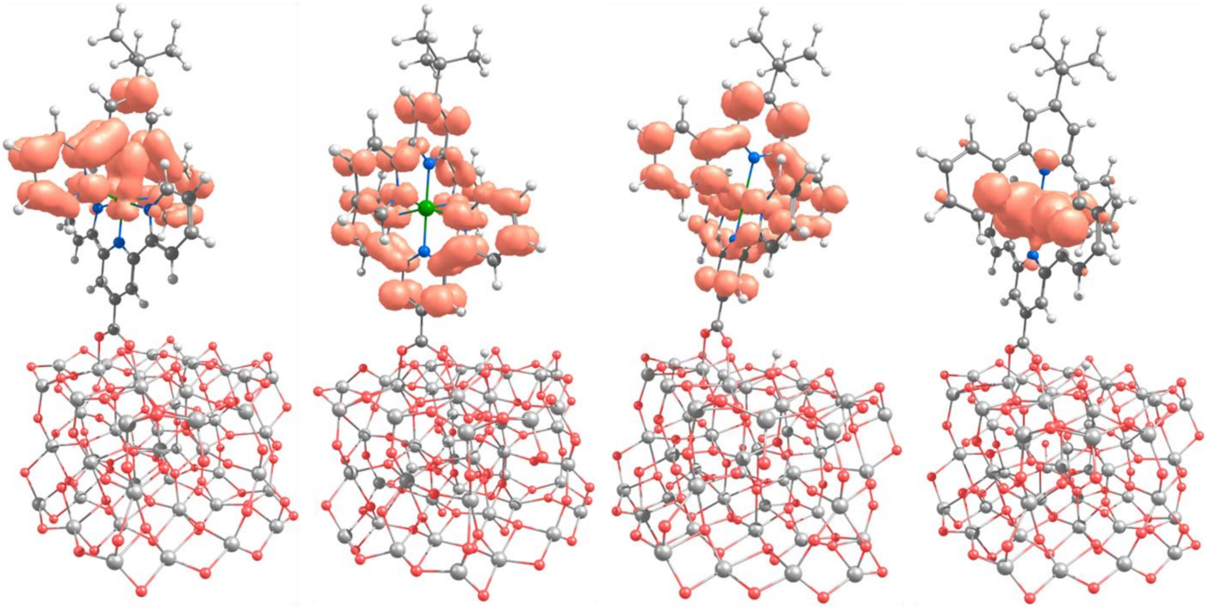

LUMO + 1 LUMO + 2 LUMO + 3 LUMO + 5

Figure S31. Non-electron injecting dye-extended *Hückel* molecular orbitals of [**S1**] – $(TiO_2)_{46}$ assembly.

References:

1. M. Schlosser and F. Cottet, *Eur. J. Org. Chem.*, 2002, **2002**, 4181–4184.
2. U. S. Schubert, C. Eschbaumer and M. Heller, *Org. Lett.*, 2000, **2**, 3373–3376.
3. J. Husson, J. Dehaudt and L. Guyard, *Nat. Protoc.*, 2014, **9**, 21–26.
4. E. C. Constable, N. Hostettler, C. E. Housecroft, P. Kopecky, M. Neuburger and J. A. Zampese, *Dalton Trans.*, 2012, **41**, 2890–2897.
5. C. Barolo, M. K. Nazeeruddin, S. Fantacci, D. Di Censo, P. Comte, P. Liska, G. Viscardi, P. Quagliotto, F. De Angelis and S. Ito, *Inorg. chem.*, 2006, **45**, 4642–4653.
6. S. Grimme, S. Ehrlich and L. Goerigk, *J. Comput. Chem.*, 2011, **32**, 1456–1465.
7. S. Grimme, J. Antony, S. Ehrlich and H. Krieg, *J. Chem. Phys.*, 2010, **132**, 154104.

8. F. Neese, *Wiley Interdiscip. Rev. Comput. Mol. Sci.*, 2022, **12**, e1606.
9. F. Neese, F. Wennmohs, U. Becker and C. Riplinger, *J. Chem. Phys.*, 2020, **152**, 224108.
10. A. D. Becke, *J. Chem. Phys.*, 1993, **98**, 1372–1377.
11. C. Lee, W. Yang and R. G. Parr, *Phys. Rev. B*, 1988, **37**, 785–789.
12. S. Kossmann and F. Neese, *Chem. Phys. Lett.*, 2009, **481**, 240–243.
13. A. D. Kulkarni and D. G. Truhlar, *J. Chem. Theor. Comput.*, 2011, **7**, 2325–2332.
14. M. Pastore, F. De Angelis and C. Angeli, *Theor. Chem. Acc.*, 2016, **135**, 108.
15. F. Perrella, X. Li, A. Petrone and N. Rega, *JACS Au*, 2022, **3**, 70–79.
16. F. Weigend and R. Ahlrichs, *Phys. Chem. Chem. Phys.*, 2005, **7**, 3297–3305.
17. Z.-F. Zhang and M.-D. Su, *RSC Adv.*, 2019, **9**, 2626–2640.
18. A. V. Marenich, C. J. Cramer and D. G. Truhlar, *J. Phys. Chem. B .* 2009, **113**, 6378–6396.
19. M. P. Mitoraj, A. Michalak and T. Ziegler, *J. Chem. Theory Comput.*, 2009, **5**, 962–975.
20. M. P. Mitoraj, M. Parafiniuk, M. Srebro, M. Handzlik, A. Buczek and A. Michalak, *J. Mol. Model.*, 2011, **17**, 2337–2352.
21. G. Bistoni, S. Rampino, F. Tarantelli and L. Belpassi, *J. Chem. Phys.*, 2015, **14**, 1286–1296.
22. D. Sorbelli, P. Belanzoni and L. Belpassi, *Eur. J. Inorg. Chem.*, 2021, **2021**, 2401–2416.
23. GitHub – BERTHA-4c-DKS/pycubescd, can be found under https://github.com/BERTHA-4c-DKS/pycubescd).
24. T. Lu and F. Chen, *J. Comput. Chem.*, 2012, **33**, 580–592.
25. D. R. Hamann, *Phys. Rev. B*, 2013, **88**, 085117.
26. J. P. Perdew, K. Burke and M. Ernzerhof, *Phys. Rev. Lett.*, 1996, **77**, 3865–3868.
27. P. E. Blöchl, *Phys. Rev. B*, 1994, **50**, 17953–17979.
28. D. N. Bowman, J. H. Blew, T. Tsuchiya and E. Jakubikova, *Inorg. Chem.*, 2013, **52**, 8621–8628.
29. D. N. Bowman, J. Chan and E. Jakubikova, in *Photoinduced Processes at Surfaces and in Nanomaterials*, American Chemical Society, 2015, vol. 1196, ch. 8, pp. 169–188.
30. E. Jakubikova, *Toward the Computational Design of Iron-Based Chromophores*, North Carolina State University Raleigh United States, 2018.
31. S. Mukherjee, D. N. Bowman and E. Jakubikova, *Inorg. Chem.*, 2015, **54**, 560–569.
32. S. Mukherjee, C. Liu and E. Jakubikova, *J. Phys. Chem. A*, 2018, **122**, 1821–1830.
33. C. R. Tichnell, J. N. Miller, C. Liu, S. Mukherjee, E. Jakubikova and J. K. McCusker, *J. Phys. Chem. C*, 2020, **124**, 1794–1811.
34. H. Lin, G. Fratesi, S. Selçuk, G. P. Brivio and A. Selloni, *J. Phys. Chem. C*, 2016, **120**, 3899–3905.
35. E. Mosconi, A. Selloni and F. De Angelis, *J. Phys. Chem. C*, 2012, **116**, 5932–5940.
36. S.-H. Liu, H. Fu, Y.-M. Cheng, K.-L. Wu, S.-T. Ho, Y. Chi and P.-T. Chou, *J. Phys. Chem. C*, 2012, **116**, 16338–16345.
37. N. M. O'boyle, A. L. Tenderholt and K. M. Langner, *J. Comput. Chem.*, 2008, **29**, 839–845.
38. L. G. C. Rego and V. S. Batista, *J. Am. Chem. Soc.*, 2003, **125**, 7989–7997.
39. G. Ramesh, R. K. P, M. Pillegowda, G. Periyasamy, P. A. Suchetan, R. J. Butcher, S. Foro and G. Nagaraju, *New Journal of Chemistry*, 2020, **44**, 11471-11489.
40. M. Abrahamsson, H. Wolpher, O. Johansson, J. Larsson, M. Kritikos, L. Eriksson, P.-O. Norrby, J. Bergquist, L. Sun, B. Åkermark and L. Hammarström, *Inorganic Chemistry*, 2005, **44**, 3215-3225.
41. Y.-Q. Fang, N. J. Taylor, F. Laverdière, G. S. Hanan, F. Loiseau, F. Nastasi, S. Campagna, H. Nierengarten, E. Leize-Wagner and A. Van Dorsselaer, *Inorg. Chem.*, 2007, **46**, 2854 – 2863.
42. J. M. Cole, K. S. Low and Y. Gong, *ACS Applied Materials & Interfaces*, 2015, **7**, 27646-27653.
43. Y. Gao, X. Ding, J. Liu, L. Wang, Z. Lu, L. Li and L. Sun, *J. Am. Chem. Soc.*, 2013, **135**, 4219–4222.
44. M. R. Norris, J. J. Concepcion, D. P. Harrison, R. A. Binstead, D. L. Ashford, Z. Fang, J. L. Templeton and T. J. Meyer, *J. Am. Chem. Soc.*, 2013, **135**, 2080−2083.
45. S. Zhang, H. Ye, J. Hua and H. Tian, *J. Energy Chem.*, 2019, **1**, 100015.